

**EFFECTS OF MANGANESE PROMOTION ON
REACTANTS AND INTERMEDIATES OF
FISCHER TROPSCH SYNTHESIS ON A MODEL
COBALT SURFACE– A DENSITY FUNCTIONAL
THEORY INVESTIGATION**

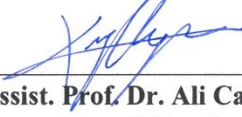
**A Thesis Submitted to
The Graduate School of Engineering and Sciences of
İzmir Institute of Technology
in Partial Fulfillment of the Requirements for the Degree of
MASTER OF SCIENCE
in Materials Science and Engineering**

**by
Merve GENÇOĞLU**

**July 2019
İZMİR**

We approve the thesis of **Merve GENÇOĞLU**

Examining Committee Members:




Assist. Prof. Dr. Ali Can KIZILKAYA

Department of Chemical Engineering, İzmir Institute of Technology



Assist. Prof. Dr. Başar ÇAĞLAR

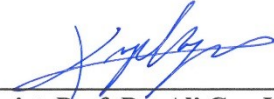
Department of Energy Systems Engineering, Yaşar University



Assoc. Prof. Dr. Özgeç EBİL

Department of Chemical Engineering, İzmir Institute of Technology

12 July 2019



Assist. Prof. Dr. Ali Can KIZILKAYA

Supervisor, Department of Chemical
Engineering
İzmir Institute of Technology



Assoc. Prof. Dr. Haldun SEVİNÇLİ

Co-Supervisor, Department of Materials
Science and Engineering
İzmir Institute of Technology



Assoc. Prof. Dr. Haldun SEVİNÇLİ

Head of the Department of Materials
Science and Engineering

Prof. Dr. Aysun SOFUOĞLU

Dean of the Graduate School of
Engineering and Sciences

ACKNOWLEDGMENTS

Firstly, I would like to thank my supervisor of this research, Assist. Prof. Dr. Ali Can Kızılkaya. He inspired me greatly to work in this project. His willingness to motivate me contributed tremendously to my project.

Besides, I would like to thank the authority of TUBITAK ULAKBİM and EFES for providing me with good facilities to complete this project. Also, I would like to take this opportunity to thank my co-advisor of this study, Assoc. Prof. Dr. Hâldun Sevinçli. This research project would not have been possible without the support of many people. Special thank my graduate friend Mustafa Neşet Çınar for invaluable assistance. Especially group member Yiğit Hatipoğlu for sharing his friendship. I am thankful that Yağmur Dağa calms and helps me in the most complicated situations. Not forgetting to my best friends who always been there.

Finally, yet importantly, I would like to express my heartfelt thanks to my beloved parents. Taner Gençoğlu, Aysel Gençoğlu, for their blessings for their help and wishes for the successful completion of this project.

ABSTRACT

EFFECTS OF MANGANESE PROMOTION ON REACTANTS AND INTERMEDIATES OF FISCHER TROPSCH SYNTHESIS ON A MODEL COBALT SURFACE– A DENSITY FUNCTIONAL THEORY INVESTIGATION

The effects of manganese promotion on the adsorbates and specific elementary reactions of Fischer-Tropsch Synthesis (FTS) was investigated using periodic Density-Functional Theory (DFT) calculations on a close packed cobalt surface, Co(111). In particular the effects of MnO promotion on the adsorbates of CO, HCO, CH, CH₂, C₂H₂, OH, H₂O, C, O and on the reactions of direct CO dissociation, H-assisted CO dissociation and carbon hydrogenation were studied for MnO coverages of 0.25 ML and 0.11 ML.

Mn was modeled in the chemical form of MnO. MnO was modeled as a singular monomer on the Co(111) surface, based on the findings from experimental studies. The results indicate that MnO promotion increases the adsorption energies of all adsorbates, except H and C₂H₂. In particular, CO and H₂O adsorption energies increase significantly, which indicate that the selectivity increases to long chain hydrocarbons is mainly due to an increased surface coverage of CO with respect to H. The results also indicate that the relative effect of MnO on adsorption energies are strongly dependent on MnO coverage.

MnO promotion is found to decrease the activation barriers for HCO and CH formation, while increasing the activation barriers for direct CO dissociation and HCO dissociation. The results point out that MnO does not promote the direct dissociation of CO and the activity increase due to Mn promotion is most probably due to a H or OH assisted CO dissociation pathway or another rate limiting step.

Keywords: Density Functional Theory, Fischer-Tropsch Synthesis, Catalysis, Promoter, Cobalt, Manganese

ÖZET

MANGANEZ AKTİFLEŞTİRİCİSİNİN MODEL KOBALT YÜZEYİ ÜZERİNDE FISCHER- TROPSCH SENTEZİNDEKİ REAKTANTLARA VE ARA ÜRÜNLERE ETKİSİNİN YOĞUNLUK FONKSİYONELİ TEORİSİ ARAŞTIRMASI

Sık istiflenmiş Co(111) yüzeyi üzerinde Mn aktifleştiricisinin adsorbatlar ve belirli temel Fischer-Tropsch reaksiyonlarını periyodik Yoğunluk Fonksiyoneli Teorisi (YFT) kullanılarak çalışıldı. Mn aktifleştiricisinin belirli etkisi CO, HCO, CH, CH₂, C₂H₂, OH, H₂O, C, O adsorbatları ve direk CO, H yardımcı CO parçalanma reaksiyonları ve carbon hidrojenlenmesi reaksiyonu için 0.25 ve 0.11 kaplama yüzey oranlarında MnO çalışıldı.

MnO kimyasal yapısı ile Mn model oluşturuldu. Deneysel bulgulara dayandırılarak MnO tekli monomer olarak Co(111) yüzeyi üzerinde model oldu. Bu sonuçlar MnO aktifleştiricisinin H ve C₂H₂ hariç tüm adsorbatlar için adsorpsiyon enerjilerini arttırdığını gösterdi. Özellikle CO ve H₂O adsorpsiyon enerjileri önemli ölçüde artması CO yüzey kaplama oranının Hidrojene göre daha fazla olması nedeniyle uzun hidrokarbon zincirli ürünlere seçiciliği arttı. Bu sonuçlar MnO'in adsorpsiyon enerjilerine etkisinin MnO yüzey kaplama oranına bağlı olduğunu göstermektedir.

MnO aktifleştiricisi direkt CO ve HCO parçalanma reaksiyonlarının aktivasyon bariyerlerine arttırırken, HCO ve CH oluşum aktivasyon bariyerlerini düşürür. Bu sonuçlar MnO'in direkt CO parçalanma reaksiyonunun aktifleştirmediğini ve Mn aktifleştiricisinin H veya OH yardımı ile CO parçalanma yoluyla veya reaksiyonu hızının belirleyici başka bir basamak için aktiviteyi arttırdığına işaret etmektedir.

Anahtar Kelimeler: Yoğunluk Fonksiyoneli Teorisi, Fischer-Tropsch Sentezi Co, Mn, Kataliz, Aktifleştirici

To my family,

TABLE OF CONTENTS

ABSTRACT.....	iv
ÖZET.....	v
LIST OF TABLES.....	ix
LIST OF FIGURES.....	xi
LIST OF ABBREVIATIONS.....	xi
CHAPTER 1. INTRODUCTION.....	1
1. CATALYSIS.....	1
1.1. Principles of Catalysis.....	1
1.2. Fundamentals of Heterogeneous Catalysis.....	3
1.3. Sabatier Principle.....	4
1.4. Fischer-Tropsch Synthesis.....	5
1.4.1. The Basics of Fischer-Tropsch Synthesis.....	5
1.4.2. Catalytic Materials Used for Fischer-Tropsch Synthesis.....	5
1.4.3. Catalyst Preparation Methods.....	6
1.4.4. Promoter Effects on Fischer-Tropsch Synthesis.....	8
1.4.5. Surface Effects on Fischer-Tropsch Synthesis.....	9
1.4.6. Main Steps at The Catalyst Surface in Fischer-Tropsch Reaction.....	10
1.5. Computational Quantum Chemistry.....	12
1.5.1. Born-Oppenheimer Approximation.....	13
1.5.2. Variational Principle and Hartree-Fock Theory.....	14
1.5.3. Principles of Density Functional Theory (DFT).....	15
1.6. The primary approximation of Exchange & Correlation.....	15
1.6.1. Capabilities of DFT.....	16
1.6.2. Main Approach in Quantum Chemical Modelling of Catalytic Systems.....	16
1.6.3. The Aim of this Thesis.....	16
CHAPTER 2. LITERATURE SURVEY.....	18
2.1. Promoter Effects on Catalytic Activity.....	18
2.2. MnO Promotion Effects on Co-catalyzed FTS.....	21
2.3. MnO promoter model on Co-Catalysts.....	33

CHAPTER 3. COMPUTATIONAL METHODOLOGY.....	35
3. Summary of Computational Methods	35
3.1. General	36
3.1.1. Bulk Optimization	36
3.1.2. Clean Surface Optimization.....	37
3.1.3. Molecule and Atomic Optimization	37
3.1.4. Adsorption Energy Calculations.....	37
3.1.5. Coadsorption Energy Calculations	38
3.1.6. The Vibrational Frequency for Adsorbed Surface and Molecule.....	39
3.1.7. Nudged Elastic Band (NEB) Calculations.....	40
3.1.8. Transition State Calculation	41
3.1.9. MnO Promoter Model	41
CHAPTER 4. RESULTS.....	42
4.1. Structural Model for MnO promoted Co(111) Surface	42
4.1.1. CO Adsorption Energy	45
4.1.2. C, O, H Adsorption Energies	51
4.1.3. CH and OH Adsorption Energies	55
4.1.4. CH ₂ Adsorption Energy	58
4.1.5. H ₂ O Adsorption Energy	59
4.1.6. C ₂ H ₂ Adsorption Energy	60
4.2. Effect on MnO Promotion on CO Dissociation and Carbon Hydrogenation...	65
4.2.1. CO Dissociation: Direct and H-assisted.....	66
4.2.2. Carbon Hydrogenation.....	69
CHAPTER 5. DISCUSSION.....	76
5.1. Effect of MnO on Adsorption Energies of Surface Species.....	76
5.1.1. Effect of MnO on Activation Barriers for CO Dissociation and Carbon Hydrogenation.....	79
CHAPTER 6. CONCLUSIONS.....	81
REFERENCES	82
APPENDIX A. INPUT AND OUTPUT FILES.....	90

LIST OF TABLES

<u>Table</u>	<u>Page</u>
Table 1.1. Different catalyst shapes [10].....	10
Table 2.1. Promoter Analysis on Co-Based Fischer-Tropsch Synthesis Source Adapted from. [34] promoter effects on Co-based Fischer-Tropsch Synthesis.....	22
Table 2.2. Mn promotion effect on unsupported Co catalysts [6].....	23
Table 2.3. Mn promotion effect on supported Co catalysts [6].....	26
Table 2.3. Mn promotion effect on supported Co catalysts [6] (cont.).....	27
Table 2.4. MnO Promotion Effects on Adsorption Energies, kJ/mol [34].....	31
Table 2.5. Two Different Mn Promotion Models Effect on Adsorption Energies, eV [68].....	34
Table 4.1. MnO Monomer Model (0.25 ML coverage) on Co(111) (a) fcc model and (b) hcp model.....	45
Table 4.2. CO Adsorption energies kJ/mol.....	50
Table 4.3. HCO Adsorption Energies kJ/mol.....	51
Table 4.4. CO Coadsorption Energies on 0.25 ML Co(111) kJ/mol.....	52
Table 4.5. Bare CO+H and CH+O Coadsorption on 0.25 ML Bare Co(111) kJ/mol.....	53
Table 4.6. C Adsorption Energies, kJ/mol.....	53
Table 4.7. O Adsorption Energies, kJ/mol.....	54
Table 4.8. H Adsorption Energies, kJ/mol.....	55
Table 4.9. CH Adsorption Energies, kJ/mol.....	56
Table 4.11. OH Adsorption Energies, kJ/mol.....	57
Table 4.12. CH ₂ Adsorption Energies, kJ/mol.....	58
Table 4.13. H ₂ O Adsorption Energy, kJ/mol.....	59
Table 4.14. C ₂ H ₂ Adsorption Energies, kJ/mol.....	60
Table 4.15. Adsorption energies 0.25 ML and 0.11 ML Bare Co(111).....	61
Table 4.16. Adsorption Energy Results (kJ/mol).....	62

<u>Table</u>	<u>Page</u>
Table 4.17. Zero Point Correction Effect on 0.25 ML Bare and HCP MnO Promoted Co(111) Surfaces.....	64
Table 4.18. Zero Point Correction Effect on 0.11 ML Bare and HCP MnO Promoted Co(111) Surfaces.....	65
Table 4.19. MnO Promotion Effect on Bond Lengths, A°.....	66
Table 4.20. MnO Promotion Effect for Activation Barrier Energies, kJ/mol on 0.25 ML Bare and HCP MnO Promoted Co(111).....	66
Table 5.1. Adsorption Energy Variation for Different Coverages.....	74
Table 5.2. Promoter Effect on Adsorption Energy.....	75

LIST OF FIGURES

<u>Figure</u>	<u>Page</u>
Figure 1.1. Catalyst cycle source adapted from [1]	1
Figure 1.2. Energy profile of a catalytic reaction source adapted from [1].....	2
Figure 1.3. Volcano Curve for Catalyst Activity, Source Adapted from [5].....	4
Figure 1.4. Variations Interest in Fischer-Tropsch Synthesis [6].....	5
Figure 1.5. Classification of promoters	9
Figure 1.6. Different adsorption site of the surfaces [11].....	10
Figure 1.7. Elementary Fischer-Tropsch Reactions.....	11
Figure 1.8. Fundamental reactions of Fischer-Tropsch Synthesis.....	12
Figure 2.1. Different MnO promoter models on Co Catalyst [34]	30
Figure 2.2. Mn promoted Co models [66]	32
Figure 3.1. NEB Calculation for CO Dissociation on 0.25 ML Co (111) Surface.....	40
Figure 4.1. Adsorption sites for bare Co(111) surface.....	43
Figure 4.2. 0.25 ML hcp and fcc MnO adsorption sites.....	44
Figure 4.3. Adsorption sites for 0.11 ML hcp MnO monomer models.....	45
Figure 4.4. Elementary Steps of FTS investigated in this thesis.....	65
Figure 4.5. MnO Promotion Effect for direct CO Dissociation.....	67
Figure 4.6. MnO Promotion Effect for HCO Formation on 0.25 ML Co(111) Surface.....	68
Figure 4.7. MnO Promotion Effects on HCO Formation on 0.25 ML Bare and.....	68
Figure 4.8. MnO Promotion Effect for Carbon Hydrogenation.....	69
Figure A.1. A sample INCAR file.....	84
Figure A.2. A sample KPOINTS file.....	85
Figure A.3. A sample POSCAR file.....	85
Figure A.4. A sample “POTCAR” file (first lines).....	86
Figure A.5. A sample POTCAR files (first lines).....	86
Figure A.6. A sample POTCAR (some last lines).....	87
Figure A.7. A sample “slurm.out” file (first lines).....	88

<u>Figure</u>	<u>Page</u>
Figure A.8. A sample "slurm.out" (last lines).....	88
Figure A.9. A sample of "OUTCAR" (first lines)	89
Figure A.10. A sample "OUTCAR" file (last lines)	90

LIST OF ABBREVIATIONS

- FTS:** Fischer-Tropsch Synthesis
- DFT:** Density Functional Theory
- TPR:** Temperature Programmed Reduction
- TPD:** Temperature Programmed Desorption
- ASF:** Anderson-Schulz-Flory
- FCC:** Face Centered Cubic
- XRD:** X-Ray Diffraction
- XPS:** X-Ray Photoelectron Spectroscopy
- TPRS:** Temperature Programmed Surface Reduction
- ZSM-5:** Pentasil Zeolites
- SBA-15:** Mesoporous Silica
- HCP:** Hexagonal closed packed
- BR:** Bridge
- Ads.:** Adsorption
- DRS:** Diffuse Reflectance Spectroscopy
- XAS:** X-Ray Absorption Spectroscopy
- TEM:** Transmission Electron Microscopy
- VASP:** Vienna Ab-Initio Simulation Package
- DRIFTS:** Diffuse Reflectance Infrared Transformed Spectroscopy
- STEM-EELS:** Scanning Transmission Electron Microscopy and Monochromated Electron Energy Loss Spectroscopy
- TOF:** Turnover Frequency
- CNF:** Carbon Nano Fiber
- GGA-RPBE:** Generalized Gradient Approximation- Revised Perdew- Burke- Ernzerhof
- MEP:** Minimum Energy Path
- GGA:** Generalized Gradient Approximation
- LDA:** Local Density Approximation

CHAPTER 1

INTRODUCTION

1. CATALYSIS

1.1. Principles of Catalysis

Catalysis has an important place in daily life. Most of the biological reactions in the human body and chemical reactions in various industrial applications cannot be accomplished without a catalyst [1]. Besides, catalysis provides solutions to chemical industry in terms of environmental pollution issues and sustainable energy conversion [2].

A catalyst is a substance that increases the rate of a chemical reaction without being consumed [2]. Catalysts provides favorable operating conditions with respect to non-catalytic reactions, such as lower operating temperature, which provide possibilities for economic operation. Catalytic operation can also help to minimize undesired side products [1].

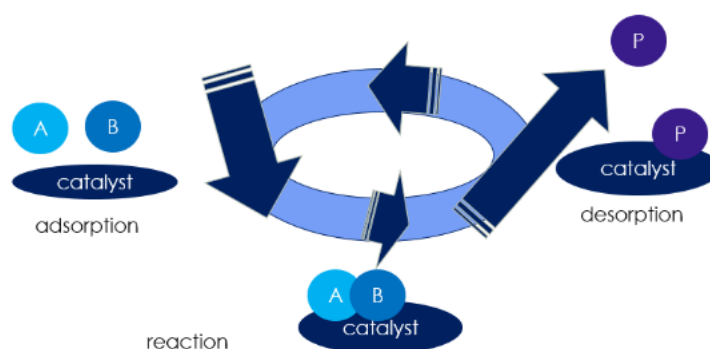


Figure 1.1. Catalyst cycle source adapted from [1]

The adsorbate helps to saturate the surface's free valences. The removal of species from the adsorbed state back to the gas phase is called desorption.

The fundamental reason that catalysts accelerate chemical reactions is that they decrease the activation barriers with respect to non-catalytic reaction [2].

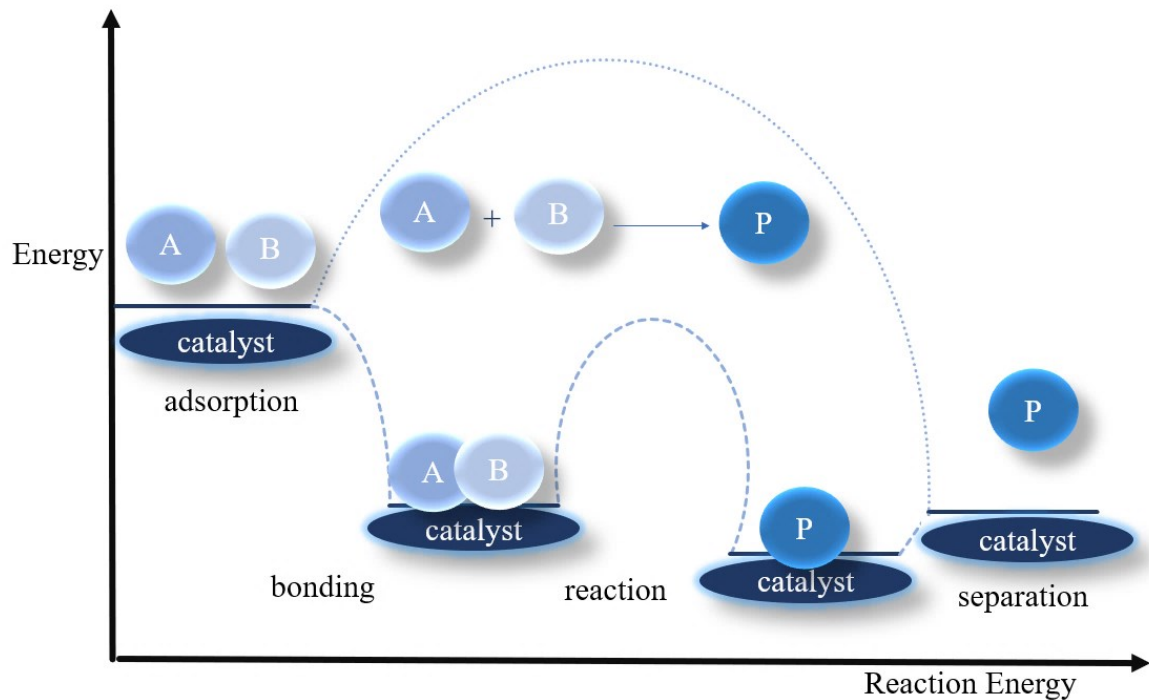


Figure 1.2. Energy profile of a catalytic reaction source adapted from [1]

There are different categorizations of catalysts that is related to the issue of concern. The most general classification is done by using the phase of a system including a catalyst. Catalysts can be mainly divided into two parts: homogeneous and heterogeneous catalysis [1].

In homogeneous catalysis, catalysts and reactants have the same physical phase, such as gas phase or liquid (solution) phase. For example, chlorine as a homogeneous catalyst accelerates ozone decomposition [1]. Typical examples of homogenous catalysts include metal complexes, metal ions, organometallic complexes, biocatalysts [1].

The heterogeneous catalysis system includes reactant and catalyst at different physical phases.

This kind of catalytic systems occurs for solid catalyst and gas phase reactants generally. The cleaning process of the automotive exhaust, for example CO oxidation on noble metals, can be given as an example of heterogeneous catalysis [1]. The catalyst and products are easily separable in heterogeneous catalysis, due to their phase differences [1].

Various industrial applications that are related to chemical and petrochemical industries depend on heterogeneous catalysis [1].

1.2. Fundamentals of Heterogeneous Catalysis

Catalysts are typically composed of an active substance (typically metallic), support and promoter. The expense of catalyst requires that heterogeneous catalytic reactions are done generally by using an inert and porous supported catalyst in nano size [1]. The catalytic reactions take part on the surface of the active component of the catalyst material.

The most important properties of catalysts are activity, selectivity and stability. Activity is a measure of how much a catalyst increases the rate of reaction. Selectivity as a catalytic feature causes specific desired products to increase at the end of the reaction. Same reactants with different catalysts have different product selectivities. Catalyst stability in terms of chemical, thermal and mechanical properties is associated with catalytic life in industrial reactors [1, 3]. There are some specific important features which define an industrially acceptable catalyst. The catalyst must be chemically resistant to impurities. These impurities on the active catalyst surface should not react with active metal. The large surface area is required to increase chemical reactivity. Catalyst activity must be specific because side products should be minimized at the end of the catalytic reaction. In terms of economics, catalyst materials should also have a feasible cost [4].

Heterogeneous catalytic reactions occur in several steps. Reactants diffuse and adsorb on catalyst active site [4]. Adsorption is one of the most essential elementary processes which activates the decisive chemical bond of the (adsorbed) reactants [2].

After surface reactions occur, products desorb from the catalyst active site. The last step is the diffusion of products from the catalyst surface to the reaction medium [4].

Heterogeneous catalysis is a multidisciplinary research area, including chemistry, physics, chemical engineering, material science, and engineering.

The issue can be studied with the contribution of various branches of science. These disciplines cover various research areas in catalysis, including catalyst preparation techniques, characterization of catalyst properties, measurement of catalyst stability and reaction kinetics. In addition to these topics, heterogeneous catalytic reactions can be investigated by using theoretical methods. Calculated results are beneficial to learn elementary steps of the reaction, catalyst structure, stability, and reactivity, which can provide a screening tool for experiments, compliment experimental findings or provide information that cannot be provided by experiments.

These calculations are done with the help of Density Functional Theory (DFT), currently the most modern tool in Computational Quantum Chemistry. Experimental techniques are generally more expensive and difficult to apply compared to computational techniques. Besides, experiments can be insufficient to measure complicated reactions on the surface [4].

1.3. Sabatier Principle

Catalytic activity is an ability that results in increased reaction rate and it is related to adsorption on the surface. Sabatier has explained the relation between adsorption properties and the catalytic capability of the surface for the first time. The principle expresses that catalytic reactions occur well when interaction strength between adsorbate and surface is intermediate. Adsorbates with too weak interactions with the catalyst surface may not be accommodated on the surface and then dissociation of chemical bonds cannot be occurred. On the other hand, as the surface has strong interaction with products and reactants, the desorption of adsorbates may be hindered, deactivating the catalyst.

Having strong interaction between molecules and surface obstructs to adsorb new molecules, so convenient open surface site on catalyst surface decreases.

When there is an interaction that is strong or weak between surface and reactants and products, so catalytic activity is decreased [1, 3]. An optimum rate of catalytic reaction can be revealed based on the heat of adsorption [1].

Volcano plots show that optimum adsorption strength at a maximum point depends on the Sabatier principle [5].

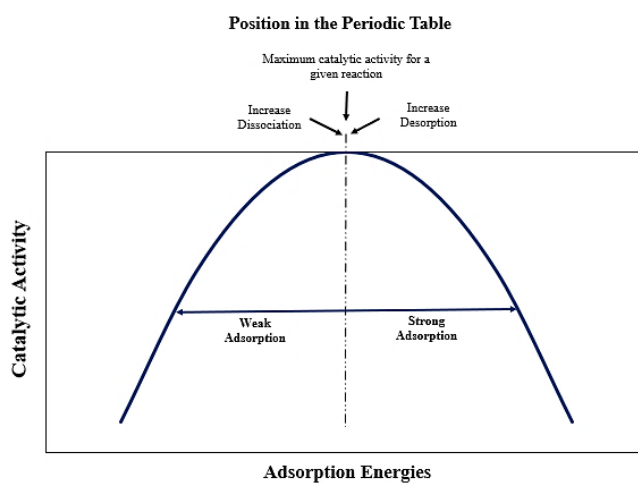


Figure 1.3. Volcano Curve for Catalyst Activity, Source Adapted from [5]

1.4. Fischer-Tropsch Synthesis

In this part, reasons for interest in Fischer-Tropsch Synthesis, catalytic materials for FTS, catalyst preparation methods, promoter and surface effects and main steps of FTS are explained.

1.4.1. The Basics of Fischer-Tropsch Synthesis

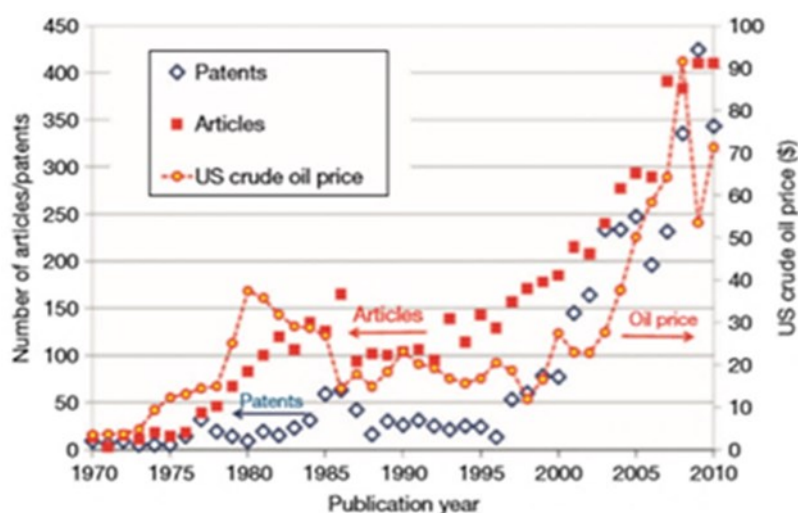
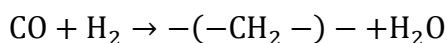


Figure 1.4. Variations Interest in Fischer-Tropsch Synthesis [6]

The variations (typically in forms of sudden increases) in crude oil prices, geographical differences in crude oil availability and environmental problems related the crude oil are the reasons for remarkable interest in Fischer-Tropsch Synthesis [6, 7].

Fischer-Tropsch Synthesis is a catalytic process for converting natural gas and coal-derived synthesis gas to long-chain hydrocarbons [8].

There is one main reaction of the Co-based Fischer-Tropsch Synthesis that is polymerization to produce long chain hydrocarbon [9]:



1.4.2. Catalytic Materials Used for Fischer-Tropsch Synthesis

Support material, active material, and promoters typically make up Fischer-Tropsch catalysts [6]. In support material, TiO_2 and Al_2O_3 have strong interaction with catalyst. However, there is a weak interaction between SiO_2 and catalyst [6, 7].

Co, Fe, Ni, Ru can be given as examples of active catalyst metal. Ru is expensive and has limited sources. This situation restricts the use of Ru.

Ni increases the production of methane (main component of natural gas) which is an undesired product for Fischer-Tropsch Synthesis. Ni is not favorable because of this reason. Fe has a higher water-gas-shift activity which leads to the greenhouse effect. Fe is not preferable in terms of environmental reasons.

Co is the typical catalyst used for converting natural gas derived syngas, despite its higher cost compared to Fe.

When Co-based Fischer-Tropsch Synthesis is performed, the amount of Co used is in general small. Co and Fe are more accessible for Fischer-Tropsch Synthesis than others.

Promoters (additives) are doping agents added to catalyst materials in small amounts to improve their activity, selectivity, and/or stability. Poisons decrease or diminish catalytic activity. Being a promoter or poison depend on the quantity of additive and the exact preparation method [6, 7].

1.4.3. Catalyst Preparation Methods

Solid catalysts are synthesized from chemicals by using a lot different procedures. The physical and chemical catalytic properties are affected differently for each various preparation step [10].

Experimental conditions (temperature, pH, pressure, concentration), instrumentals are important parameters for synthesis of heterogeneous catalyst [10].

Preparation techniques vary depending on catalyst types. Bulk catalyst and support, impregnated catalyst, and mixed-agglomerated catalyst are derived from chemicals by using different preparation steps [10].

Bulk catalyst mainly contains active catalyst metal. Silica-alumina support for hydrocarbon cracking can be an important example. Supports such as silica, alumina, silica-alumina are prepared with the same procedure [10].

Impregnation catalysts are produced that support material is impregnated on catalyst metal. A number of hydrogenation catalyst can be synthesized by impregnation method.

Mixed-agglomerated catalyst is done by mixing active element with a powdered support or a precursor support material and agglomerating the mixture [10].

There are several unit operations to synthesize catalyst [10]:

1. Precipitation:

In this step, a solid solution is produced from a liquid solution.

There are 3 main steps; supersaturation, nucleation, and growth. Supersaturation is unstable region. Precipitation appears with small disorder. Homogeneous nucleation may proceed spontaneously. Otherwise, seed materials are used to initiate heterogeneous nucleation. Addition of seed facilitates acceleration of nucleation. Concentration, pH and temperature are effective factors on growth process. Amorphous solids can be produced that depend on precipitation conditions.

Precipitation method can be used for one component catalyst and support material or mixed catalyst. Higher supersaturation leads to occur very small particle size. pH must be optimized and kept constant during precipitation operation [10].

2. Gelation:

Micelles are produced from hydrophilic colloidal solutions.

Micelles located separately because of the electrical charge on the surface and in the surrounding surface.

The micelle concentration, the ionic strength of solution and especially the pH are important parameters for gelation process. Sol-gel method is better than precipitation. Control of surface area, pore volume and pore size distribution can be done well with the help of sol-gel method [10].

3. Hydrothermal transformation:

The modification of precipitates, gels, flocculates are considered by activating temperature, aging, ripening in the presence of mother liquor. This transformations are occurred at 100 -300°C [10].

4. Decantation, filtration, centrifugation:

These are unit operations to separate from mother liquor [10].

5. Washing:

Mother liquor is completely removed, and impurities are eliminated by washing [10].

Separation methods are specified that particle size of the solids. Precipitates solid catalysts can be separated from mother liquor easily than flocculates. There is no usage of separation for gel catalysts [10].

6. Drying:

Solvent elimination from pores of the solids can be done with this step.

Drying is important for flocculates and gel catalyst [10].

7. Calcination:

There are several processes for calcination. These are loss of the chemically bonded water or carbon dioxide, modification of texture through sintering, modification of the structure, active phase generation, stabilization of mechanical properties [10].

8. Forming operations:

Suitable sized particles in the reactor can be obtained by using forming operations. This step is essential for forming and shaping supports and catalyst. Catalytic activity, strength the particle resistance to crushing and abrasion, minimization of bed pressure drops, lessening fabrication cost and distribute dust build-up uniformly can be provided by optimizing catalyst shape and dimension [10].

Depending on height (h), length (l), diameter (d) catalyst has different shapes [10].

9. Impregnation [10]

10. Crushing and grinding [10]

11. Mixing [10]

12. Activation [10]

Preparation procedures for supported catalysts starts from powder of support or support precursors.

Then, all unit operations are done. Precipitation and impregnation method are common types for supported catalyst formation [10].

There are three steps in impregnation method. The support material and the impregnation solution are contacted for a certain period. Then, drying is applied for support to remove imbedded liquid. Finally, catalyst is activated by calcination, reduction, or other appropriate treatment [10].

Table 1.1. Different catalyst shapes [10]

Shape	Size	Reactor
Extrude	d=1-50 mm l=3-30 mm	Fixed bed reactor
Pellet	d=3-15 mm h=3-15 mm	Fixed bed reactor
Granule, bead	d=1-20 mm d=1-5 mm	Fixed bed reactor
Sphere	d=1-10 mm	Fixed bed reactor Moving bed reactor
Microspheroidal	d=20-100 μm	Fluid bed reactor Slurry reactor

In this thesis, nanometer scale catalyst is considered [10].

1.4.4. Promoter Effects on Fischer-Tropsch Synthesis

There are three types of promotion effects including structural effect, electronic effects, and synergistic effects [6].

Structural promoters affect the formation and stability of the active phase of the catalyst material [6].

Electronic promoters affect the local electronic structure of an active metal by adding or withdrawing electron density near the Fermi level in the valence band of the metal [6].

Synergistic promotion effects: Promoter is considered as catalytically active. Promoter activity may indirectly affect the behavior of the catalytically active element. They influence overall reaction product distribution [6].

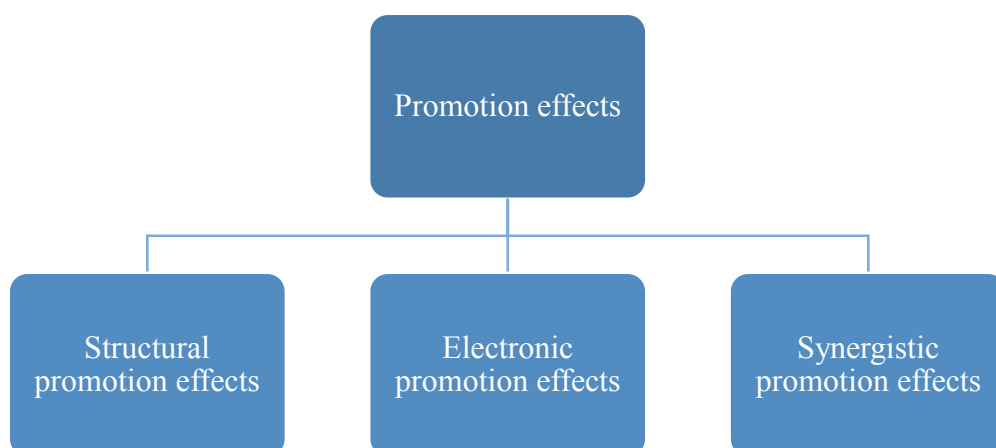


Figure 1.5. Classification of promoters

1.4.5. Surface Effects on Fischer-Tropsch Synthesis

Due to different electronic structures, geometrically different sites on the surface have different chemical activity. In kinks and stepped sites (atoms that have a lower coordination number compared to the bulk and close packed surface facets), chemical reactivity increases. For example, CO dissociation occurs easily in these sites [11].

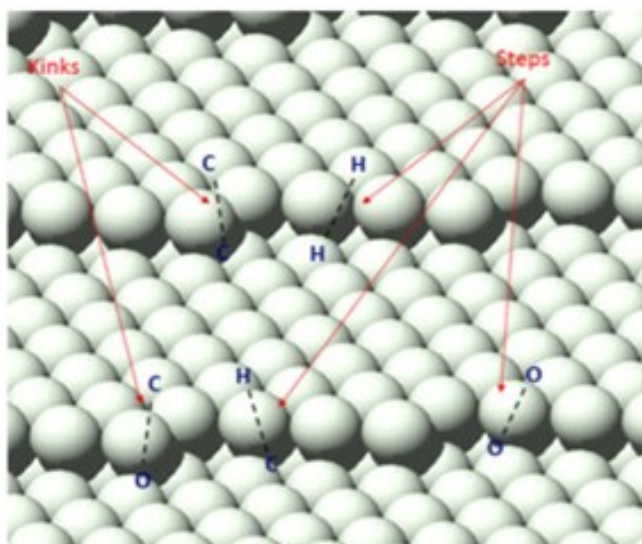


Figure 1.6. Different adsorption site of the surfaces [11]

1.4.6. Main Steps at The Catalyst Surface in Fischer-Tropsch Reaction

Important information about essential FTS mechanism steps can be obtained using surface science studies. Microkinetic models for FTS can be studied in more detail with the help of knowledge about reaction mechanisms and activation barriers for individual reactions[12].

It is proposed that either water formation or carbon monoxide dissociation determine reaction rate in Fischer-Tropsch mechanism [12]. On close-packed surfaces, the chain growth mechanism is predicted by adding CH to chain initiation reactant and hydrogenation is done as a final step. There must be a large surface area to the chain growth mechanism for a single chain. Growth ensemble on a large surface lead to form CH_x monomer. The situation results in different chain growth mechanisms simultaneously.

Diffusion of surface species that include hydrocarbon group is important to understand as a whole reaction sequence. Coupling reactions are considered as a source of chain growth mechanism [12].

Even though Fischer-Tropsch Synthesis is extensively studied in the literature, its reaction mechanism is still under debate and considered to be one of the most complicated mechanisms in heterogeneous catalysis. This is since various products can be formed, starting from the main building blocks of CO and H_2 [12, 13].

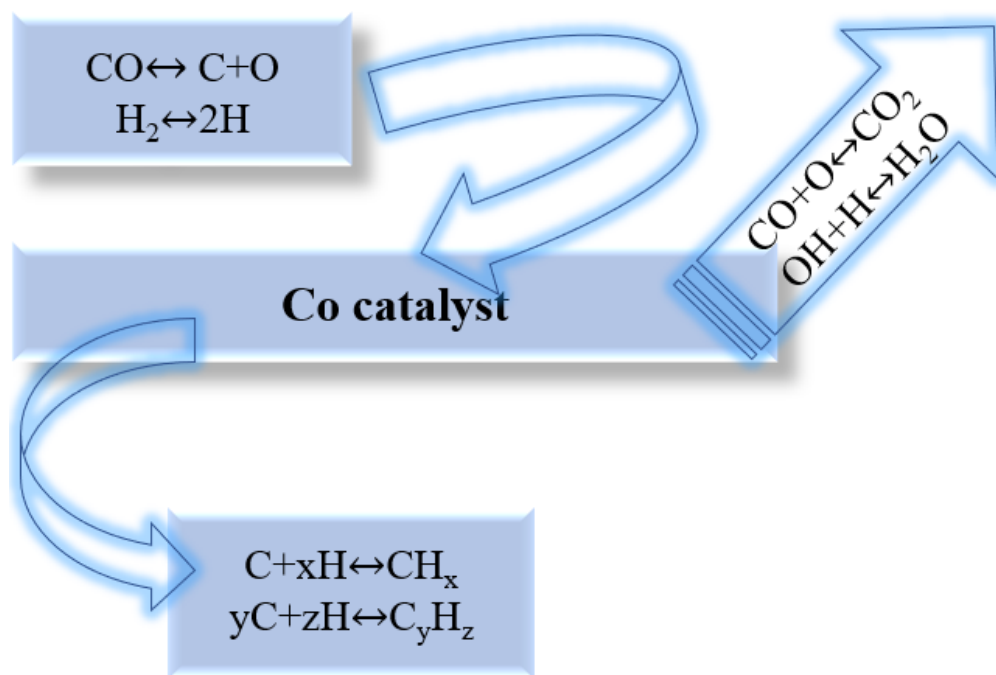


Figure 1.7. Elementary Fischer-Tropsch Reactions

Figure 1.7. explains that there are 4 essential reactions that the catalyst should be active for, including H_2 and CO dissociation, removal of oxygen as water or carbon dioxide, carbon-carbon coupling, hydrogenation/dehydrogenation reaction C_1H_x and C_yH_z . The surface geometry of Co is effective for CO bond breaking and the CH_aOH_b reaction mechanism.

Previous theoretical studies that are done with Density Functional Theory are about direct CO dissociation on stepped surface [13], H -assisted CO dissociation on terrace and stepped surface [14, 15], and CO insertion mechanism [16, 17] [13].

Another important topic is how a chain growth mechanism occurs. Because, CH_x ($x=0, 1, 2$) and CO can be used as adding monomer [12, 18, 19]. There are experimental studies to express detailed information about Fischer-Tropsch chain growth reaction mechanisms [12, 20, 21]. Besides, there are theoretical studies for the same topic at the molecular level [12, 15, 22, 23].

In surface science using single crystal structures, there are more theoretical studies than experimental studies [12, 24].

Figure 1.8 can be explained in this way. CO can adsorb on the catalyst and may be dissociated. Then H_2 adsorbs the surface and dissociate. Next, surface reactions occur on the catalyst and lead to hydrocarbon products. Finally, hydrocarbon products desorb from the catalyst surface. Secondary reactions can occur from hydrocarbon products.

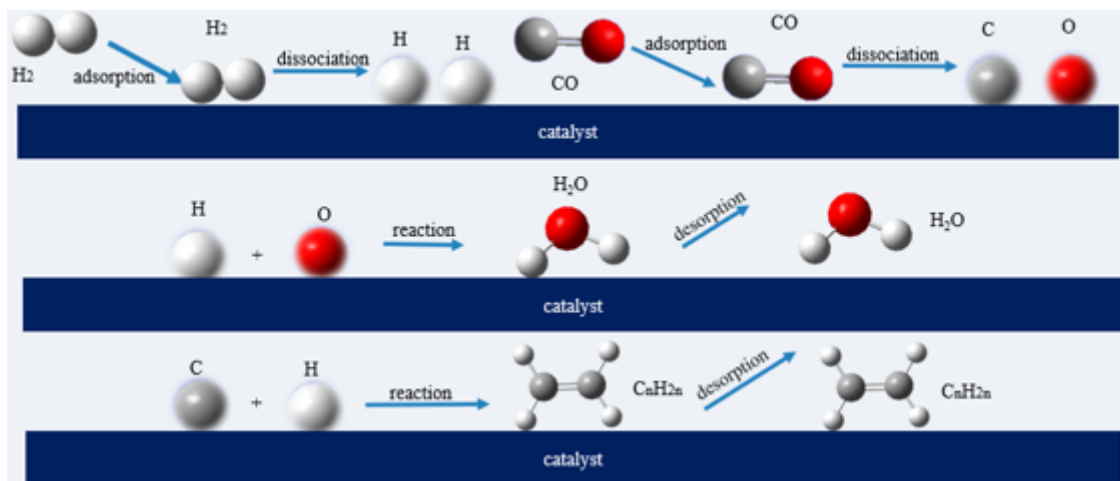


Figure 1.8. Fundamental reactions of Fischer-Tropsch Synthesis

1.5. Computational Quantum Chemistry

Computational techniques can be used to investigate various problems in chemistry due to the fast advancement of computers and computational power.

These issues include molecular geometry prediction, molecule energy calculation, specification of reaction intermediates and transition states, the visualization of orbital structures and IR, UV, NMR spectra, investigation of chemical reactivity, and the physical properties of substances [25, 26]. These techniques are based on Quantum Chemical principles.

Classical mechanics is interested in trajectories of particles that can be calculated theoretically by using initial conditions and Hamilton structure of electrons.

$$H = T + V \quad (1)$$

In (1) 1.1, H is the Hamilton that is the sum of the kinetic energy of particles, T , and potential energy of particles, V .

Electrons have wave and particle dualities so electronic motion is crucial to calculate the total energy of the system.

Unlike classical physics, quantum mechanics is used to expressing wave-particle duality behavior of electrons correctly, so total energy calculation can be done by considering the existence of electronic motion.

$$H = \hat{T}\Psi + \hat{V}\Psi \quad (2)$$

Schrödinger has expressed that the calculation of total energy of the system by using wave function that is Ψ .

The behavior of all particles can be found by using wave functions. The Hamiltonian operator can be written like below in quantum mechanics.

$$H = \hat{T} + \hat{V} \quad (3)$$

Kinetic, \hat{T} , and \hat{V} potential, energy operators can be expressed as a formulation like below for one electron system. h is Planck constant, m is electron mass, ∇^2 is Laplacian operator that is written with cartesian coordinates in kinetic energy formula. Besides, Z , the atomic number, e , the unit of electronic charge, and v , take place in potential energy operator.

$$\hat{T} = -\frac{h}{8\pi^2 m} \nabla^2, \hat{V} = -\frac{Ze^2}{v} \quad (4)$$

The Hamiltonian operator in quantum mechanics for a molecule consists of kinetic energy and electrostatic interactions mainly.

m mass particle's kinetic energy formula in SI units is

$$KE = \hat{T} - \frac{1}{2h^2 m} \nabla^2 \quad (5)$$

Coulomb Law applies to the interaction between all charged particles in a molecule, so the total energy of the system is related to the interaction of these particles.

Electrostatic interaction, \hat{I} , can be expressed with the help of position vector of a typical charge, \vec{r}_i and the typical charge, q_i .

$$\hat{I} = \sum_{i=1}^N \sum_{j=1, j>1}^N \frac{q_i \times q_j}{4\pi\epsilon_0 |\vec{r}_i - \vec{r}_j|} \quad (6)$$

1.5.1. Born-Oppenheimer Approximation

The Hamiltonian operator can be written in Schrödinger Equation (1) for molecular systems in atomic units:

$$\left(\sum_{i=1}^N -\frac{1}{2m_i} \nabla^2 (i) + \sum_{i=1}^N \sum_{j=1, j>1}^N \frac{q_i \times q_j}{4\pi\epsilon_0 |\vec{r}_i - \vec{r}_j|} \right) \Psi(\vec{x}_1, \vec{x}_2, \vec{x}_3, \dots, \vec{x}_n; t) = \sqrt{-1} \frac{\partial}{\partial x} \Psi(\vec{x}_1, \vec{x}_2, \dots, \vec{x}_n; t) \quad (7)$$

Schrödinger Equation (7) cannot be separated in smaller dimensions because of the existence of $\frac{1}{|\vec{r}_i - \vec{r}_j|}$ and partial derivative so the solution of this cannot be done easily.

In order to solve this (7), there are some electronic structure approximations including, the Born-Oppenheimer model and the variational principle.

Born-Oppenheimer model explains that nuclei have much greater mass than an electron. A nucleus can be thought immovable for lots of systems. Schrödinger (7) can be solved as a product of electronic and nucleus wave functions as wave function can be divided into two different parts as electronic and nuclei.

$$\Psi(\vec{x}_1, \vec{x}_2, \dots, \vec{x}_n) = \Psi_{\text{elec}}(\chi_{\text{elec}}; r_{\text{nuc}}) \times \Psi_{\text{nuc}}(r_{\text{nuc}}) \quad (8)$$

Wave function involves electronic and nucleic motion and can be reduced by considering the center of mass, CM, and relative coordinates.

$$\Psi_{\text{trans}} \approx \Psi_{\text{trans}}(\text{CM}) \Psi_{\text{rot}} \Psi_{\text{vib}} \quad (9)$$

The translational, vibrational and rotational contribution is calculated by using the center of mass.

Schrödinger Equation (1) must be divided into two parts as the electronic motion and translational motion of the center of mass and the vibrational and rotational wavefunctions and this situation can be interpreted as a disadvantage of Born-Oppenheimer approximation. The solution of complicated structured molecules is difficult by using this approach. Schrödinger Equation (1) can be written to calculate electronic energy for complex molecules that have many electrons.

n signifies included electron number in complicated molecules.

$$\hat{H}_{\text{elec}}(1, 2, \dots, n) \Psi_{\text{elec}} = E_{\text{elec}} \Psi_{\text{elec}}(1, 2, \dots, n) \quad (10)$$

With the use of stationary bound states and only single continuous eigenvalues, finite solution for Eqn 1 can be obtained.

E_i is the eigenvalue of the electronic Schrödinger (1)

$$\hat{H} \Psi_i = E_i \Psi_i \quad (11)$$

The suitable condition can be provided when eigenfunctions are orthonormal that has both orthogonality and normalization properties.

$$\int \Psi_i \Psi_j d\tau = \langle \Psi_i | \Psi_j \rangle = \delta_{ij} \quad (12)$$

δ_{ij} , Kronecker delta is the result of the electron interaction in terms of volume element and this (1) is called the matrix or Dirac notation.

1.5.2. Variational Principle and Hartree-Fock Theory

The variational principle expresses that the mean value of total energy can be calculated by using normalized wave functions. The result is found a bigger value than true total energy quantitatively, so the circumstance is a disadvantage [27].

The Hartree-Fock approximation is the modification of the variational principle and is used to describe the many-particle system wavefunctions [27].

1.5.3. Principles of Density Functional Theory (DFT)

Electronic structure calculations in solid state physics have been done by using Density functional theory (DFT) since 1970 [28,29].

In many body systems, the calculation of ground state total energy is done with the help of density Functional Theory, which is the best-known quantum chemical method.

Density functional theory is used because of its accuracy in calculating catalytic properties in detail.

Density functional theory provides lots of advantages ordered like below: [29, 30]

- Catalytic surfaces can be analyzed at the atomic level with density functional theory calculations.
- The identification of surface intermediates which cannot be afforded with the help of current experimental conditions can be investigated by using computational techniques.
- The investigation of the different reaction energies and the estimation of the reliable catalyst model can be made consistent with the experimental results.

Exchange-correlation potential covers all other electron-electron interactions.

1.6. The primary approximation of Exchange & Correlation

Local density approximation (LDA) is the simplest approach in density functional theory. It causes an inaccurate solution of quantum chemical problems and unreliable solid-state calculations [27].

Generalized gradient approximation (GGA) is more reliable than the local density approximation (LDA) as a density functional theory (DFT) approach.

GGA facilitates the solution of more complicated quantum chemistry problems. The use of GGA and hybrid functions reduces the error rate in results as 5-fold [27].

Becke and Perdew corrections (BP86), Perdew-Wang exchange functional (PW91), Perdew-Burke-Erzerhof (PBE) or Revised PBE (RPBE) can be given as examples of GGA functional types [27].

B3LYP is the most well-known function in hybrid functionals [31].

Hybrid functionals are used to information about different molecular properties, including structural, thermodynamic, vibrational of large molecules [31, 32].

Hartree-Fock exact exchange function is expensive to calculate metallic properties for large molecules and solids [31].

1.6.1. Capabilities of DFT

In literature, molecular modeling studies are generally done by Density Functional Theory, in the recent years. It is helpful to obtain information about reaction mechanisms relevant at the molecular level, transition states, adsorption energies, activation energies, heats of reaction and promoter effects on the catalyst [25, 26].

1.6.2. Main Approach in Quantum Chemical Modelling of Catalytic Systems

Metallic surface modeling is done by using two different approaches that are cluster model and periodic [33].

A metallic surface that is formed up to a few tens of atoms uses a cluster model. The model reports the band structure of metals restricted. Besides, adsorption energies are obviously related to cluster size. In addition to these, it facilitates calculation of local properties including adsorption geometries and vibrational frequencies for low coverage metallic surfaces. Adsorption energies can be calculated accurately by using a cluster model that is composed of 80 and 150 atoms [33].

In the periodic slab approach, under controllable numbered layers are used to solve artificial cluster boundaries. Basis set choice and superposition error problems are prevented by using a plane wave basis set in the periodic slab model for the description of electron density. Periodic calculations for very high number of atoms are time-consuming and require optimization heavily [33].

1.6.3. The Aim of this Thesis

The aim of this thesis is to investigate the effects of Mn promotion on the properties of adsorbates and intermediates of FTS, as well as the effects of Mn promotion on the main elementary reactions, using Density Functional Theory calculations.

There are three main scientific questions associated with this study:

- How does MnO coverage effect these results?

- How does Mn promotion affect the adsorption energies of reactants/intermediates?
- How does MnO affect elementary reactions of CO dissociation and carbon hydrogenation?

So far mainly experimental methods have been used to investigate MnO promoter effects on Co catalyzed Fischer-Tropsch Synthesis, where very limited number of computational studies have appeared in the last 2 years.

These studies will be discussed in the Literature Survey Section. Characterization techniques provide valuable information which is related to the effective catalyst model. The interaction between catalyst and support material and/or promoter, the physicochemical properties, the structural properties, particle size, the shape can be characterized by spectroscopic techniques.

These results have an influence on the construction of the catalyst model. Unfortunately, there is still no consensus about the details of the promotion mechanism of Mn, especially related to specific adsorption characteristics of the reactants and the reactions that are affected by the promotion. These effects will be investigated in this thesis, by investigating properties like adsorption sites, adsorption energies, bond lengths between surface and adsorbates, transition state structures and activation energies using Density Functional Theory.

CHAPTER 2

LITERATURE SURVEY

2.1. Promoter Effects on Catalytic Activity

Previous studies indicate that twenty-two various promoters are investigated in Co based catalytic reactions. Catalytic activity, selectivity, and stability vary depending on promoter kind [6]. Amount of promotion elements, experimental conditions during the catalytic reaction, catalyst preparation techniques also play important roles in specification of the promoter effect. Depending on these, promoter properties may change, also resulting in the change of catalytic activity product selectivity [6].

Apart from these, when promoter quantity is increased on catalyst active sites, adsorption features change. If great quantities of oxide promoter are used on active metal surface, catalyst active sites may be blocked. Catalytic activity decreases as a result of this promoter blockage [6].

Promoters have different chemical properties that affect the Co-based Fischer-Tropsch reaction [6].

Some transition metal oxides show water gas shift reagent features. The variation of CO/H₂ ratio leads to coverage change. Promoters may affect hydrogenation/dehydrogenation reactions. The ratio of alkane/alkene changes at the end of the reaction that the promoter is used. Promoter addition can also prevent catalyst against sintering of supported catalyst clusters.

Most studies in the literature are done about Ru, Re, Pt promoted Co-catalyzed Fischer-Tropsch reactions [21]. Ru has electronic and structural promotion effects [6].

Ru-promoted catalysts have typically increased C₅₊ selectivity compared to other promoters.

By addition of little Ru promoter to unsupported or supported Co-based catalysts, turnover frequency increases.

The maximum catalytic activity is observed for Ru/Co ratio smaller than 0.008 value [6].

Rhenium has a structural promotion effect on catalyst.

It leads to increase reducibility of Co, so Co dispersion increases by the increment of hydrogen spillover. Fischer-Tropsch activity increases by adding Re promoter, whereas site specific activity of Co sites is not affected. The product selectivity topic for Re promoted Co catalysts is not well established [6].

Pt as a structural promoter helps to increase the dispersion of cobalt nanoparticles. It also results in the decrease of Co_3O_4 reduction temperature especially for alumina supported Cobalt catalyst. The hydrogenation reaction rate increases without changing product selectivity [6].

Nb promoted $\text{Co}/\text{Al}_2\text{O}_3$ effect is characterized by using temperature programmed surface reaction (TPRS) and diffuse reflectance spectroscopy (DRS). Nb promoter has an influence on CO hydrogenation selectivity [6].

For Mg promoted $\text{Co}/\text{Al}_2\text{O}_3$ system there is a decrease in the formation of metallic cobalt surface phase, while the formation of MgO-CoO is characterized by XPS. The small quantity consumption of Mg results in increased catalytic activity. When Mg quantity is increased, reducibility of catalyst decreases because of MgO-CoO mixed phase formation[6].

The catalytic performance of alumina supported Co can be increased by using the Zirconium promoter. Catalytic activity improves by providing increased production of intermediate product that is $(-\text{CH}_2-)$, which results in increased selectivity to long chain hydrocarbons. Zirconium has an increasing effect on cobalt reducibility and catalytic activity [35-40].

Lanthanum can be used as a promoter for supported Co catalysts to increase CO adsorption with reference to the unpromoted catalyst. $\gamma\text{-Al}_2\text{O}_3$ supported Co catalyst catalytic activity and selectivity can be enhanced by using La promoter [38].

Although it increases catalytic lifetime and activity, it leads to a change in the chemical structure support material [41]. Reactor operating conditions can be important parameters for La promoted catalyst [42].

Many transition metal oxides took place in Co-based catalyst as potential promoter. Although transition metal oxide promoters are considered as electronic promoters, they also illustrate synergistic and structural promotion effects [4].

Transition metal oxide promoters tend to disperse on the Co surface. The spread promoter causes a change in features of active adsorption sites on Co surface.

Table 2.1. Promoter Analysis on Co-Based Fischer-Tropsch Synthesis Source Adapted from [34] promoter effects on Co-based Fischer-Tropsch Synthesis

Effect Types	Elements	Tasks	Activity	Selectivity	Stability
Structural	Mg. Si. Zr. Nb. Rh. La. Ta. Re. Pt	Support stabilization	X		X
	B. Mg. Zr	Co gluing	X		X
	Ti. Cr. Mn. Zr. Mo. Ru. Rh. Pd. Ce. Re. Ir. Pt. Th	Co dispersion increase	X		X
Electronic	B. Mg. K. Ti. V. Cr. Mn. Zr. Mo. La. Ce. Gd. Th	Decorating Co surface	X	X	X
	Ni. Cu. Ru. Pd. Ir. Pt. Th	Co alloying	X	X	X
Synergistic	B. Mn. Cu. Ce	Water shift	X	X	
	Pt*	Hydrogenation/ Dehydrogenation		X	
	Ni. Zr. Gd	Coke burning			X
	B. Mn. Zn. Zr. Mo	H ₂ S resistance			X
Note*: Apart from Pt as a (de-)hydrogenation element. other metals and metal oxides can be used for this reaction.					

TiO₂ supported Co catalysts have higher catalytic activity than alumina, silica, magnesia supported Co catalysts. There is a strong metal strong support interaction between TiO₂ and Co catalyst.

The electronic promotion effect can be expressed with the help of the strong metal support interactions (SMSI). V, Ce and Mg oxides have an effect to increase the activity of Co catalyst. When these metal oxide promoters are used for a Co-based catalyst, product selectivity towards long chain hydrocarbons is increased. Similar results are found for Cr promoted Co/ZSM-5 catalyst. Catalytic activity and long-chain hydrocarbon production are increased by using Cr promoter for the system. Two important results are obtained by analyzing the interaction between metal oxides and cobalt oxides. These results are improvement of Co dispersion and inhibition of Co reduction. CO and H₂ chemisorption, TPD and TPR results have an important role to interpret these. Although the bond between CO and Co strengthens, the Co-H bond weakens. Hydrogenation reaction rate lowers for Cr promoted Fischer-Tropsch reactions. Cr, Ti, Mn, and Mo promoter effects are investigated for Fischer-Tropsch reaction. Catalytic activity and long-chain hydrocarbon product selectivity increase are found for these promoters. Besides, decreases in Co particle size are found as a result of structural promoter effect [4].

CO dissociation at interface region that was between metal oxide promoter and active catalyst metal surface is facilitated. Inactive mixed oxides are formed from promoter and support material which have resistance against carbon deposition. The use of metal oxide promoters results in increased CO conversion, C₅₊ selectivity, olefin/paraffin ratio [9, 43, 44].

Co reducibility can be increased with the addition of the CeO₂ promoter. Product selectivity to long chain hydrocarbons is also found to increase when CeO₂ is used as a promoter in alumina or silica supported Co catalytic systems [45, 46].

H₂ and CO have an affinity against ceria covered surface [47]. Besides, there is a decreasing effect on the formation rate of CO₂, CH₄, and C₂-C₄ [48].

2.2. MnO Promotion Effects on Co-catalyzed FTS

There are various experimental and a limited number of theoretical studies that investigate Mn promotion effects on adsorption energy, activation barrier, product selectivity, vibrational frequencies on Co catalyst surface [7, 47, 62, 53, 6, 63, 64].

Co/Mn ratio, location of Mn promoter on active metal surface, vibrational frequency changes, desorption temperature can be found by using spectroscopic techniques [21, 49-62, 65]. Theoretical studies allow to explore in detail about catalyst structure, adsorption energies, reactivity, vibrational frequencies, activation barrier, electronic structure of the surface, product selectivity [6, 66]. The function of MnO has not been understood completely yet.

In the following paragraphs, the general findings from the literature are summarized. Some studies focused on MnO location and MnO promotion effects on CO adsorption energy and CO dissociation barrier on Co catalyst [42, 47].

EXAFS results showed that MnO is a highly dispersed on cobalt catalyst surfaces. Highly dispersed metal oxide promoters cannot be characterized by X-Ray Diffraction (XRD).

The interaction of the promoter with neighbors and its oxidation state can be found with the help of X-Ray Absorption Spectroscopy (XAS). When MnO is adjacent to Co, catalytic activity increases [42, 47, 64, 65, 6]. Metal-metal oxide interfaces increase higher hydrocarbon (C₅₊) selectivity and decrease methane selectivity compared to unpromoted Co catalyst [44].

In order, for the promotion effects to be observed, species must be bound in the close vicinity of the promoter. When species are not located at these interfaces, promotion effects are not observed. There is a cooperative interaction between MnO, and CO adsorbate. Mn tends to the O atom in CO molecule, as it has a Lewis acid character. Knowledge of oxidation state is crucial to predict Lewis acidity. The location and crystal structure are considered for determination of Lewis acidity of oxide promoters [42, 46].

Mn/Co and Mn/Ti ratio. The maximum C₅₊ selectivity is found when Co/Mn ratio is 0.1. When Co/Mn ratio is bigger than 0.1, product selectivity does not change [67]. Results show that promoter facilitates C-O bond cleavage.

When Mn/Co ratio is less than 0.1, although product selectivity decreases for CH₄, C₅₊ selectivity increases [67]. CO dissociation rate increases [42].

Based on the TEM and H₂ chemisorption measurements, Mn promotion was found to increase [6], decrease [21] and have no effect [65] on the particle size of cobalt crystallites. These studies show the importance of the support used and the complexity of separating promotion and support effects. Most research shows that turnover frequency is not associated with above 6-10 nm particle sized Co based FTS [42], so whether the effects observed are due to promotion or particle size are not clear.

Table 2.2. Mn promotion effect on unsupported Co catalysts [6]

	Authors	Topic of Study	Main Results
Unsupported Co Catalyst	Van der Riet et al. [49].	CO hydrogenation on Mn-Co catalyst	High selectivity to C ₃ products
	Hutchings et al. [50].	CO hydrogenation on Mn-Co catalyst	CH ₄ production yield is lowered. Coupling reactions occur between electrophilic and nucleophilic C ₁ surface intermediates (In situ XRD).
	Liang et al. [51].	Oxidized Co-Mn catalysts preparation methods Co/Mn ratio effect on CO hydrogenation	Different Co/Mn ratio causes different spinel structures.
	Jiang et al. [52].	Mn effects on surface properties	Mn increases catalytic activity and stability. These effects are related to the fact that Co-Mn catalyst has a bigger particle size than Co catalyst. Mn promotion also increases catalyst stability and tolerance against H ₂ S (In situ IR)
	Riedel et al. [55].	Water gas shift activity	The removal of CO ₂ occurs when MnO takes place in Co-based Fischer-Tropsch catalysts. MnO is a water gas shift promoter.

There is a strong connection between the promoter quantity and the spatial association between the promoter and Co catalyst [67]. XPS is used to obtain information about the

TPR shows that CO adsorption temperature increases for Mn promoted Co catalyst supported and MnO promoted Co catalyst reduction take a longer time [42]. Previous experimental studies showed that CO adsorption energy increases on MnO promoted Co surface [42]. IR results signifies that Mn promoter weakens carbonyl bond. Lewis acid-base interaction facilitates bond cleavage for CO [42].

At low pressures (1 atm) conditions, MnO promoted Co surface has high CO adsorption constant and rate constant, resulting in the increase of CO surface coverage. At higher pressures (10 atm), CO adsorption constant is higher than low pressured medium. Surface is saturated nearly with CO adsorbates. At these pressures, MnO promotion may lead to the decrease in activity and/or selectivity [47, 65].

When pressure increases, product selectivity is towards higher hydrocarbons production for Co based FTS. Pressure is optimized above 5 bar for Mn promoted Co, CH₄ production decreases and C₅₊ selectivity increases [53]. Turnover frequency is increased as a result of pressure increase. MnO promoted Co catalyst has two times higher turnover frequency compared to unpromoted Co catalyst [44].

Early pioneering experimental studies about the effect of Mn promotion on cobalt FTS catalysts came from Morales et al. [6]. and Bezemer et al. [47].

Morales et al. [6]. investigated TiO₂ supported Mn promoted cobalt catalysts by XAS, TEM, XRD and TPR measurements to reveal interactions between preparation method, structure and performance. They found that Mn is present in the MnO₂ form for the passivated and MnO form for the reduced catalyst. MnO reduces cobalt reducibility. Mn promotion resulted in the formation of larger particle sizes for cobalt crystallites.

Manganese was also found as an alloy with cobalt, in the form of rock salt solid solution, in the calcined form. For large (>5 nm crystallites), MnO decreased CH₄ selectivity, increased hydrogenation activity (based on TOF measurements) and improved catalyst stability.

Bezemer et al. [47]. investigated Mn promotion effects on carbon nano fiber (CNF) supported cobalt catalysts using XPS, STEM-EELS and kinetic measurements. MnO effects were already studied on Co catalysts supported on oxidic materials, which complicated the analysis of cobalt reduction.

In this study, effects were studied on CNF supported (inert) cobalt catalysts, with the purpose of evaluating the effect of MnO on cobalt reducibility.

XPS and STEM-EELS indicated that MnO is closely associated with cobalt. Using TPR and H₂ chemisorption, they found that MnO reduces cobalt reduction degree.

XPS and STEM-EELS indicated that MnO is closely associated with cobalt. Using TPR and H₂ chemisorption, they found that MnO reduces cobalt reduction degree. They found that TOF increases 20% for 1 bar, while it increases 130% at 20 bar. This was explained by severe conditions at high pressure, resulting in the possible creation of active sites. For selectivity, they observed increase for 1 bar, while they observed decrease in 20 bar. At 1 bar, increase was attributed to the decrease in H₂ coverage (due to increase in CO coverage). For 20 bar, the catalyst was already operating at high CO coverage, resulting in overpromotion with MnO and therefore decreased selectivity. They concluded that the main function of MnO was the moderation of hydrogenation reactions. Morales et al. [63]. later investigated effects of MnO promotion for TiO₂ supported catalysts on CO and H₂ adsorption using in situ DRIFTS, focusing on the electronic promotion effect of MnO.

The structural characterization performed by XRD, TPR, TEM and H₂-chemisorption confirmed their previous results that MnO hampered cobalt reducibility. However, this time the association of MnO with cobalt resulted in decrease of the cobalt particle sizes from 24 nm to 11-14 nm. However, this can be also due to the loss of crystallinity of CO₃O₄ particles. They also observed that MnO is also found dispersed on the TiO₂ support. They also proposed that the support itself may be responsible for the decreased reducibility of cobalt, comparing their results with CNF supported cobalt [21]. Based on DRIFTS results using CO as a probe, they pointed three conclusions: MnO decreases CO adsorption capacity at high loadings. MnO results in disappearance of bridge bonded CO. This was proposed to be due to the Lewis acid character of MnO, withdrawing electron density from cobalt surface, and resulting in decrease of bridge bonded CO. MnO results in a change of intensity of linearly bonded CO at 2030 and 2050, however no blue shift is observed. More CO is located at 2030 cm peak. This may be due to a weakening of CO bond at high MnO loadings.

The selectivity continues to increase with MnO loading, while activity increases slightly for initial small MnO loadings, while it decreases after some optimum value.

Table 2.3. Mn promotion effect on supported Co catalysts [6]

Supported Co catalyst	Authors	Topic	Investigation
	Das et al. [56, 57].	Lower hydrocarbon synthesis on Co and Co-Mn catalysts (Silica supported)	Mn promoted supported Co catalyst has a decreasing effect on reduction temperature for Co_3O_4 . Water gas shift activity decreases. Product selectivity is maximized $\text{C}_2\text{-C}_4$ hydrocarbons. while catalytic activity increases.
	Zhang et al. [58].	Mn promotion effects on selectivity (Alumina supported)	Mn promoted Co catalyst has lower hydrogenation features than bare Co catalyst. Product distribution is toward more olefinic. C_{5+} selectivity increases. Co active phase dispersion increases.
	Klabunde et al. [59].	Characterization (Silica supported)	Although Mn takes place in oxidized state. Co is partially oxidized state. EXAFS results indicate that Mn is an oxyphilic metal and Mn shows electronic promotion effect on Co catalyst.
	Voß et al. [60].	Mn promotion effects on titania supported Co	XPS results show that Mn located more on support than Co active metal. MnO is reduced form of Mn and it serves as a support material.
	Martinez et al. [61].	Mn promotion effects on Co/SBA-15 catalyst	Mn promoter increases production of C_{10+} . Methane selectivity decreases. Although the activity is found to decrease for promoted system.

cont. on next page

Table 2.3. (cont.)

		Authors	Investigation
Supported Co catalyst	Bezemer et al. [47].	MnO promotion effect on carbon nanofiber-supported Co catalyst for FTS	Pressure increase leads to enhance C ₅₊ product selectivity . MnO locates near site of Co nanoparticles. There is not an interference between support material and MnO promoter.
	Johnson et al. [8].	MnO promotion effect on activity and selectivity of Co/SiO ₂ for FTS	MnO takes place at the edge Co nanoparticles. There is a Lewis acid-base interaction between Mn ⁺² and O in CO molecule. Coadsorption and dissociation are done by using MnO promoter. The C-O bond scission is facilitated.
	den Breejen et al. [21].	MnO promotion effect on activity and selectivity for Co based silica supported FTS	Experiments show that there is a relation between surface coverages of CH _x intermediate on Co surface and C ₅₊ selectivity.
	Dinse et al. [62].	Mn promotion effect on activity and selectivity for co based silica supported FTS	Experimental conditions and Mn amount effect on FTS activity and selectivity

Under FTS conditions, they observed a blue shift of CO peak from 2012 to 2031 cm, concluding C---O bond is strengthened. They also observed carbonate peaks at 1570 and 1330 cm, with increasing MnO content, indicating CO₂ is formed on the surface and water gas-shift reaction is catalyzed.

They also observed a selectivity increase for olefinic products compared to paraffinic products, concluding that this may be due to the decreased likelihood of hydrogenation reactions in FTS [63].

den Breejen et al. [21]. investigated MnO promotion effects on SiO₂ supported catalysts using STEM-EELS, IR and SSITKA. A relation between C₅₊ selectivity and CH_x coverages were established. A decrease in particle size of cobalt crystallites were found as a result of MnO promotion. MnO is found to be homogeneously well dispersed on the surface of both cobalt and silica. MnO promotion decreased the reducibility of NO calcined catalysts from 94 to 62% while no change in reducibility could be detected for air calcined catalysts (94%) using XANES analysis.

For the NC reduced catalyst, both activity and selectivity increased as a result of MnO promotion, while for AC reduced catalyst activity decreased. For smaller particles ($4\text{nm} <$) obtained by NC method, the activity increase may be due to the different cobalt surface structure or particle shape (possibly inducing of more defective surface facets by MnO).

IR spectroscopy indicated that MnO promotion resulted in lower coverage of CO, possibly due to blocking of surface by MnO. Next to a peak at 2057 cm^{-1} , a second peak is observed at 2012 cm^{-1} , attributed to CO adsorbed on undercoordinated sites. This is explained by creating of undercoordinated sites due to MnO promotion.

SSITKA results showed that CO coverage and residence time were decreased while CH_x coverage and residence time increased. Also, higher TOF was found for MnO promoted catalysts, which indicates MnO promotes activity. In conclusion, the selectivity increase due to MnO promotion was attributed to higher CH_x coverage and the resulting higher probability of coupling reactions. The promotion of activity was not explained in detail [21].

Dinse et al. [62].investigated MnO promotion effects in SiO_2 supported catalysts, focusing on the changes in activity and selectivity.

Based on their H_2 uptake results, they concluded that MnO promotion slightly decreased cobalt crystallite size and reducibility of cobalt particles. MnO was found to be highly dispersed on the cobalt surfaces.

In terms of selectivity, they found that MnO promotion increases the selectivity to C_{5+} and olefins, while decreasing the selectivity to C_1 , $\text{C}_2\text{-C}_4$ and paraffins. They proposed increased CO coverage and decreased H coverage, as the main reason for increased selectivity to C_{5+} , due to MnO promotion.

Similar to the results of Bezemer et al., they found conflicting effects of MnO on activity for operation under 1 atm and 10 atm.

MnO promotion resulted in slight increase in activity for 1atm.For 10 atm operation, MnO loading decreased activity significantly.

The loss of activity was attributed to the blockage of active cobalt sites by MnO and the fact that MnO also reduces the number of metallic cobalt sites, which were assumed to be the only active form of cobalt for FTS. The loss of activity may be also due to the decrease in particle sizes.

Johnson et al. [65]. performed a detailed investigation related to the effects of Mn promotion on activity and selectivity of FTS, using a combination of experimental techniques on SiO₂ supported cobalt catalysts. In particular, they investigated how Mn interacts with CO and how this interaction effects activity and selectivity.

Their STEM-EDS measurements revealed that Mn preferentially accumulates on the surface of Co nanoparticles up to loadings of Mn/Co > 0.1. After this loading, MnO starts to appear on the surface of SiO₂ support, in the form of nanometer scale particles. Mn is found highly dispersed on cobalt nanoparticles and found in the chemical form of MnO (Mn is found to have an oxidation state of +2). Also, they did not observe a change in cobalt particle size due to MnO promotion, in contrast to the previous experimental studies [6, 47].

Based on kinetic analysis they concluded that MnO increases the CO adsorption constant and the and the apparent rate constant for FTS. In-situ IR revealed that MnO promotion increases the abundance of CO with weakened carbonyl bonds. It is proposed that CO cleavage is facilitated by Lewis acid-base interactions between Mn²⁺ cations located at the edge of MnO islands covering cobalt surfaces and the O atom of CO atom. The observed decrease in selectivity to CH₄ and the increased selectivity to C₅₊ products with increasing Mn/Co ratio are attributed to a decrease in the ratio of adsorbed H to CO on the surface of the supported Co nanoparticles.

Despite numerous experimental studies that investigated the MnO promotion effects on cobalt catalysts, only two theoretical studies, one MSc thesis [34] and one article [66], appeared in the last two years.

van Doorslaer [34] studied the nature of the promoter under reaction conditions and the effect of Mn promotion on the kinetics of CO and H₂O dissociation by studying the adsorption energies of CO, OH, H and H₂O. Based on experimental and DFT based phase diagrams, MnO was predicted to be the chemical state of the promoter in agreement with previous experimental studies.

Six MnO ring model was proposed as the most stable occurrence of MnO promoter. In this model Mn locates on bridge position and oxygen atoms locates on top position. On the stepped Co(211) surface, one MnO (monomer) model located on the step edge was found as the most stable model, as shown in Figure 2.1.

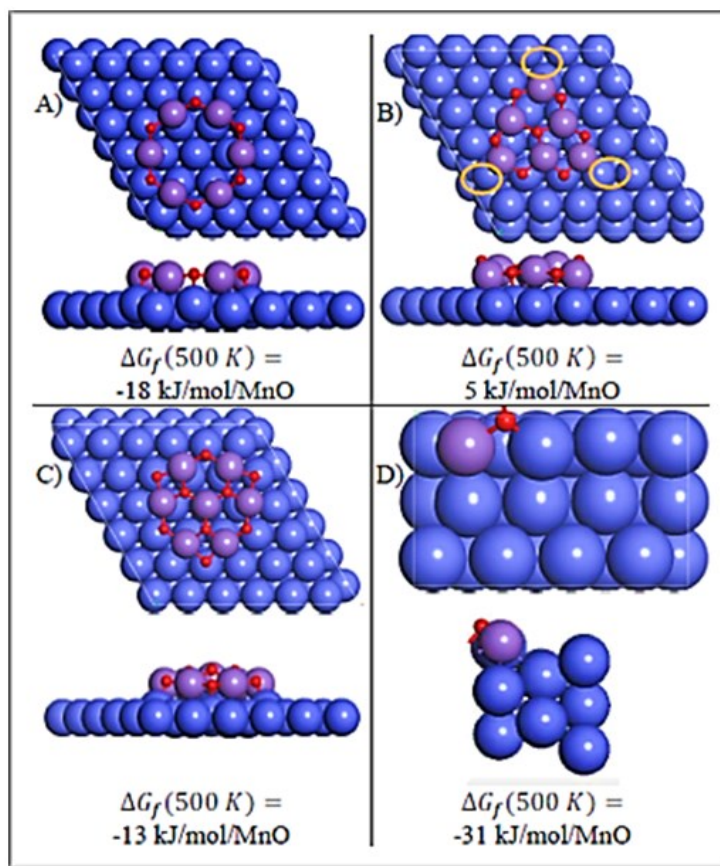


Figure 2.1. Different MnO promoter models on Co Catalyst [34]

CO, H, OH and H₂O adsorption energies were studied on six MnO ring model on Co(111) surface and one MnO (monomer model) on Co(211) surface. On the Co(111) surface, CO adsorption energy has the least MnO promotion effect among other species. CO adsorption energy decreases from -133 kJ/mol to -130 kJ/mol. H adsorption energy also decreased from -273 kJ/mol to -252 kJ/mol. OH adsorption energy decreases from -338 kJ/mol to -321 kJ/mol. Otherwise, H₂O adsorption energies increased from -27 kJ/mol to -53 kJ/mol [34]. H and OH adsorption on Co(111) surface cause the deformation of six MnO ring model. H₂O is found to be adsorbed on MnO promoter [34].

On the MnO promoted stepped Co(211) surface, there was an increase for CO, H, OH adsorption energies. CO adsorption energy increased from -137 kJ/mol to -155 kJ/mol. H adsorption energy enhanced from -263 kJ/mol to -281 kJ/mol. There was an increase from -360 kJ/mol to -397 kJ/mol for OH adsorption energy. However, H₂O adsorption energy decreased from -68 kJ/mol to -62 kJ/mol [34]. The change in adsorption energies are shown in Table 2.4.

Table 2.4. MnO Promotion Effects on Adsorption Energies, kJ/mol [34]

Adsorbed Species	Electronic Adsorption Energy [kJ/mol]			
	Unpromoted		Promoted	
	Co(111)	Co(211)	Co(111)	Co(211)
CO	-133	-137	-130	-155
H	-273	-263	-252	-281
OH	-338	-360	-321	-397
H₂O	-27	-68	-53	-62

Pedersen et al. [66] investigated MnO promotion effects in a combined experimental and theoretical study.

In the experimental part, Mn promoted Co/Al₂O₃ catalysts are prepared, characterised and tested at industrially relevant FTS conditions favouring light olefin formation.

The effect of preparation procedure, i.e. co-impregnation vs. sequential impregnation, is investigated as well as the order of component addition. Compared to the Co catalyst, the Mn promoted catalysts displayed a larger intrinsic activity, larger selectivity to light olefins and C₅₊ species, whereas the selectivity to CH₄ was considerably lower.

Mn was found to be closely associated with Co, and a surface enrichment of Mn was observed during the course of operation.

DFT calculations were performed to obtain adsorption energies surface species as well as the activation barriers for elementary reactions of direct CO dissociation and methane formation. The authors obtained their results on two models: a model of metallic Mn completely covering the fcc Co(111) surface and a model where the 2nd surface layer in a Co(111) slab is replaced with a metallic Mn layer [66].

When two models were analyzed, CH₄ adsorption energy decreases and there were increases for O, H, C, CO, OH, CH, CH₂, CH₄ adsorption energies. These energy values were in Table 2.5.

The authors point out that their DFT results indicate that the adsorption energies of all surface species (CO, H, C, O, CH_x (0<x<4)) except CH₄ for both of their models.

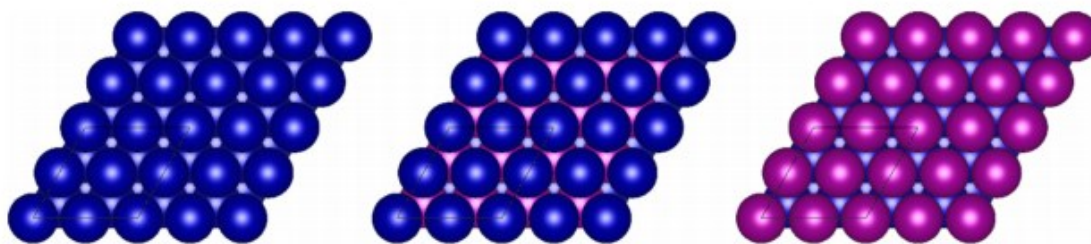


Figure 2.2. Mn promoted Co models [66]

For the activation barriers, CO dissociation was found to have a lowered activation barrier for both models, while the hydrogenation reactions to form methane was lowered for the Mn terminated model and increased for the cobalt terminated model. Based on these results the authors postulated that the increased selectivity to C_{5+} may be due to increased coverage of olefin precursors, such as CH_2 , while the increased activity may be due to the lowered activation barrier for direct CO dissociation [66]. The activation barriers for direct CO dissociation based on two models are shown in Figure 2.3.

Table 2.5. Two Different Mn Promotion Models Effect on Adsorption Energies, eV [68]

Species surface	E_{ads} , [eV]			Literature values
	Co (111)	Co/Mn/Co (111)	Mn/Co (111)	
CO	-1.76	-2.13	-2.55	-1.61 [68], -1.88 [69], -1.66 [70], -1.43 [71]
C	-6.95	-7.43	-8.15	-6.80 [68], -6.71 [69], -6.46 [70], -6.54 [23], -6.62 [72] -7.09 [73]
O	-5.73	-6.19	-7.27	-5.61 [68], -5.43 [69], -5.34 [70], -5.42 [74]
H	-2.84	-3.25	-3.75	-2.88 [69], -2.72 [70], -2.94 [72], -2.85 [74]
CH	-6.42	-6.83	-7.55	-6.31 [69], -6.54 [23], -5.99 [72]
CH₂	-4.02	-4.54	-5.44	-3.86 [69], -3.86 [23], -3.85 [72]
CH₃	-1.93	-2.38	-3.03	-2.00 [23], -1.89 [72]
CH₄	-0.02	-0.02	-0.02	

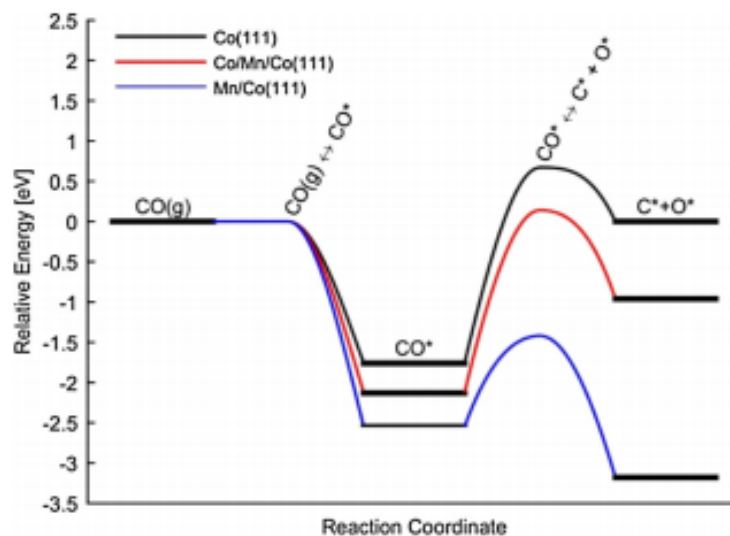


Figure 2.3. Mn Promoter Effect on CO Activation Barrier [66]

However, based on various experimental studies (including their own study), Mn promoter is found to be located on the surface of cobalt crystallites in the form of highly dispersed MnO, instead of the metallic Mn substitution model used in this study. This makes the validity of the results highly questionable, which can also be seen in conflicting change of activation barriers on metallic Mn promoted surfaces for carbon hydrogenation in their two different models.

2.3. MnO promoter model on Co-Catalysts

There is a consensus in the literature that Mn is found mainly in the +2-oxidation state (in the form of MnO), highly dispersed and in direct contact with the active cobalt surfaces [65, 47, 63, 21].

It is also stressed in these studies that MnO is found in the form of very small nanoparticles, or isolated patches of MnO either covering or in direct contact with cobalt surfaces.

Yang et al. [75] investigated the conversion of syngas to higher oxygenates on MnO promoted Rh surfaces by a combined experimental and computational approach using TEM, FTIR measurements and DFT modelling. Based on their experimental results, they have concluded that MnO is highly dispersed on Rh surfaces.

In the computational literature, Yang et al. [75] applied a relevant model based on MnO covering Rh surfaces.

For the DFT modelling, they obtained energy barriers for the syngas conversion mechanism on the “MnO monomer” model, illustrated in Figure 2.7a, which were consistent with their experimental findings.

As bigger aggregates of MnO clusters on Rh surfaces cannot be ruled out experimentally, they have also tested their DFT results on a “MnO stripe” model, shown in Figure 2.7b. As the results were consistent for both models, they concluded that the “MnO monomer” model is a realistic representation for highly dispersed MnO on Rh surfaces.

Based on these findings, we have also employed a “MnO monomer” model in the calculations performed in this study.

In Figure 2.7. different MnO promoter models on a Rh (111) surface is shown [75]. These models are monomer model and stripe model.

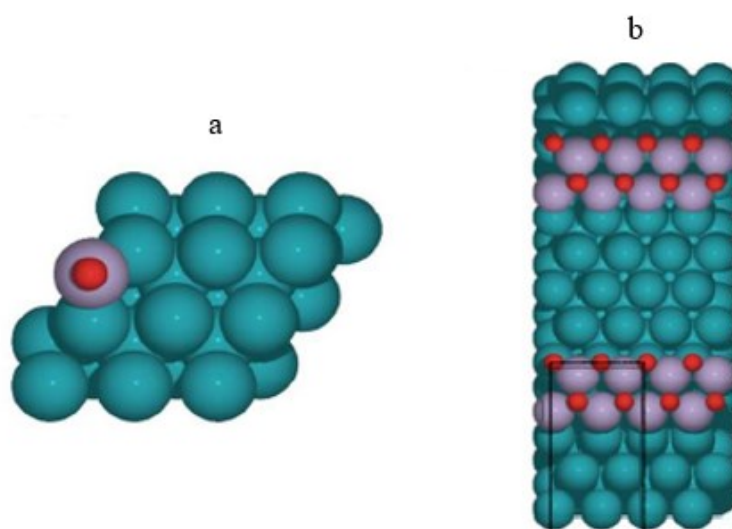


Figure 2.7. MnO promoter model on Rh (111) a.Monomer model, b.Stripe model. [75]

CHAPTER 3

COMPUTATIONAL METHODOLOGY

3. SUMMARY OF COMPUTATIONAL METHODS

In this study, Vienna Ab-Initio Simulation Package (VASP) was used to evaluate spin polarized DFT calculations. The Generalized Gradient Approximation of Perdew, Burke and Ernzerhof (GGA-PBE) was incorporated with the Projector Augmented of Perdew, Burke and Ernzerhof (GGA-PAW) as the exchange-correlation function to resolve the Kohn-Sham equations. The Kohn-Sham orbitals were expanded in a plane wave basis set using a 600-eV kinetic energy cut off, and a 5x5x1 and 3x3x1 Monkhorst-Pack grid of kpoints was used for numerical integration in reciprocal space.

Fermi smearing was used and the convergence criteria for the geometry optimizations were 10^{-6} eV for the total energy and 10^{-2} eV \times A $^{-1}$ for the forces acting on the ions. The conjugate-gradient (CG) method was used for the geometry optimizations. Previous studies have shown that the catalytic properties and reaction energies are affected by the surface orientation, steps and defects and that cobalt particles have shapes exhibiting (111) facets for this study. The cobalt facet was, therefore, used to study the CO, HCO, and CH dissociation and HCO formation. Surfaces were constructed using 2 \times 2 and 3x3-unit cells with five layers, and periodic boundary conditions in two directions to model a semi-infinite crystal surface. The two upper layers were free to relax while the three bottom layers of the slab were fixed to maintain the bulk crystal structure. This surface had 15 A $^{\circ}$ vacuum. This periodic box size, which corresponds to a 1/9 and 1/4 monolayer (ML) coverage when there are one and two adsorbates, respectively, has been widely used in previous investigations of adsorption on transition metal surfaces [29-31] and yields converged results in a computationally tractable time. Transition states were identified using the climbing image–nudged elastic band (CI-NEB) method [33, 76], where the lowest energy reactant and product configurations are selected as the initial and final states.

In NEB calculations, reaction steps were produced with 8 images.

Eight images were placed along the minimum energy path (MEP) and a $5 \text{ eV/\text{Å}^2}$ spring force constant between images was used to relax all the images until the maximum force acting on each atom was less than $0.015 \text{ eV/\text{Å}}$. Although bare surface NEB calculations were accomplished by relaxing the top 2 layer atoms, MnO promoted Co(111) surface had a complicated structure MnO and species atoms were relaxed for MnO promoted surfaces. Calculations using a $0.1 \text{ eV/\text{Å}^{-3}}$ convergence criteria showed that the activation energy differs from that obtained with $0.1 \text{ eV/\text{Å}^{-1}}$ by at most 0.2 meV .

All calculations were accomplished spin polarized and with dipole correction. MnO had antiferromagnetic properties and this feature were set INCAR file. All optimizations were done by using IBRION=2 to found global minimum and maximum points. Vibrational frequency calculations were done by using IBRION=5.

3.1. General

In this project Mn promoter effect is investigated for main Fischer-Tropsch reactants, intermediates and main elementary reactions on flat p (2x2) and p (3x3) Co(111) surfaces. There is a specific calculation order to find adsorption energy:

- Bulk optimization
- Clean surface optimization
- Adsorption energy calculations,
- Coadsorption energy calculations,
- Molecule optimization
- The vibrational frequency for adsorbed surface
- The vibrational frequency for molecule
- NEB calculations
- Transition state calculation
- The vibrational frequency for the transition state
- Frequency analysis

3.1.1. Bulk Optimization

Bulk optimization includes volume relaxation, encut optimization, and kpoint optimization. Volume relaxation is necessary to give information about lattice constant.

Bulk structure lattice constant was calculated as 3.51612766874. Besides, bulk Co has a face-centered cubic structure.

Bulk includes 4 Co atoms. This geometry has an FM-3M space group. $p(2 \times 2)$ and $p(3 \times 3)$ Co(111) surfaces are created by using lattice constant and entering space group. Layer numbers were entered as thickness number when Co(111) surface is created. The vacuum was optimized 15 Å after the surface was formed.

Supercells including $p(2 \times 2)$ and $p(3 \times 3)$ were done. Encut optimization is done to reach maximum cut-off energy. This value must be greater than all of atoms encut energy value. The optimum encut value was calculated at 600 eV. Then, kpoints optimization was done and found as $19 \times 19 \times 19$. Clean surface optimization was done after bulk optimization was completed.

3.1.2. Clean Surface Optimization

In clean surface optimization, kpoints were entered as $5 \times 5 \times 1$. Encut value was entered 600 eV. Co had 27 electrons. When the electron number was odd, the spin-polarized calculation was done. In addition to this, Co magnetic properties were added in input parameters. All atoms in the bare Co surface were relaxed when a clean surface was optimized. If the result reached accuracy, its CONTCAR file was used for adsorption calculations.

3.1.3. Molecule and Atomic Optimization

CO, HCO, CH₂, C₂H₂, H₂O, OH, CH, H, C, and O optimizations were done. For each optimization, all atoms were relaxed. CO included 2 atoms and all of them were relaxed.

3.1.4. Adsorption Energy Calculations

Minimum energy configurations for adsorbates were calculated on an optimized clean surface. Adsorbate structure was important to obtain correct adsorption energy. There were 4 adsorption sites, and these were top, bridge, hcp, fcc. The top site was on Co atom. Bridge position was average 2 Co atoms x, y, z coordinates. Bridge horizontal located line position between 2 Co atoms. The bridge diagonal took place at the corner. Hollow adsorption site was calculated from 3 Co atoms average x, y, z coordinates. There are 2 hollow adsorption sites; hcp and fcc. There was an atom under 3 atoms when there was an hcp hollow site.

In general, molecules are known to preferred top and bridge sites, while atoms are found in hollow sites. Nevertheless, in order to find the experimentally observed adsorption structure and energy, adsorbates must be optimized for each site, and their adsorption energies need to be calculated. Different potential function, kpoint, encut value, vacuum space, the lattice constant, layer number, supercell size was effective to result in different adsorption sites for adsorbates.

A global energy minimum, corresponding to the optimized structure was obtained by using the global minimization scheme in VASP. After accurate results were obtained, CONTCAR files were used to calculate vibrational frequency.

Adsorption Energy Calculation

Bare Surface:

$$E_{ads} = E_{(slab+adsorbate)} - (E_{slab}) - (E_{adsorbate(g)})$$

MnO Promoted Surface:

$$E_{ads} = E_{(MnO\ promoted\ slab+adsorbate)} - (E_{MnO\ promoted\ slab}) - (E_{adsorbate(g)})$$

3.1.5. Coadsorption Energy Calculations

After adsorption energies were obtained, the most stable adsorption site was decided. The smallest energy value was the most stable configuration. Molecule dissociates near the most stable adsorption site. All possible coadsorption calculations were done. For example, CO dissociated produces C and O atoms.

The most stable adsorption site was found as an hcp and fcc sites. Because of this reason, coadsorption possibilities were investigated near the location of the fcc and hcp adsorption site. Coadsorption input parameters were like adsorption input parameters. Both were spin polarized and magnetic properties were considered.

The most stable coadsorption energy was found.

(C+O) coadsorption:

- Bare Surface:

$$E_{(C+O)coadsorption} = E_{(slab+C+O)} - (E_{slab}) - (E_{C(g)}) - (E_{O(g)})$$

- MnO Promoted Surface:

$$E_{(C+O)coadsorption} = E_{(MnO\ pro.\ slab+C+O)} - (E_{MnO\ pro.\ slab}) - (E_{C(g)}) - (E_{O(g)})$$

(CO+H) coadsorption:

- Bare Surface:

$$E_{(CO+H)coadsorption} = E_{(slab+CO+H)} - (E_{slab}) - (E_{CO(g)}) - (E_{H(g)})$$

- MnO Promoted Surface:

$$E_{(CO+H)coadsorption} = E_{(MnO\ pro.\ slab+CO+H)} - (E_{MnO\ pro.\ slab}) - (E_{CO(g)}) - (E_{H(g)})$$

(CH+O) coadsorption:

- Bare Surface:

$$\begin{aligned} E_{(CH+O)coadsorption} \\ = E_{(slab+CO+H)} - (E_{slab}) - (E_{(CH+O)(g)}) - (E_{CH(g)}) - (E_{O(g)}) \end{aligned}$$

- MnO Promoted Surface:

$$\begin{aligned} E_{(CH+O)coadsorption} \\ = E_{(MnO\ pro.\ slab+CH+O)} - (E_{MnO\ pro.\ slab}) - (E_{CH(g)}) - (E_{O(g)}) \end{aligned}$$

(C+H) coadsorption:

- Bare Surface:

$$E_{(C+H)coadsorption} = E_{(slab+C+H)} - E_{(slab)} - E_{C(g)} - E_{H(g)}$$

- MnO Promoted Surface:

$$E_{(C+H)coadsorption} = E_{(MnO\ pro.\ slab+C+H)} - E_{(MnO\ pro.\ slab)} - E_{C(g)} - E_{H(g)}$$

3.1.6. The Vibrational Frequency for Adsorbed Surface and Molecule

The vibrational frequency was calculated for adsorbed surfaces. After vibrational frequency for molecules was calculated to find zero-point correction energy.

There was a frequency calculation for an adsorbed slab that depended on adsorbates degrees of freedom. In the adsorbed slab, only adsorbates were relaxed.

Other atoms were fixed. When molecule vibrational energy was calculated, all the atoms were relaxed. Then, the sum of frequencies was divided the number of frequencies. For example, CO had 2 atoms, and these were C and O. They had vibrational motion in x, y, and z-direction. There were 6 frequencies at the end of the vibration calculation. The 6 frequency Zero-point vibrational energy formula required that result must be divided 2. Then, the unit must be converted to meV to eV.

Corrected energy

- Bare Surface:

$$E_{corrected\ energy} = (E_{(slab+ads.)} + E_{ZPE}) - (E_{slab}) - (E_{ads.(g)})$$

- MnO Promoted Surface:

$$E_{corrected\ energy}$$

$$= (E_{(MnO\ pro.\ slab+ads.)} + E_{ZPE}) - (E_{MnO\ pro.\ slab}) - (E_{ads.(g)})$$

3.1.7. Nudged Elastic Band (NEB) Calculations

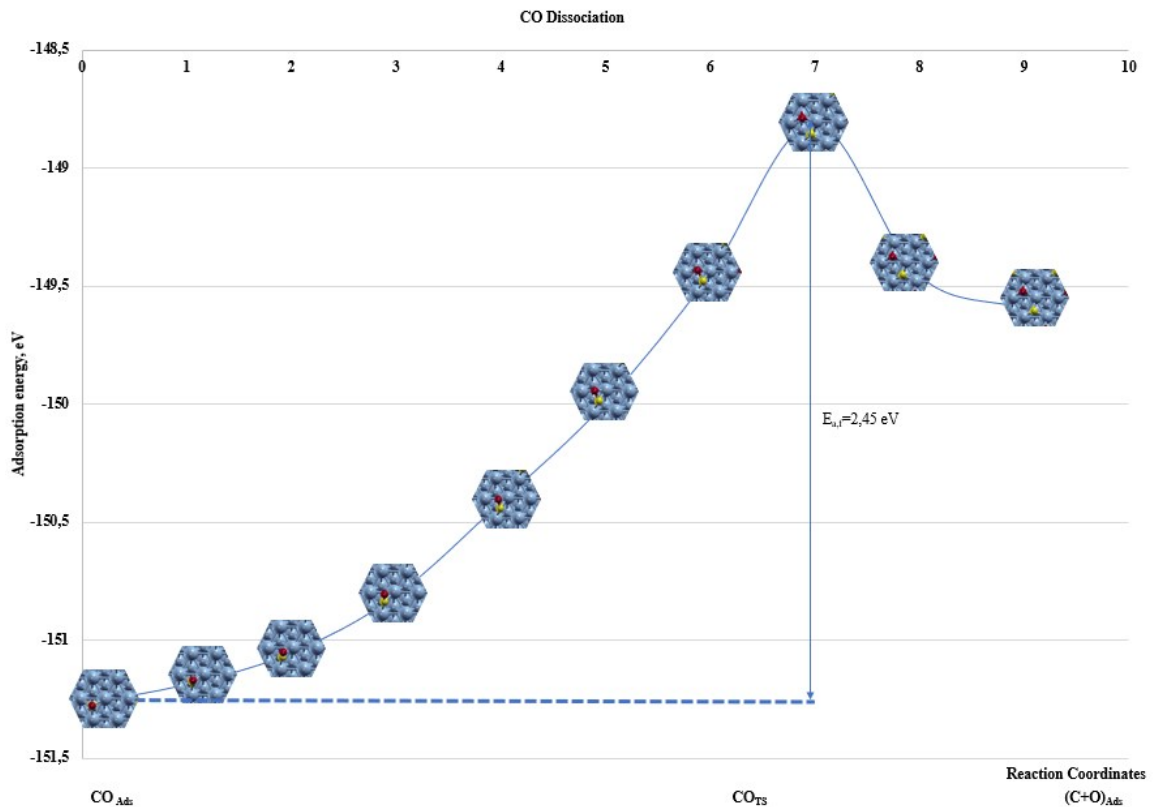


Figure 3.1. NEB Calculation for CO Dissociation on 0.25 ML Co (111) Surface

The most stable adsorption site specified initial state and the most stable coadsorption site was the final state. Molecule dissociated atoms on the active catalyst surface.

Minimum energy path required from the initial state to the final state. This was called a climbed nudge elastic band. Molecule dissociation was visualized before CI-NEB calculation. Neb video was helpful to decide the logical dissociation path. When dissociation reaction occurred step by step, neb calculation was done.

After 100 electronic steps passed, adsorption energy versus the dissociation reaction pathway was drawn. The volcano curve was needed to detect the transition state.

The peak of the volcano curve was the transition state candidate. In addition to this information, one more neb calculation may be required to reach the transition state candidate. The narrow range can be calculated two times neb.

After NEB calculation, the CONTCAR movie was reoccurred from CONTCAR files. CONTCAR movies must be continuous to understand the correct step for the transition state.

3.1.8. Transition State Calculation

The highest energy geometry coming out of the NEB calculations is also the highest energy point in the volcano curve for the reaction potential energy diagram. This geometry is taken as the input for transition state calculations and further optimized. When the optimization reaches the required accuracy, a vibrational frequency analysis must be performed to verify the transition state. If the correct transition state structure is optimized, the frequency analysis must yield a singular imaginary frequency.

3.1.9. MnO Promoter Model

The monomer MnO model was calculated at different adsorption sites. MnO had antiferromagnetic properties. This model was also calculated spin polarized.

The most stable MnO monomer model was detected hcp MnO monomer model. Adsorption and coadsorption energy were calculated on MnO promoted monomer model.

Different adsorption sites that occurred in MnO promoted the monomer model. MnO location was effective to specify adsorption sites. Different adsorption energies were obtained depending on the MnO neighbor number.

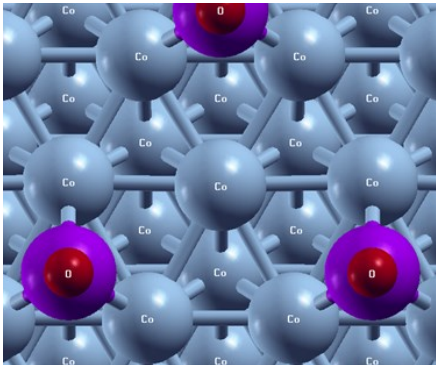
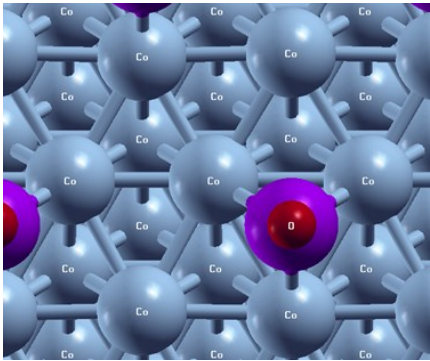
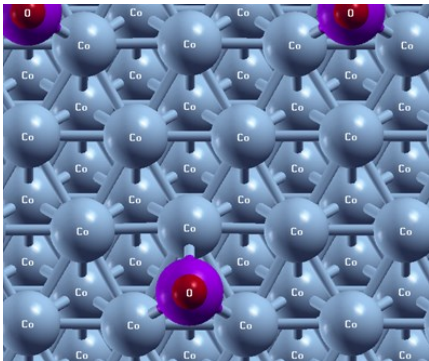
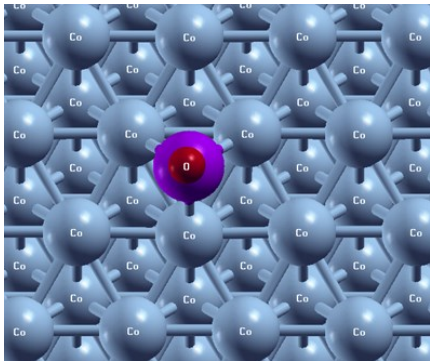
MnO promoted Co adsorbed slab and molecular vibrational frequency, neb, transition state and vibrational analysis for transition state analysis were done. They were like bare Co calculations.

CHAPTER 4

RESULTS

4.1. Structural Model for MnO promoted Co(111) Surface

Table 4.1. MnO Monomer Model (0.25 ML coverage) on Co(111) (a) fcc model and (b) hcp model

0.25 ML HCP MnO Monomer Model	0.25 ML FCC MnO Monomer Model
 <p data-bbox="432 1252 592 1285">-235 kJ/mol</p>	 <p data-bbox="1059 1252 1219 1285">-226 kJ/mol</p>
0.11 ML HCP MnO Monomer Model	0.11 ML FCC MnO Monomer Model
 <p data-bbox="432 1865 592 1899">-254 kJ/mol</p>	 <p data-bbox="1059 1865 1219 1899">-248 kJ/mol</p>

In this study, monomer model was studied to investigate the MnO promotion effect on Co catalyst $p(2 \times 2)$ [periodic structure corresponding to one MnO monomer for 4 cobalt atoms, resulting in 0.25 ML MnO coverage], and $p(3 \times 3)$ [periodic structure corresponding to one MnO monomer for 9 cobalt atoms, resulting in 0.11 ML MnO coverage] models of promoted Co(111) surfaces where studied to investigate how MnO coverage effects the adsorption energies of surface species.

MnO was adsorbed top, bridge, hcp and fcc on clean Co surface for 0.25 ML and 0.11 ML surface models. At the end of the calculation, top and bridge site MnO on the Co surface shifted to the hcp site. There were fcc and hcp MnO monomer model in this research. HCP MnO monomer model was the most stable adsorption site both 0.25 ML and 0.11 ML bare Co surface.

There were 4 adsorption sites for bare 0.25 ML and 0.11 ML bare Co(111) surfaces.

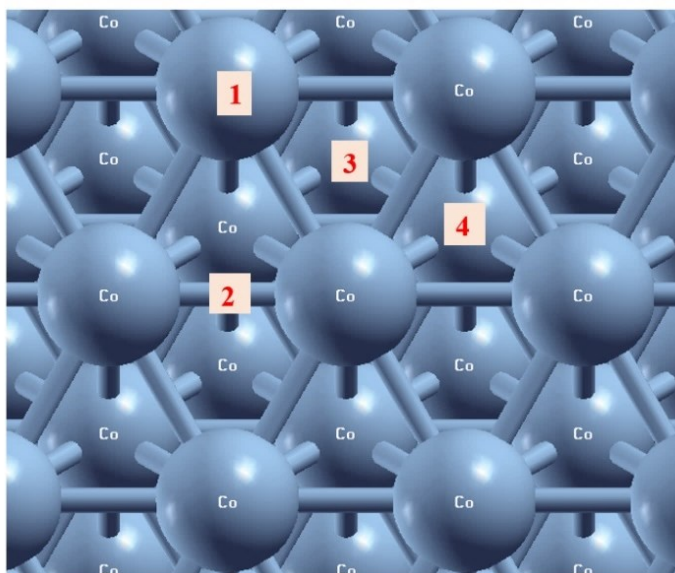


Figure 4.1. Adsorption sites for bare Co(111) surface

Figure 4.1. illustrated the adsorption sites for these two different coverages. Numbers signified adsorption sites. The top site was 1, the bridge site was 2, the fcc site was 3 and the hcp site was 4.

There were 8 adsorption sites for hcp and fcc MnO monomer models for 0.25 ML Co(111) surface. There were 2 top adsorption sites for these two models. One of the top sites was neighbor of MnO (1) and the other had farther distance from MnO (2).

2 different kinds of bridge sites took place for these models as 1 MnO neighbored (3) and 2 MnO neighbored (4) bridges.

Hcp and fcc adsorption sites number differ from hcp and fcc MnO monomer models. In the hcp model, 1 MnO neighbored (8) and 2 MnO neighbored (7) hcp sites were formed.

1 MnO neighbored fcc (5) and 3 MnO neighbored fcc (6) sites were observed for hcp MnO monomer models. Otherwise, in fcc MnO monomer models 2 MnO neighbored fcc (5) and 1 MnO neighbored fcc (8) sites.

Apart from these, there were 2 kinds of hcp sites including 1 MnO neighbored hcp (6) and 3 MnO neighbored hcp (7) sites.

The number of MnO neighbor affected adsorption energies, due to the MnO promotion effect.

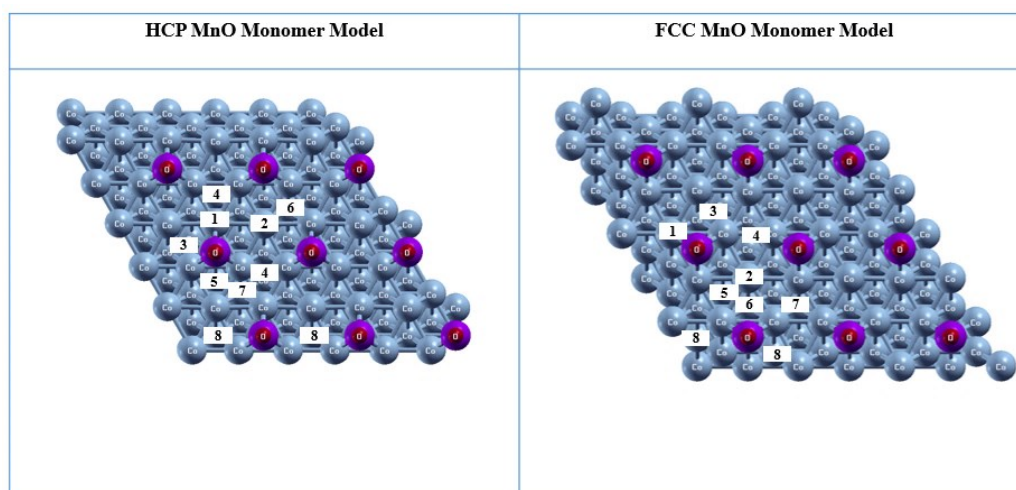


Figure 4.2. 0.25 ML hcp and fcc MnO adsorption sites

MnO monomer promoter models had different adsorption sites where some adsorption sites were close to MnO and others were far away from MnO promoters, as shown in Figure 4.2.

For this 0.11 ML MnO covered, p(3x3) model, only the closest region of MnO was investigated, including MnO neighbored top (1), bridge (2), fcc (3), and hcp(4) sites.

Hcp and fcc MnO monomer models were again calculated for this coverage to evaluate the most stable MnO monomer model.

0.11ML MnO promoted p(3x3) Co(111) surface model and the investigated adsorption sites are shown in Figure 4.3.

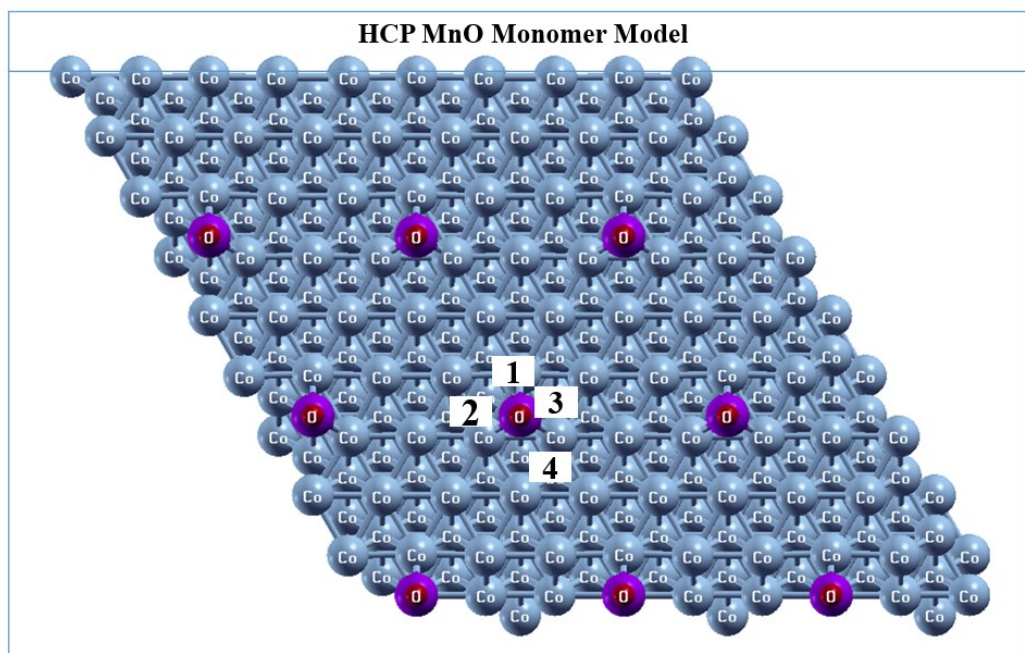


Figure 4.3. Adsorption sites for 0.11 ML hcp MnO monomer models

Based on our calculations, hcp MnO monomer had an adsorption energy of -235 kJ/mol while the fcc MnO monomer model had an adsorption energy of -229 kJ/mol, for a coverage of 0.25 ML.

For the 0.11 ML coverage, the adsorption energies were calculated to be -254 kJ/mol for hcp model and -248 kJ/mol for the fcc model.

Although the hcp model was 6 kJ/mol more stable than the fcc model, and thus the minimum energy structure, due to the small difference in their stability, both models were used to calculate the adsorption energies of CO, OH, C, O and H.

These hcp and fcc MnO monomer promoter model's adsorption energies were compared with bare clean Co(111) adsorption energies to investigate the effects of MnO promotion on surface species.

4.1.1. CO Adsorption Energy

CO molecule adsorption energy was found as -170 kJ/mol and its adsorption site was hcp in 0.25 ML surface coverage.

When surface coverage decreased from 0.25 ML to 0.11 ML, adsorption energy was -179 kJ/mol with hcp site.

Various DFT functionals affected results in the VASP software program.

GGA-PBE function resulted in -168 kJ/mol, unlike this another GGA-RPBE function resulted in -129, -137 and -135 kJ/mol.

Calculations using PW91 functional resulted in -171, -188 kJ/mol adsorption energies on cobalt surfaces [69, 77-80].

Hybrid functionals including van-der-Waals interactions resulted in the top adsorption site [23].

When non-hybrid functionals were used such as, PBE functional, the most stable adsorption site was found as hcp.

The CO adsorption energy calculated in this thesis are consistent with the DFT results in the literature obtained using My results were calculated by using the PAW-PBE function were consistent with the literature results [78].

In p (2×2) hcp MnO promoted Co(111), the most stable CO adsorption site was hcp site that had 1 Mn neighbor and -297 kJ/mol adsorption energy.

O in CO molecule had a bond with Mn. The most stable adsorption site was found -228 kJ/mol top site for CO by using a 0.25 ML fcc MnO promoter model.

Based on these results, the hcp MnO monomer model is postulated to be most stable structural model for MnO promoted Co(111) surfaces.

Like a 0.25 ML hcp promoted model, 0.11 ML hcp promoted Co (111), the most stable CO adsorption site was hcp site that had 1 Mn neighbor and -340 kJ/mol adsorption energy.

There was also an interaction between Mn and O atom.

In literature, different models reached different adsorption energies for CO. A subsurface monolayer (Co/Mn/Co) resulted in -213 kJ/mol and a top (Mn/Co) reached -255 kJ/mol for CO molecule [66].

In order to calculate the potential energy diagrams (volcano curves) for reactions using NEB calculations, minimum energy structures for initial and final states for the reaction has to be calculated.

Initial states were found from the most stable adsorption calculations.

Final states were calculated from the most stable coadsorption results. Reactions were considered between initial state and final state coordinates.

When volcano curve is not observed at the end of the neb calculation, the second most stable initial and final structure are used for neb calculation.

Table 4.2. CO Adsorption energies, kJ/mol

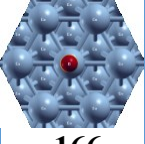
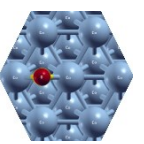
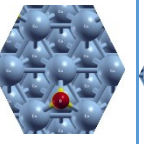
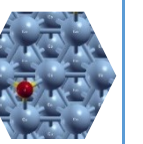
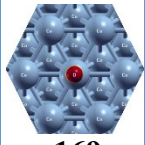
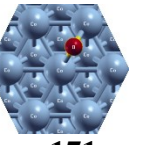
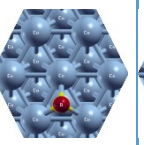
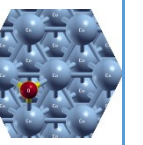
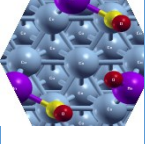
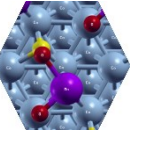
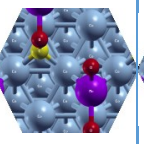
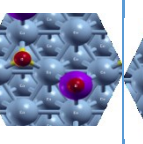
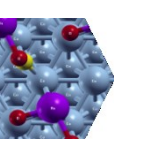
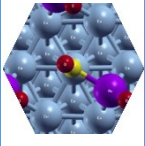
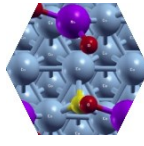
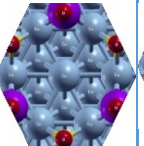
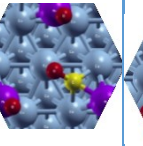
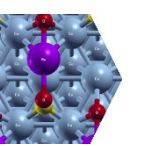
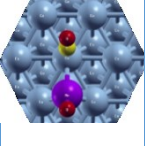
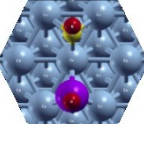
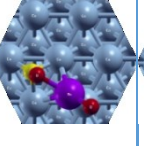
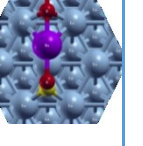
CO Adsorption Energies (kJ/mol)					
0.25 ML Bare Co(111)	 -166 TOP	 -163 BRIDG E	 -170 HCP	 -169 FCC	
0.11 ML Bare Co(111)	 -169 FCC	 -171 BRIDG E	 -179 HCP	 -176 FCC	
0.25 ML FCC MnO promoted Co(111)	 -128 TOP 1	 -228 HCP 2	 -184 HCP 3	 -120 HCP 3	 -228 BRIDGE 2
0.25 ML HCP MnO promoted Co(111)	 -118 TOP 1	 -178 HCP 2	 -119 FCC 3	 -124 FCC 1	 -297 FCC 3
0.11 ML HCP MnO promoted Co(111)	 -170 TOP 1	 -172 FCC 1	 -181 FCC 1	 -340 HCP 1	

Table 4.3. HCO Adsorption Energies, kJ/mol

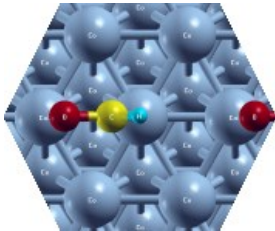
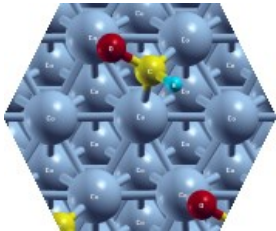
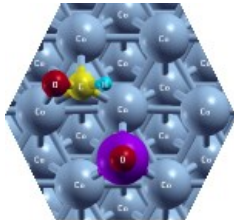
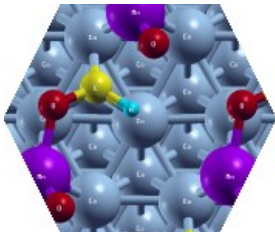
HCO Adsorption Energies (kJ/mol)		
0.25 ML Bare Co(111)	 <p>-210 TOP</p>	 <p>-208 BRIDGE</p>
0.25 ML HCP MnO promoted Co(111)	 <p>-233 HCP 1</p>	
0.11 ML HCP MnO promoted Co(111)	 <p>-245 HCP 1</p>	

Table 4.4. CO Coadsorption Energies on 0.25 ML Co (111), kJ/mol

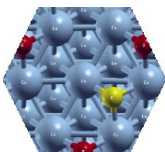
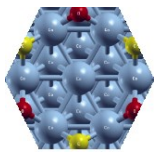
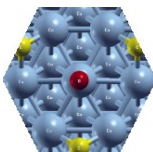
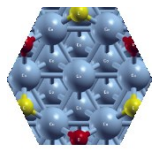
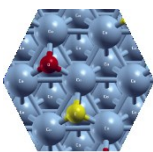
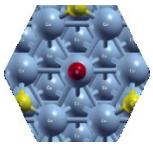
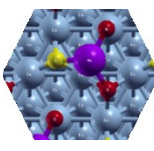
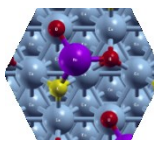
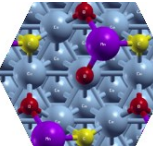
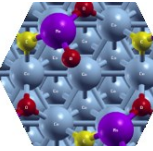
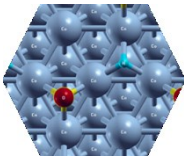
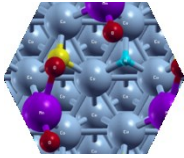
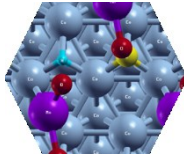
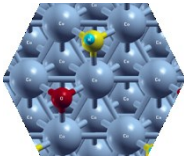
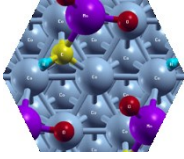
C+O Coadsorption Energies on 0.25 ML Bare Co(111). kJ/mol					
					
-1174 C _{fcc} +O _{fcc}	-1208 C _{fcc} +O _{hcp}	-1052 C _{fcc} +O _{top}	-1223 C _{hcp} +O _{fcc}	-1195 C _{hcp} + O _{hcp}	-1074 C _{hcp} + O _{top}
C+O Coadsorption Energies on 0.25 ML HCP MnO Promoted Co(111). kJ/mol					
					
-1336 C _{hcp} +O _{fcc}	-1328 C _{fcc} +O _{hcp}	-1297 C _{fcc} +O _{hcp}	-1306 C _{fcc} +O _{hcp}		

Table 4.5. Bare CO+H and CH+O Coadsorption on 0.25 ML Bare and
0.25 ML HCP MnO Promoted Co(111), kJ/mol

<p>CO+H Coadsorption Energies on 0.25 ML Bare Co(111). kJ/mol</p>	 <p>-454 CO_{fcc}+H_{hcp}</p>	
<p>CO+H Coadsorption Energies on 0.25 ML HCP MnO Promoted Co(111). kJ/mol</p>	 <p>-417 CO_{hcp}+H_{hcp}</p>	 <p>-433 CO_{hcp}+H_{hcp}</p>
<p>CH+O Coadsorption Energies on 0.25 ML Bare Co(111). kJ/mol</p>	 <p>-1175 CH_{fcc}+O_{fcc}</p>	
<p>CH+O Coadsorption Energies on 0.25 ML HCP MnO Promoted Co(111). kJ/mol</p>	 <p>-1288 CH_{hcp}+O_{top}</p>	

4.1.2. C, O, H Adsorption Energies

C, O atoms adsorbed on hcp sites and H preferred the fcc adsorption site. Adsorption energies were calculated -698 kJ/mol hcp; -598 kJ/mol hcp; -280 kJ/mol fcc for 0.25 ML coverage and -708 kJ/mol hcp; -601 kJ/mol hcp; -282 kJ/mol fcc site for 0.11 ML coverage of C, O, H atoms. Jiao et al. found that C had -637 kJ/mol hcp site, O had -543 kJ/mol hcp site and H had -268 kJ/mol fcc site [77].

Different functionals were also used in the literature to calculate adsorption energies. In SIESTA software using PAW-PBE function calculated -654 kJ/mol as C adsorption energy. GGA-PW91 function led to -671 kJ/mol C adsorption energy [77, 23, 69]. O adsorption energy was calculated as -592 kJ/mol with the use of GGA-PBE function, -548 kJ/mol with GGA-RPBE and GGA-PW91 function calculations resulted in -658 kJ/mol and -671 kJ/mol [78, 69]. The calculated results are consistent with the literature.

H adsorption energy was calculated -269 kJ/mol fcc site for 0.25 ML hcp MnO monomer model and -275 kJ/mol fcc site for the fcc MnO monomer model.

Hcp MnO promoted 0.11 ML Co(111) surface had -282 kJ/mol fcc site. Like 0.25 ML promoter models, this H also had 1 Mn neighbor.

In the literature, H adsorption energy was calculated as -325 kJ/mol for the sub monolayer model and -375 kJ/mol for the top model [23].

0.25 ML hcp MnO monomer models showed that C preferred hcp site and had 1 Mn neighbor.

Although the hcp model had -763 kJ/mol hcp site adsorption energy, the fcc model had -769 kJ/mol hcp site adsorption energy.

In 0.11 ML hcp MnO monomer model, C had -831 kJ/mol fcc site and it had also 1 Mn neighbor.

C adsorption energy was calculated literature as -743 kJ/mol for the sub monolayer model and -815 kJ/mol for the top model [23].

O adsorption energy was calculated -638, -643, -682 kJ/mol fcc sites for 0.25 ML hcp, fcc and 0.11 ML hcp MnO promoter models

All the models had 1 Mn neighbor. -619 and -727 kJ/mol adsorption energies were calculated for two different MnO models [52].

Table 4.6. C Adsorption Energies, kJ/mol

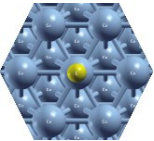
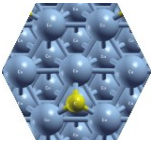
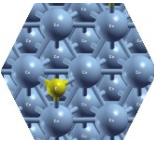
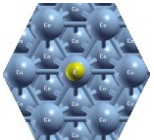
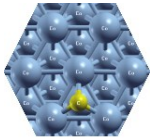
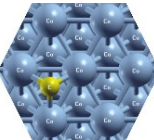
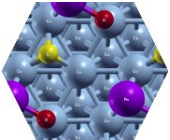
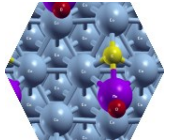
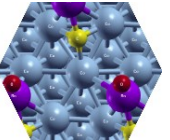
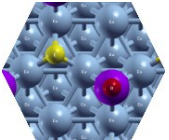
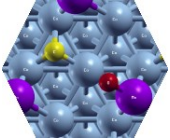
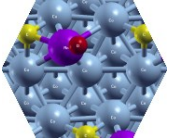
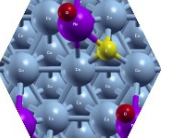
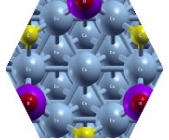
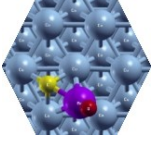
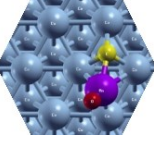
C Adsorption Energies (kJ/mol)				
0.25 ML Bare Co(111)	 -492 TOP	 - 698HCP	 -675 FCC	
0.11 ML Bare Co(111)	 -675 TOP	 -708 HCP	 -690 FCC	
0.25 ML FCC MnO promoted Co(111)	 -749 HCP 2	 -769 HCP 1	 -759 FCC2	 -685 HCP 3
0.25 ML HCP MnO promoted Co(111)	 -694 HCP 2	 -757 FCC 1	 -763 HCP 1	 -666 FCC 3
0.11 ML HCP MnO promoted Co(111)	 -772 FCC 1	 -777 HCP 1		

Table 4.7. O Adsorption Energies, kJ/mol

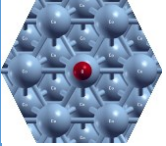
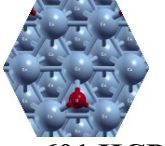
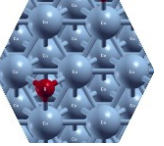
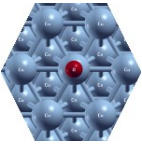
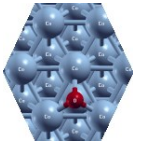
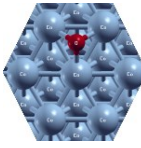
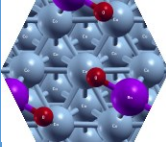
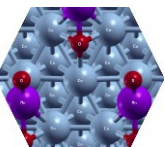
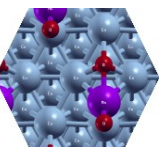
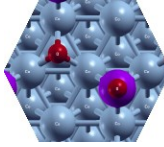
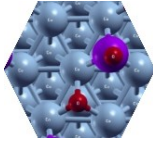
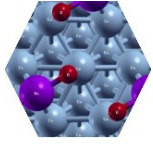
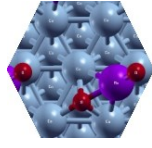
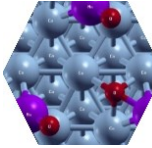
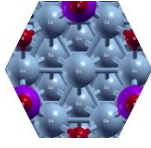
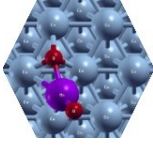
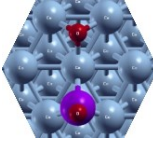
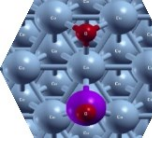
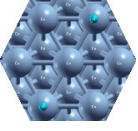
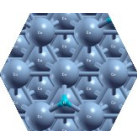
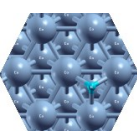
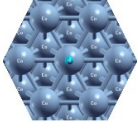
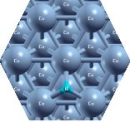
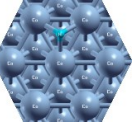
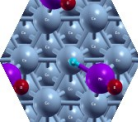
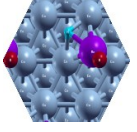
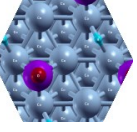
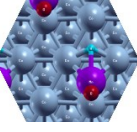
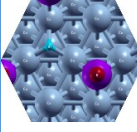
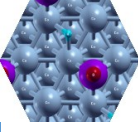
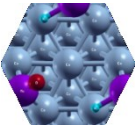
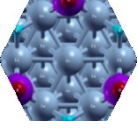
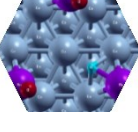
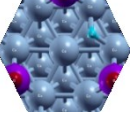
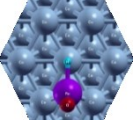
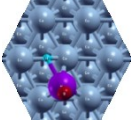
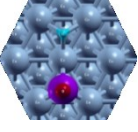
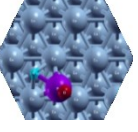
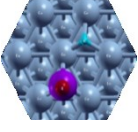
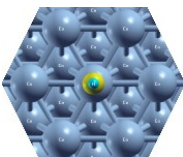
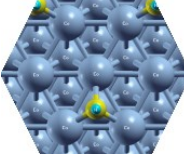
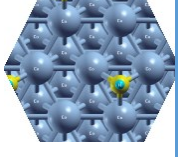
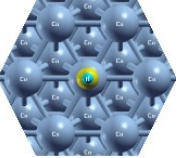
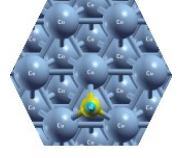
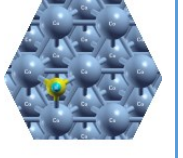
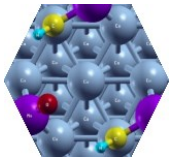
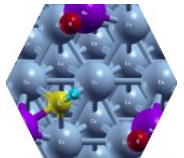
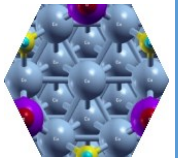
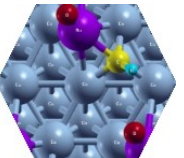
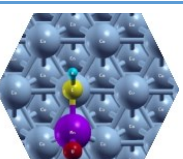
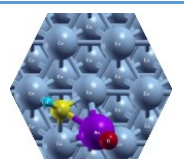
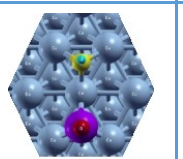
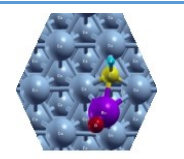
O Adsorption Energies (kJ/mol)					
0.25 ML Bare Co(111)	 -447 TOP	 -601 HCP	 -597 FCC		
0.11 ML Bare Co(111)	 -444 TOP	 -601 HCP	 -597 FCC		
0.25 ML FCC MnO promoted Co(111)	 -629 TOP 1	 -638 FCC 1	 -643 HCP 1	 -539 HCP 3	
0.25 ML HCP MnO promoted Co(111)	 -537 HCP 2	 -623 TOP 1	 -638 HCP 1	 -633 FCC 1	 -531 FCC 3
0.11 ML HCP MnO promoted Co(111)	 -644 HCP 1	 -581 FCC 1	 -646 FCC1		

Table 4.8. H Adsorption Energies, kJ/mol

H Adsorption Energies (kJ/mol)						
0.25 ML Bare Co(111)	 -215 TOP	 -277 HCP	 -280 FCC			
0.11 ML Bare Co(111)	 -218 TOP	 -280 HCP	 -282 FCC			
0.25 ML FCC MnO promoted Co(111)	 -271 TOP 1	 -275 FCC 1	 -256 BRIDGE 2	 -270 HCP 1	 -267 HCP 3	 -262 FCC 2
0.25 ML HCP MnO promoted Co(111)	 -266 TOP 1	 -269 FCC 3	 -269 FCC 1	 -261 HCP 2		
0.11 ML HCP MnO promoted Co(111)	 -276 TOP 1	 -274 BRIDGE 1	 -282 FCC 3	 -279 FCC 1	 -276 HCP 1	

4.1.3. CH and OH Adsorption Energies

Table 4.9. CH Adsorption Energies, kJ/mol

CH Adsorption Energies (kJ/mol)				
0.25 ML Bare Co(111)	 -472 TOP	 -646 HCP	 -636 FCC	
0.11 ML Bare Co(111)	 -481 TOP	 -653 HCP	 -649 FCC	
0.25 ML HCP MnO promoted Co(111)	 -610 TOP 1	 -685 FCC 1	 -659 FCC 3	 -687 HCP 2
0.11 ML HCP MnO promoted Co(111)	 -618 TOP 1	 -707 FCC 1	 -660 FCC 1	 -705 HCP 1

CH and OH adsorption energies were found as -646 kJ/mol hcp site and -361 kJ/mol hcp site in 0.25 ML and -653 kJ/mol hcp site, -346 kJ/mol hcp in 0.11 ML Co catalyst.

CH had -642 kJ/mol, -631 kJ/mol, -654 kJ/mol, -599 kJ/mol adsorption energy [23]. OH, adsorption energy was calculated -319 kJ/mol and O connected with catalyst from hcp site [77]. GGA-PBE function resulted in -360 kJ/mol, -365 kJ/mol, GGA-RPBE function found -322 kJ/mol, PAW-PW91 calculations concluded -367 kJ/mol and -321 kJ/mol as OH adsorption energies. OH, adsorption energy was found the same with GGA-PBE function in literature [78, 69, 23].

OH had -449 kJ/mol top site for 0.25 ML hcp model, kJ/mol for 0.25 ML fcc model, -440 kJ/mol top site for 0.11 ML hcp model. They had also 1 Mn neighbor.

CH had -687 kJ/mol hcp site for 0.25 ML hcp model and -707 kJ/mol fcc site for 0.11 ML hcp model.

Table 4.10. C+H Coadsorption Energies on 0.25 ML Bare Co(111)

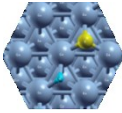
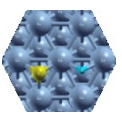
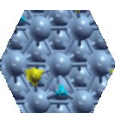
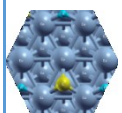
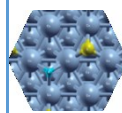
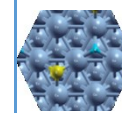
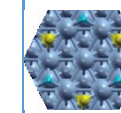
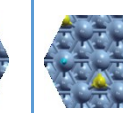
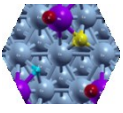
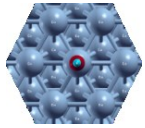
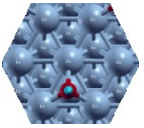
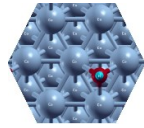
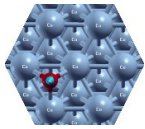
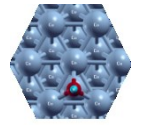
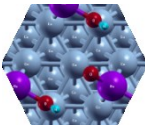
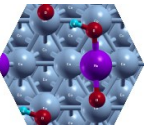
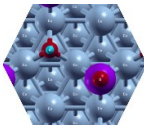
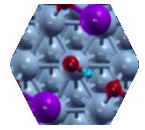
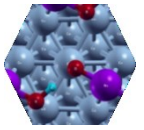
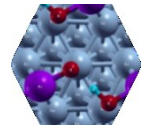
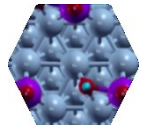
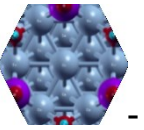
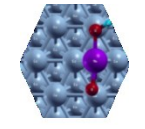
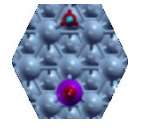
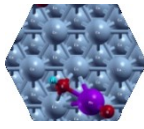
C+H Coadsorption Energies on 0.25 ML Bare Co(111). kJ/mol							
							
-954	-934	-887	-953	-591	-603	-957	-874
C_{hcp+}	C_{fcc+}	C_{fcc+}	C_{hcp+}	C_{hcp+}	C_{fcc+}	C_{fcc+}	C_{hcp+}
H_{hcp}	H_{fcc}	H_{hcp}	H_{hcp}	H_{fcc}	H_{hcp}	H_{hcp}	H_{top}
C+H Coadsorption Energies on 0.25 ML HCP MnO Promoted Co(111). kJ/mol							
							
-1033							
C_{hcp+}							
H_{fcc}							

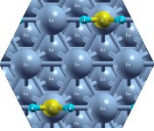
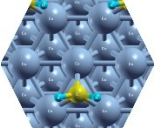
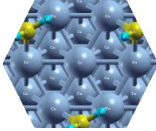
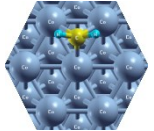
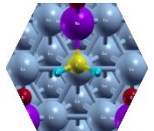
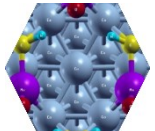
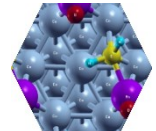
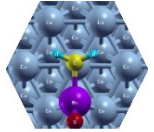
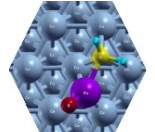
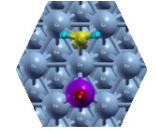
Table 4.11. OH Adsorption Energies, kJ/mol

OH Adsorption Energies (kJ/mol)					
0.25 ML Bare Co(111)	 -255 TOP	 -361 HCP	 -333 FCC		
0.11 ML Bare Co(111)	 -343 FCC	 -346 HCP			
0.25 ML FCC MnO promoted Co(111)	 -388 TOP 1	 -443 TOP 1	 -275 HCP 3		
0.25 ML HCP MnO promoted Co(111)	 -396 TOP 0	 -437 TOP 1	 -449 TOP 1	 -444 BRIDGE	 266 FCC 3
0.11 ML HCP MnO promoted Co(111)	 -440 TOP 1	 -341 HCP	 -344 BRIDGE 1		

4.1.4. CH₂ Adsorption Energy

Most stable adsorption site for CH₂ was found as fcc for bare and hcp for MnO promoted surfaces. Adsorption energies were calculated on the bare surface as -396 kJ/mol for 0.25 ML coverage and -399 kJ/mol for 0.11 ML coverage, and on the MnO promoted surface as -420 kJ/mol for 0.25 ML coverage and -442 kJ/mol for 0.11 ML coverage

Table 4.12. CH₂ Adsorption Energies, kJ/mol

CH ₂ Adsorption Energies (kJ/mol)			
0.25 ML Bare Co(111)	 -294 TOP	 -390 HCP	 -396 FCC
0.11 ML Bare Co(111)	 -399 FCC		
0.25 ML HCP MnO promoted Co(111)	 -386 TOP 1	 -411 FCC 3	 -420 HCP 2
0.11 ML HCP MnO promoted Co(111)	 -410 TOP 1	 -442 HCP 1	 -412 FCC 1

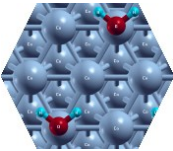
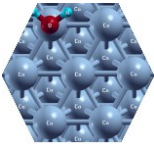
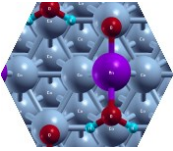
4.1.5. H₂O Adsorption Energy

H₂O had low adsorption energy. Water physisorbed on the catalyst surface. H₂O adsorption energy was calculated -24 kJ/mol top site in 0.25 ML, -27 kJ/mol top site in 0.11 ML. Jiao et al. calculated H₂O adsorption energy as -7 kJ/mol [77].

In the literature, adsorption energies were calculated by GGA-PBE functional as -9 kJ/mol, and by GGA-PW91 functional as -31 kJ/mol. According to literature, O in H₂O molecule connected from the top site [78, 69, 66].

H₂O adsorbed on Mn atom. H₂O adsorption energy was found as -213 kJ/mol hcp site.

Table 4.13. H₂O Adsorption Energy, kJ/mol

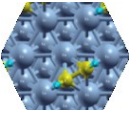
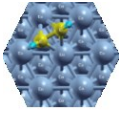
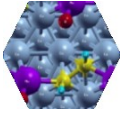
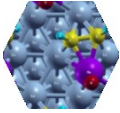
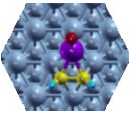
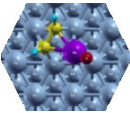
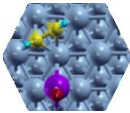
H₂O Adsorption Energies (kJ/mol)	
0.25 ML Bare Co(111)	 -24 TOP
0.11 ML Bare Co(111)	 -27 TOP
0.25 ML HCP MnO promoted Co(111)	 -213 TOP 1

4.1.6. C₂H₂ Adsorption Energy

For C₂H₂ adsorption on Co(111) surface, one of the C atoms in this molecule adsorbed on the fcc site and the other adsorbed on hcp site. C₂H₂ adsorption energy was calculated as -252 kJ/mol hcp+fcc site on 0.25 ML and -272 kJ/mol hcp+fcc site on 0.11 ML surface coverage.

On the MnO promoted Co(111), C₂H₂ had -240 kJ/mol for 0.25 ML coverage and -302 kJ/mol for 0.11 ML coverage. It had a different structure that each C connected bridge sites and had 1 Mn neighbor for both coverages.

Table 4.14. C₂H₂ Adsorption Energies, kJ/mol

C₂H₂ Adsorption Energies (kJ/mol)			
0.25 ML Bare Co(111)	 -252 HCP+FCC		
0.11 ML Bare Co(111)	 -272 HCP+FCC		
0.25 ML HCP MnO promoted Co(111)	 -207 FCC+HCP	 -240 BR+BR	
0.11 ML HCP MnO promoted Co(111)	 -301 BR+BR	 -302 BR+BR	 -276 HCP+FCC

The calculated adsorption energies are summarized in Table 4.15. for bare Co(111). The comparison of adsorption energies for bare and MnO promoted Co(111) surfaces are summarized in Table 4.15.

Table 4.15. Adsorption energies 0.25 ML and 0.11 ML Bare Co(111)

Species	Bare p(2x2) Co	HCP MnO promoted p(2x2) Co(111)	Bare p(3x3) Co	HCP MnO promoted p(3x3) Co(111)
CO	-170 HCP	-297 HCP 3	-179 HCP	-340 HCP 3
HCO	-211 TOP	-233 HCP 1	-	-246 HCP
H ₂ O	-24 TOP	-213 TOP	-27 TOP	-134 TOP
OH	-336 HCP	-449 TOP 1	-346 HCP	-440 TOP 1
CH	-646 HCP	-687 HCP 1	-653 HCP	-707 FCC 1
CH ₂	-396 FCC	-420 HCP 2	-399 FCC	-442 HCP 1
C ₂ H ₂	-252 HCP+FCC	-240 BR 1+ BR 1	-272 HCP+FCC	-302 BR 1+BR 1
C	-698 HCP	-763 HCP 1	-708 HCP	-831 FCC 1
O	-598 HCP	-638 HCP 1	-601 HCP	-682 FCC 1
H	-280 FCC	-269 FCC 3	-282 FCC	-282 FCC

Table 4.16. Adsorption Energy Results (kJ/mol)

Bare Co (111) Adsorption Energies. kJ/mol								
Species	p(2×2)				p(3×3)			
	TOP	BRIDGE	HCP	FCC	TOP	BRIDGE	HCP	FCC
CO	-166	-163	-170	-169	-169	-171	-179	-176
HCO	-210	-208	-	-	-	-	-	-
H₂O	-24	-	-	-	-27	-	-	-
CH	-472	-	-646	-636	-481	-	-653	-649
CH₂	-294	-	-390	-396	-	-	-	-399
C₂H₂	-	-	-252		-	-	-272	
OH	-255	-	-361	-333	-	-	-346	-343
C	-492	-	-698	-675	-497	-	-708	-690
O	-447	-	-598	-593	-444	-	-601	-597
H	-215	-	-277	-280	-218	-	-280	-282

Vibrational frequency calculations were done for 0.25 ML and 0.11 ML bare Co adsorbed surfaces and molecular adsorbates individually.

Zero-point energies (ZPE) can be calculated from contribution of vibrational frequency. Zero-point correction had an influence for adsorbates that included H atoms especially [82]. ZPE calculations and their effect on adsorption energies are summarized in Table 4.17. and Table 4.18.

Table 4.17. Zero Point Correction Effect on 0.25 ML Bare and
HCP MnO Promoted Co(111) Surfaces

Species	0.25 ML Bare Co(111) Ads. Energy. kJ/mol			0.25 ML HCP MnO Promoted Co(111) Ads. Energy. kJ/mol		
	Without ZPE	ZPE	with	Without	ZPE	With
CO	-170	+3	-167	-297	+5	-292
HCO	-211	+5	-206	-233	+4	-229
CH	-646	+6	-640	-687	+7	-680
CH₂	-396	+6	-390	-420	+9	-411
C₂H₂	-252	+6	-246	-240	+10	-230
OH	-336	+6	-330	-449	+7	-442
H₂O	-24	+7	-17	-213	+7	-206

Table 4.18. Zero Point Correction Effect on 0.11 ML Bare and
HCP MnO Promoted Co(111) Surfaces

Species	0.11 ML Bare Co(111) Ads. Energy. kJ/mol			0.11 ML HCP MnO Promoted Co(111) Ads. Energy. kJ/mol		
	Without	ZPE	with	Without	ZPE	With ZPE
CO	-179	+2	-177	-340	+2	-338
HCO	-	-	-	-245	-1	-246
CH	-653	+3	-650	-707	+3	-704
CH₂	-399	+6	-393	-442	+6	-437
C₂H₂	-272	+6	-266	-302	+5	-297
OH	-346	+4	-342	-440	+4	-436
H₂O	-27	+7	-20	-134	+5	-129

The bond lengths for adsorbates on bare and MnO promoted surfaces are summarized in Table 4.19.

The bond lengths for adsorbates on bare and MnO promoted surfaces are summarized in Table 4.19.

Table 4.19. MnO Promotion Effect on Bond Lengths, A°

MnO Promotion Effect on Molecular Bond Length(A °)		
Species	0.25 ML Co(111) Bare	0.25 ML MnO Promoted Co(111)
CO	C-O: 1.96	C-O: 1.36
HCO	H-C: 1.12	H-C: 1.15
	C-O: 1.27	C-O: 1.36
CH	C-H: 1.10	C-H: 1.11
OH	O-H : 0.97	O-H: 1.03
H ₂	H-H: 0.91	-
H ₂ O	H-O: 0.98	H-O: 1.01

4.2. Effect on MnO Promotion on CO Dissociation and Carbon Hydrogenation

Elementary Steps of FTS investigated in this thesis

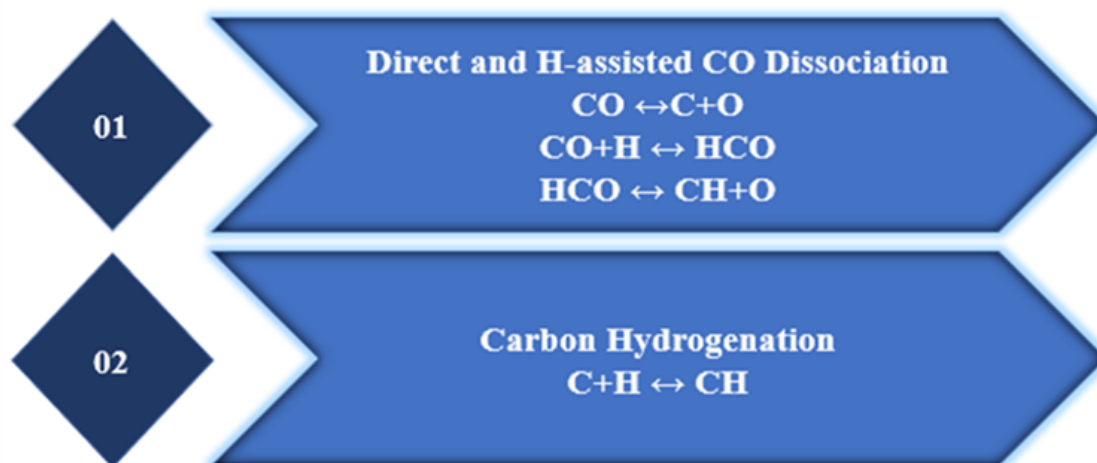


Figure 4.4. Elementary Steps of FTS investigated in this thesis

The activation barriers for the investigated reactions are summarized in Table 4.20.

Table 4.20. MnO Promotion Effect for Activation Barrier Energies, kJ/mol

on 0.25 ML Bare and HCP MnO Promoted Co(111)

NEB						
Reactions	Bare			Promoted		
	Forward	Reverse	ΔH	Forward	Reverse	ΔH
Direct CO Dissociation	245.663	78.7056	166.957	313.525	215.112	98.4134
	220 [16]	167 [16]				
HCO Formation	133.945	9.14571	124.799	81.3178	15.96	65.3579
	146 [16]	29 [16]				
HCO Dissociation	67.8512	84.1183	-16.267	111.536	179.525	-67.99
	90 [16]	187 [16]				
CH Formation	91.6678	149.54	-57.872	55.8145	79.3207	-23.506

4.2.1. CO Dissociation: Direct and H-assisted

CO dissociation can proceed via various pathways. In this thesis, the two most accepted pathways in the literature was studied: Direct and H-assisted [83, 16]. The direct CO forward activation barrier was found as 245 kJ/mol (in line with the literature value of 240 kJ/mol [16] and reverse activation barrier was found as 79 kJ/mol on bare Co(111) surface for a CO coverage of 0.25 ML ($\text{CO} \leftrightarrow \text{C} + \text{O}$).

However, 0.25 ML MnO hcp promoted Co(111) surface had 314 KJ/mol for direct CO dissociation barrier and the activation energy for reverse reaction was found as 215 KJ/mol, as shown in Figure 4.5.

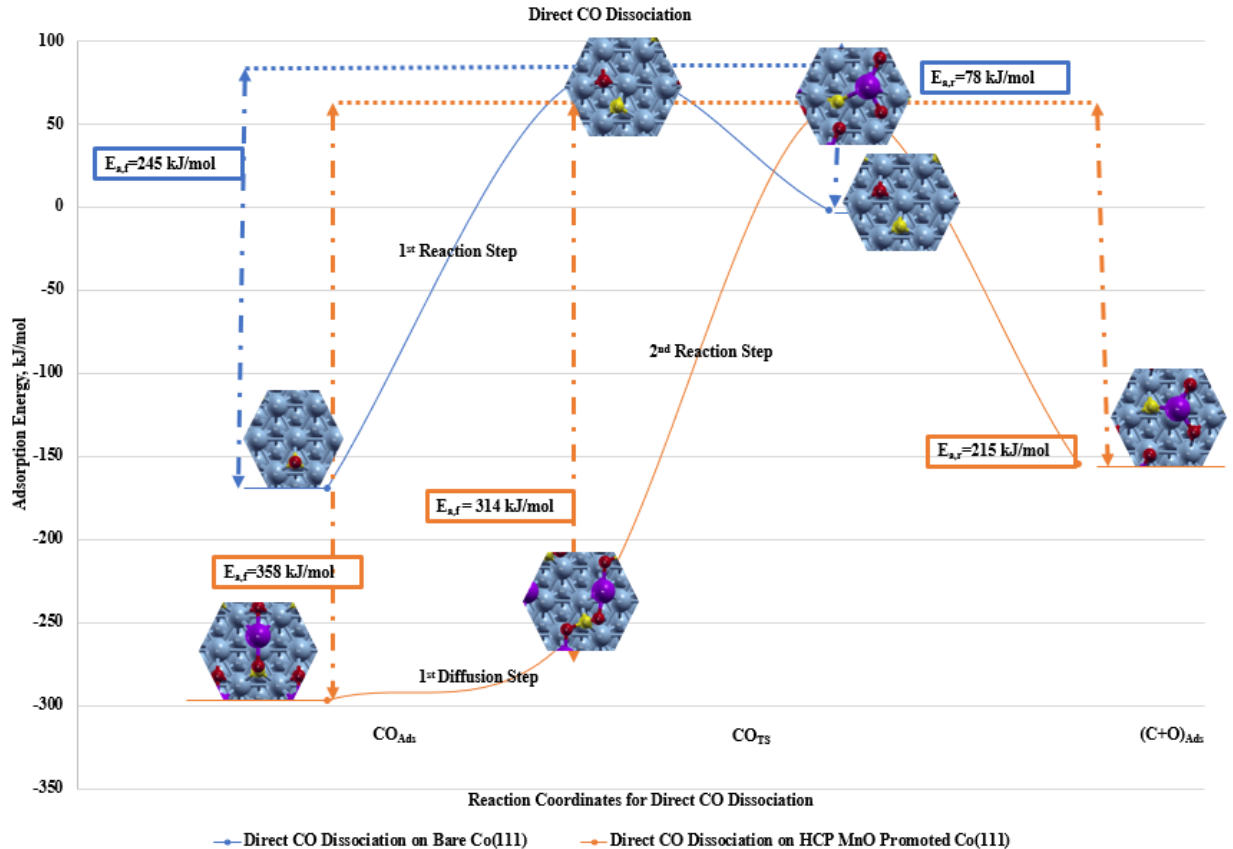


Figure 4.5. MnO Promotion Effect for direct CO Dissociation on 0.25 ML Co(111) Surface

For the H-assisted pathway, first CO have to be hydrogenated to COH [16]. $\text{CO} + \text{H} \rightarrow \text{HCO}$ forward activation barrier was found as 134 kJ/mol and reverse activation barrier was found as 9 kJ/mol on the bare Co(111), while on 0.25 ML MnO promoted Co(111) surface, HCO formation barrier was found as 81 kJ/mol and its reverse activation barrier was found as 15 kJ/mol ($\text{HCO} \leftrightarrow \text{CO} + \text{H}$), as shown in Figure 4.6.

In the H-assisted pathway HCO can undergo C-O bond scission or it can be further hydrogenated to H_xCO [16].

For simplicity, only HCO dissociation to $\text{HC} + \text{O}$ was investigated in this thesis.

The barrier for HCO dissociation increased from 67 to 111 kJ/mol as a result of MnO promotion while the barrier for reverse reaction also increased from 84 to 179 kJ/mol, as shown in Figure 4.6.

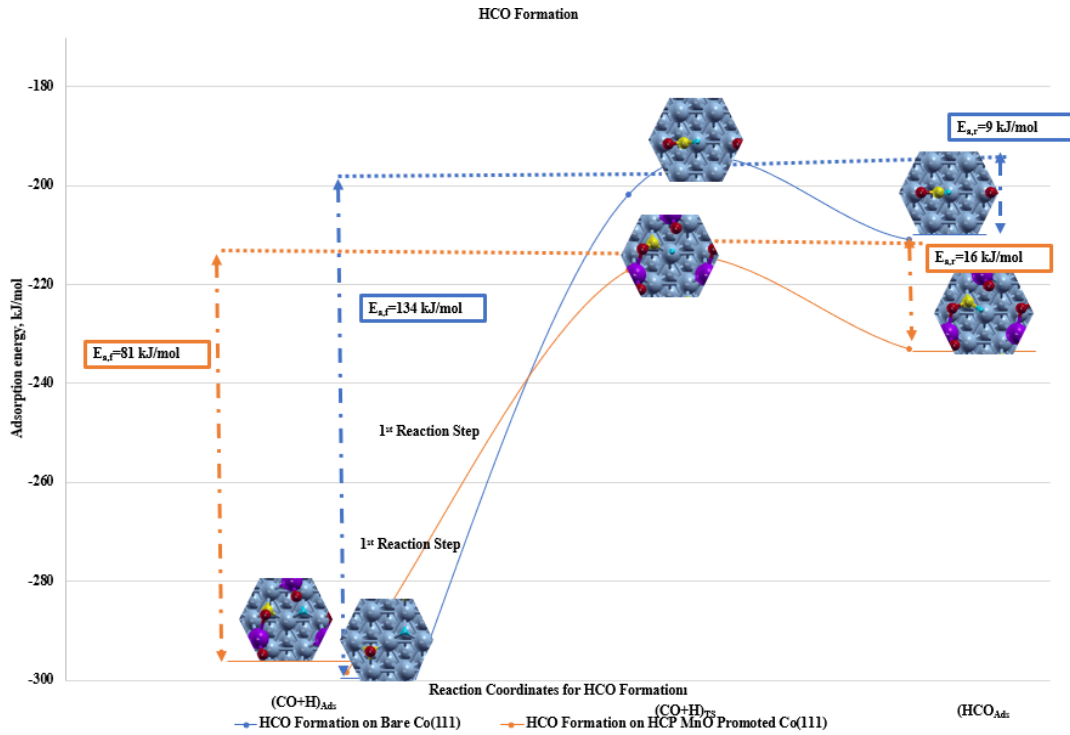


Figure 4.6. MnO Promotion Effect for HCO Formation on 0.25 ML Co(111) Surface

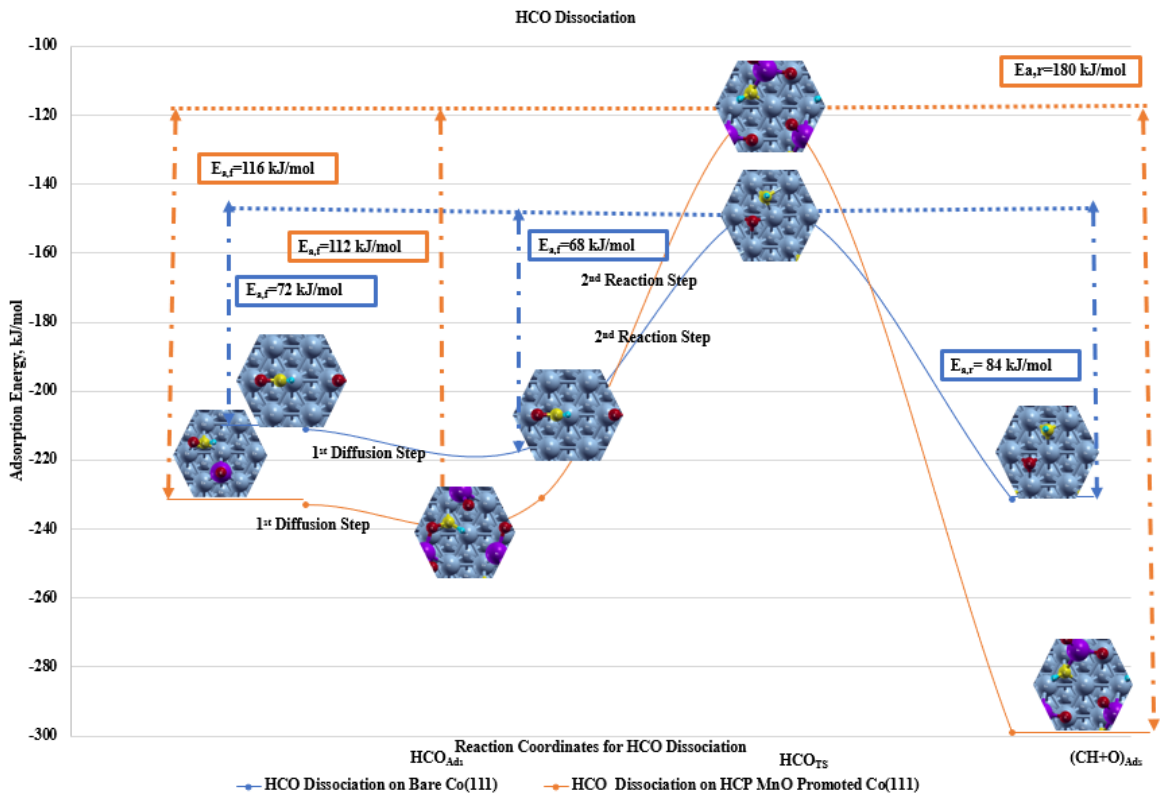


Figure 4.7. MnO Promotion Effects on HCO Formation on 0.25 ML Bare and HCP MnO Promoted Co(111) Surfaces

4.2.2. Carbon Hydrogenation

The activation barrier for the hydrogenation of atomic carbon was calculated as 92 kJ/mol for the bare and 56 kJ/mol for the MnO promoted Co(111) surfaces. The barriers for reverse reactions are calculated as 79 kJ/mol for the bare and 150 kJ/mol for the MnO promoted Co(111) surfaces.

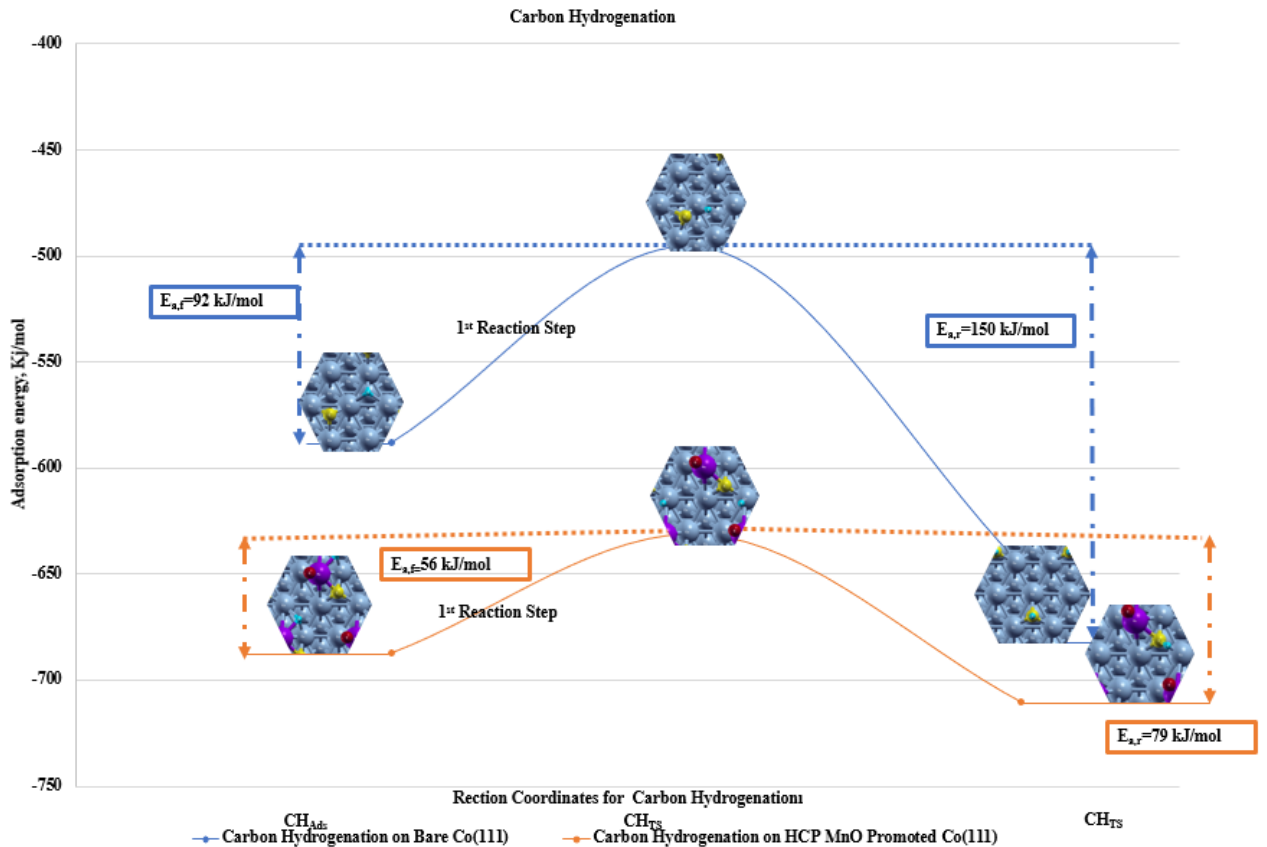


Figure 4.8. MnO Promotion Effect for Carbon Hydrogenation on 0.25 ML Co(111) Surface

CHAPTER 5

DISCUSSION

5.1. Effect of MnO on Adsorption Energies of Surface Species

First the effect of changing coverage on the adsorption energies of species is investigated on the bare (clean) Co(111) surface.

Decreasing the coverage from 0.25 ML to 0.11 ML, CO adsorption energy increased 9 kJ/mol from -170 kJ/mol to -179 kJ/mol and adsorption sites did not affect, and it remained hcp site for.

H₂O adsorption energies on bare Co surface increased 3 kJ/mol from -24 kJ/mol to -27 kJ/mol and it took place top site. Based on this low adsorption energy, H₂O adsorption can be classified as physisorption.

There was a 7 kJ/mol increase from -646 kJ/mol to -653 kJ/mol for CH (methylene) adsorption and it kept adsorption site as hcp.

CH₂ was an intermediate product for Fischer-Trosch Synthesis. Intermediates are very hard to or not possible to investigate experimentally, therefore DFT results are very important in understanding the trends in the adsorption energies of intermediates. CH₂ adsorption energy increased 3 kJ/mol from -396 kJ/mol to -399 kJ/mol and it also remained fcc site.

C₂H₂ (ethylene) adsorption energy raised 20 kJ/mol from -252 kJ/mol to -272 kJ/mol and its most stable hcp+fcc site did not change.

OH, preferred hcp adsorption site and there was a 10 kJ/mol increase from -336 kJ/mol to -346 kJ/mol.

C adsorbate had an increase of approximately 10 kJ/mol from -698 kJ/mol to -708 kJ/mol and hcp site did not change.

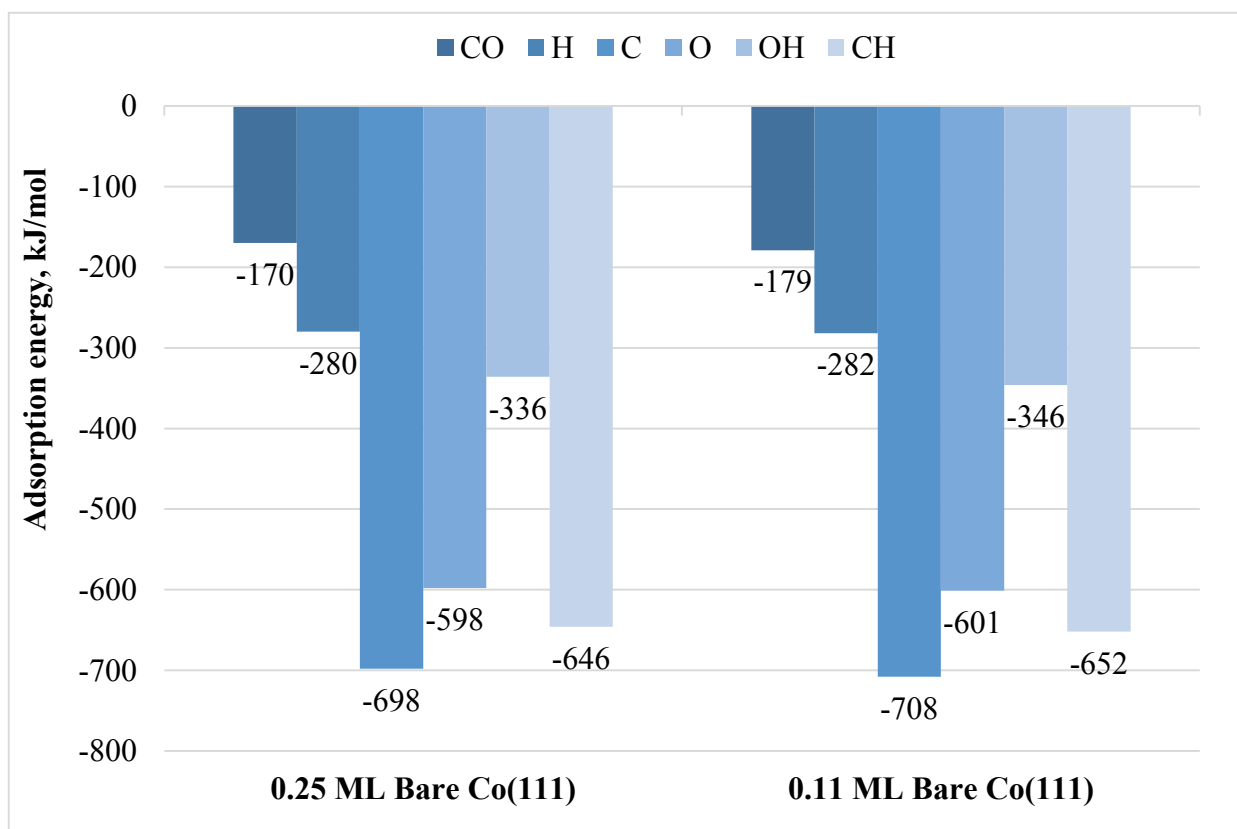
There was a 3 kJ/mol increase from -598 kJ/mol to -601 kJ/mol and the hcp adsorption site did not change for O adsorption.

H adsorption energy increased 2 kJ/mol from -280 kJ/mol to -282 kJ/mol and the fcc site was kept.

It can be interpreted that as surface coverage is decreased from 0.25 ML to 0.11 ML, the adsorption energies for all species increased. There was a little effect on CH₂, O, H adsorption energies. The more increase was observed for C₂H₂ and OH.

In order to provide an explanation to MnO effects to adsorbates, adsorption energies were compared among bare and MnO promoted models, as shown in Table 5.2.

Table 5. 1 Adsorption Energy Variation for Different Coverages



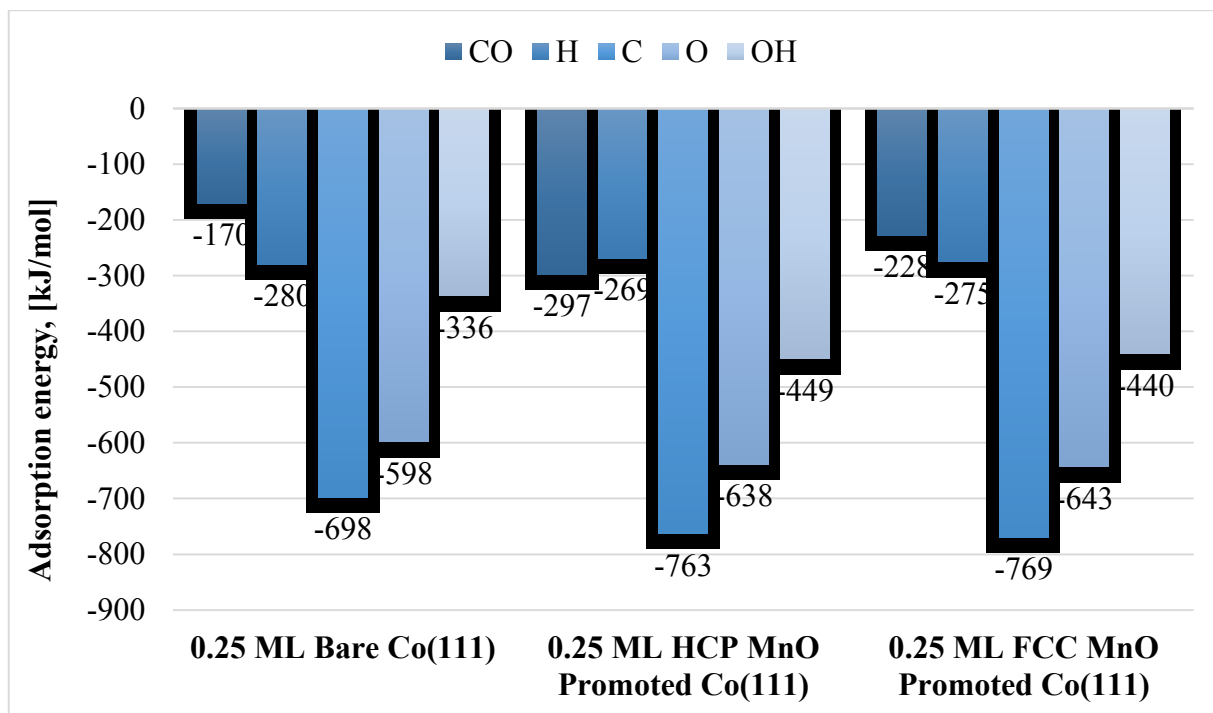
The first important effect of MnO on surface species, which can be seen from the investigation of results for 0.25 ML coverage, is that it increases the adsorption energies of the investigated surfaces species, namely CO, HCO, H₂O, CH, OH, C and O.

Within the investigated adsorbates, a decrease in the adsorption energies of only atomic H and C₂H₂ was observed. These results may have important consequences with respect to the selectivity of FTS.

The significant increase in the adsorption of CO is consistent with the experimental studies indicating that MnO promotion effects are mainly due to the increase in CO surface coverage [62, 47, 8].

Coupled with the decrease in H adsorption energy, these results indicate that the surface CO/H coverage will increase as a result of MnO promotion, which will lead to the increase in C₅₊ selectivity and the decrease in CH₄ selectivity.

Table 5. 2. Promoter Effect on Adsorption Energy



Furthermore, the increase in adsorption energy of CH, the monomer for chain growth also indicates that surface monomer coverage will increase, also resulting in a higher chain growth probability.

Another striking effect of MnO is the increase of H₂O adsorption energy from 24 to 213 kJ/mol. Removal of water as H₂O is seen as one of the candidates for the rate limiting step in FTS mechanism [84, 85].

Therefore, this significant increase in the H₂O adsorption energy implies that oxygen removal mechanism may become slower, and therefore the surface may become more crowded with H₂O and its dissociation products.

Nevertheless, this issue is complicated and needs further detailed investigations, taking into account the effect of O, OH and H₂O on FTS mechanism. The decrease in the adsorption energy of C₂H₂ may also indicate an increase in the rate of growing chains, because incorporation of C₂H₂ into the growing chains may become easier due to its decreased adsorption energy.

However, the mechanism of chain growth is highly complex and debated, therefore it is hard to make detailed inferences about chain growth from the adsorption energy of a single component. Detailed analysis about adsorption of various species and their elementary reactions have to be taken into account for a more clear picture.

When the effect of MnO coverage is considered, it can be seen that the trends in the decrease/increase of adsorption energies are the same for both 0.25 ML and 0.11 ML surface coverages. Only for C₂H₂, it is found that MnO promotion results in an increase in adsorption energy for 0.11 ML while it results in a decrease for 0.25 ML. C₂H₂ is investigated as one of the precursor in chain growth formed as a result of CH coupling. This may demonstrate that the effect of MnO on chain growth is strongly dependent on the MnO coverage, as experimentally shown by [47, 62, 8].

Further support indicating that MnO coverage is critical and dictates the effect on chemistry comes from the relative increase of the adsorption energies as MnO coverage changes. For example, for the increase in CO adsorption energy was higher for 0.11 ML MnO coverage (161 kJ/mol) compared to the increase (127 kJ/mol) for 0.25 ML coverage. For H₂O, the increase is lower (107 kJ/mol) for 0.11ML MnO promoted surface, compared to the increase for 0.25 ML MnO promoted surface.

Overall, these results indicate that the exact effect of MnO on surface species (adsorbates) is strongly dependent on the MnO coverage.

Also, the selectivity increases to C₅₊ and olefinic products and decreases to CH₄ and paraffinic products can be explained due to increasing CO and CH coverages, and decreasing H coverage, in line with the recent experimental findings [21, 47, 62, 61]. Nevertheless, the results also demonstrate the important stabilizing effect of MnO on H₂ adsorption.

Therefore, in order to have a more clear explanation of the MnO effect on selectivity, the influence of water has to be investigated.

5.1.1. Effect of MnO on Activation Barriers for CO Dissociation and Carbon Hydrogenation

The effect of MnO on activity could not be explained in detail in the previous studies, where conflicting results such as increase or decrease in activity could be obtained based on various promoter loadings, operating conditions and catalyst preparation techniques [66, 21, 47, 62, 61].

The most recent hypothesis was that MnO facilitates the CO dissociation reaction, which was assumed to be the rate limiting step for FTS [61]. Nevertheless, based on kinetic measurements the authors proposed CO dissociation to be H assisted.

Our results indicate that no decrease in the activation barrier for CO dissociation due to MnO promotion. On the contrary, it is calculated that the CO dissociation barrier increased from 246 to 314 kJ/mol, which implies that MnO promotion effect cannot be due to the increasing rate of direct CO dissociation. When H-assisted pathway is investigated, a more complex picture emerges.

The barrier for HCO formation is decreased from 133 to 81 kJ/mol, which implies that HCO formation rate will be increased due to MnO promotion. This finding is in line with the hypothesis that CO dissociation occurs via H-assisted pathway. Nevertheless, the results also indicate that HCO dissociation to HC+O has an increased barrier due to MnO promotion from 68 to 112 kJ/mol. However, it is proposed that HCO is further hydrogenated to H_xCO and then dissociation occurs. The formation of H_xCO and their dissociation was not investigated in this thesis. In order to come up with a conclusive results about the CO dissociation mechanism, these reactions have to be investigated as well as the OH assisted CO dissociation pathway.

Nevertheless, our results clearly indicate that direct CO dissociation is not favored when cobalt catalysts are promoted by MnO. These findings are in contrast with the theoretical study by Pedersen et al. [66]. As previously mentioned, they have used a metallic Mn promoter model, which is inconsistent with experimental findings.

This situation also demonstrates the importance of working with the correct surface model during computational studies.

The results about the effect of MnO on carbon hydrogenation provide a more clear picture.

It is seen that MnO promotion decreases the activation barrier for carbon hydrogenation from 92 to 56 kJ/mol. Combined with the increase in the adsorption energy of CH species, this indicates that surface monomer pool for chain growth will significantly increase, resulting in an increased selectivity to long chain (C₅₊) hydrocarbons, as reported in the literature.

CHAPTER 6

CONCLUSIONS

The effects of manganese promotion on the adsorbates and specific elementary reactions of Fischer-Tropsch Synthesis (FTS) was investigated using periodic Density-Functional Theory (DFT) calculations on a close packed cobalt surface, Co (111). In particular the effects of MnO promotion on the adsorbates of CO, HCO, CH, CH₂, C₂H₂, OH, H₂O, C, O and on the reactions of direct CO dissociation, H-assisted CO dissociation and carbon hydrogenation were studied for MnO coverages of 0.25 ML and 0.11 ML.

Mn was modeled in the chemical form of MnO. MnO was modeled as a singular monomer on the Co(111) surface, based on the findings from experimental studies. The results indicate that MnO promotion increases the adsorption energies of all adsorbates, except H and C₂H₂. In particular, CO and H₂O adsorption energies increase significantly, which indicate that the selectivity increase to long chain hydrocarbons is mainly due to an increased surface coverage of CO with respect to H. The results also indicate that the relative effect of MnO on adsorption energies are strongly dependent on MnO coverage.

MnO promotion is found to decrease the activation barriers for HCO and CH formation, while increasing the activation barriers for direct CO dissociation and HCO dissociation. The results point out that MnO does not promote the direct dissociation of CO and the activity increase due to Mn promotion is most probably due to a H or OH assisted CO dissociation pathway or another rate limiting step.

REFERENCES

1. Chorkendorff, I., & Niemantsverdriet, J. W. (2017). *Concepts of modern catalysis and kinetics*. John Wiley & Sons.
2. Niemantsverdriet, J. W. (2007). *Spectroscopy in catalysis: an introduction*. John Wiley & Sons.
3. Hagen, J. (2015). *Industrial catalysis: a practical approach*. John Wiley & Sons.
4. Dumesic, J. A., Huber, G. W., & Boudart, M. (2008). Principles of heterogeneous catalysis. *Handbook of Heterogeneous Catalysis: Online*.
5. Méndez, J., López, M. F., & Martín-Gago, J. A. (2011). On-surface synthesis of cyclic organic molecules. *Chemical Society Reviews*, 40(9), 4578-4590.
6. Morales, F., & Weckhuysen, B. M. (2006). Promotion effects in Co-based Fischer-Tropsch catalysis. *Catalysis*, 19(1), 1-40.
7. Van de Loosdrecht, J., Botes, F. G., Ciobica, I. M., Ferreira, A. C., Gibson, P., Moodley, D. J., ... & Niemantsverdriet, J. W. (2013). Fischer-Tropsch synthesis: catalysts and chemistry. In *Comprehensive Inorganic Chemistry II: from elements to applications*. Elsevier.
8. Johnson, G. R., Werner, S., & Bell, A. T. (2015). An investigation into the effects of Mn promotion on the activity and selectivity of Co/SiO₂ for Fischer-Tropsch synthesis: evidence for enhanced CO adsorption and dissociation. *ACS Catalysis*, 5(10), 5888-5903.
9. Deutschmann, O., Knözinger, H., Kochloefl, K., & Turek, T. (2000). Heterogeneous catalysis and solid catalysts, 2. development and types of solid catalysts. *Ullmann's Encyclopedia of Industrial Chemistry*.
10. Perego, C., & Villa, P. (1997). Catalyst preparation methods. *Catalysis Today*, 34(3-4), 281-305.
11. Musselwhite, N., & Somorjai, G. A. (2013). Investigations of structure sensitivity in heterogeneous catalysis: from single crystals to monodisperse nanoparticles. *Topics in Catalysis*, 56(15-17), 1277-1283.
12. Weststrate, C. J., Van Helden, P., & Niemantsverdriet, J. W. (2016). Reflections on the Fischer-Tropsch synthesis: Mechanistic issues from a surface science perspective. *Catalysis Today*, 275, 100-110.
13. Schulz, H. (1999). Short history and present trends of Fischer-Tropsch synthesis. *Applied Catalysis A: General*, 186(1-2), 3-12.

14. van Helden, P., van den Berg, J. A., & Ciobîcă, I. M. (2012). Hydrogen-assisted CO dissociation on the Co (211) stepped surface. *Catalysis Science & Technology*, 2(3), 491-494.
15. Inderwildi, O. R., Jenkins, S. J., & King, D. A. (2008). Fischer–Tropsch mechanism revisited: alternative pathways to produce higher hydrocarbons from synthesis gas. *The Journal of Physical Chemistry C*, 112(5), 1305-1307.
16. Zhuo, M., Tan, K. F., Borgna, A., & Saeys, M. (2009). Density functional theory study of the CO insertion mechanism for Fischer–Tropsch synthesis over Co catalysts. *The Journal of Physical Chemistry C*, 113(19), 8357-8365.
17. Schweicher, J., Bundhoo, A., & Kruse, N. (2012). Hydrocarbon chain lengthening in catalytic CO hydrogenation: evidence for a CO-insertion mechanism. *Journal of the American Chemical Society*, 134(39), 16135-16138.
18. Maitlis, P. M., Long, H. C., Quyoum, R., Turner, M. L., & Wang, Z. Q. (1996). Heterogeneous catalysis of C–C bond formation: black art or organometallic science? *Chemical Communications*, (1), 1-8.
19. Overett, M. J., Hill, R. O., & Moss, J. R. (2000). Organometallic chemistry and surface science: mechanistic models for the Fischer–Tropsch synthesis. *Coordination Chemistry Reviews*, 206, 581-605.
20. Schulz, H., & Claeys, M. (1999). Reactions of α -olefins of different chain length added during Fischer–Tropsch synthesis on a cobalt catalyst in a slurry reactor. *Applied Catalysis A: General*, 186(1-2), 71-90.
21. Den Breejen, J. P., Radstake, P. B., Bezemer, G. L., Bitter, J. H., Frøseth, V., Holmen, A., & De Jong, K. P. (2009). On the origin of the cobalt particle size effects in Fischer–Tropsch catalysis. *Journal of the American Chemical Society*, 131(20), 7197-7203.
22. Pilot, I. A., van Santen, R. A., & Hensen, E. J. (2014). The optimally performing Fischer–Tropsch catalyst. *Angewandte Chemie International Edition*, 53(47), 12746-12750.
23. Cheng, J., Gong, X. Q., Hu, P., Lok, C. M., Ellis, P., & French, S. (2008). A quantitative determination of reaction mechanisms from density functional theory calculations: Fischer–Tropsch synthesis on flat and stepped cobalt surfaces. *Journal of Catalysis*, 254(2), 285-295.
24. Weststrate, C. J., Ciobîcă, I. M., Saib, A. M., Moodley, D. J., & Niemantsverdriet, J. W. (2014). Fundamental issues on practical Fischer–Tropsch catalysts: How surface science can help. *Catalysis Today*, 228, 106-112.

25. Martin, R. M. (2004). *Electronic structure: basic theory and practical methods*. Cambridge university press.
26. Müller, K. (1980). Reaction paths on multidimensional energy hypersurfaces. *Angewandte Chemie International Edition in English*, 19(1), 1-13.
27. Koch, W., Holthausen, M. C., & Kaupp, M. (2001). BUCHER-A Chemist's Guide to Density Functional Theory. *Angewandte Chemie-German Edition*, 113(5), 989-989.
28. Sadaf, A., Baria, H., & Jain, N. (2017, December). Simulation of Adsorption of Gas Molecules on Carbon Nanosensors. In *International Workshop on the Physics of Semiconductor and Devices* (pp. 881-887). Springer, Cham.
29. Nørskov, J. K., Abild-Pedersen, F., Studt, F., & Bligaard, T. (2011). Density functional theory in surface chemistry and catalysis. *Proceedings of the National Academy of Sciences*, 108(3), 937-943.
30. Shan, N., Zhou, M., Hanchett, M. K., Chen, J., & Liu, B. (2017). Practical principles of density functional theory for catalytic reaction simulations on metal surfaces—from theory to applications. *Molecular Simulation*, 43(10-11), 861-885.
31. Adamo, C., Cossi, M., Rega, N., & Barone, V. (2001). New computational strategies for the quantum mechanical study of biological systems in condensed phases. In *Theoretical and Computational Chemistry* (Vol. 9, pp. 467-538). Elsevier.
32. Heyd, J., Scuseria, G. E., & Ernzerhof, M. (2003). Hybrid functionals based on a screened Coulomb potential. *The Journal of Chemical Physics*, 118(18), 8207-8215.
33. Pessoa, A. M., Fajín, J. L., Gomes, J. R., & Cordeiro, M. N. D. (2010). Cluster and of Molecular Structure: *THEOCHEM*, 946(1-3), 43-50.
34. Van Doorslaer, M. (2017). Elucidating the role of Mn promotion in Co-based.
35. Chandradass, J., Yoon, J. H., & Bae, D. S. (2008). Synthesis and characterization of zirconia doped alumina nanopowder by citrate–nitrate process. *Materials Science and Engineering: A*, 473(1-2), 360-364.
36. Heyd, J., Scuseria, G. E., & Ernzerhof, M. (2003). Hybrid functionals based on a screened Coulomb potential. *The Journal of Chemical Physics*, 118(18), 8207-8215.
37. Jongsomjit, B., Panpranot, J., & Goodwin Jr, J. G. (2003). Effect of zirconia-modified alumina on the properties of Co/ γ -Al₂O₃ catalysts. *Journal of Catalysis*, 215(1), 66-77.

38. Li, Z., Wu, J., Yu, J., Han, D., Wu, L., & Li, J. (2016). Effect of incorporation manner of Zr on the Co/SBA-15 catalyst for the Fischer–Tropsch synthesis. *Journal of Molecular Catalysis A: Chemical*, 424, 384-392.
39. Liu, Y., Chen, J., Fang, K., Wang, Y., & Sun, Y. (2007). A large pore-size mesoporous zirconia supported cobalt catalyst with good performance in Fischer–Tropsch synthesis. *Catalysis Communications*, 8(6), 945-949.
40. Miyazawa, T., Hanaoka, T., Shimura, K., & Hirata, S. (2014). Fischer–Tropsch synthesis over a Co/SiO₂ catalyst modified with Mn-and Zr under practical conditions. *Catalysis Communications*, 57, 36-39.
41. Hemmati, M. R., Kazemeini, M., Zarkesh, J., & Khorasheh, F. (2012). Effect of lanthanum doping on the lifetime of Co/ γ -Al₂O₃ catalysts in Fischer-Tropsch synthesis. *Journal of the Taiwan Institute of Chemical Engineers*, 43(5), 704-710.
42. Ledford, J. S., Houalla, M., Proctor, A., Hercules, D. M., & Petrakis, L. (1989). Influence of lanthanum on the surface structure and carbon monoxide hydrogenation activity of supported cobalt catalysts. *The Journal of Physical Chemistry*, 93(18), 6770-6777.
43. Vosoughi, V., Dalai, A. K., Abatzoglou, N., & Hu, Y. (2017). Performances of promoted cobalt catalysts supported on mesoporous alumina for Fischer-Tropsch synthesis. *Applied Catalysis A: General*, 547, 155-163.
44. Iqbal, S., Davies, T. E., Hayward, J. S., Morgan, D. J., Karim, K., Bartley, J. K., ... & Hutchings, G. J. (2016). Fischer Tropsch Synthesis using promoted cobalt-based catalysts. *Catalysis Today*, 272, 74-79.
45. Zhang, X., Su, H., Zhang, Y., & Gu, X. (2016). Effect of CeO₂ promotion on the catalytic performance of Co/ZrO₂ catalysts for Fischer–Tropsch synthesis. *Fuel*, 184, 162-168.
46. de Lima, A. E. P., & de Oliveira, D. C. (2017). In situ XANES study of cobalt in Co-Ce-Al catalyst applied to steam reforming of ethanol reaction. *Catalysis Today*, 283, 104-109.
47. Bezemer, G. L., Radstake, P. B., Falke, U., Oosterbeek, H. P. C. E., Kuipers, H. P. C. E., Van Dillen, A. J., & De Jong, K. P. (2006). Investigation of promoter effects of manganese oxide on carbon nanofiber-supported cobalt catalysts for Fischer–Tropsch synthesis. *Journal of Catalysis*, 237(1), 152-161.
48. He, L., Zhang, Y., & Fan, M. (2015). Development of composited rare-earth promoted cobalt-based Fischer–Tropsch synthesis catalysts with high activity and selectivity. *Applied Catalysis A: General*, 505, 276-283.

49. Colley, S., Copperthwaite, R. G., Hutchings, G. J., & Van der Riet, M. (1988). Carbon monoxide hydrogenation using cobalt manganese oxide catalysts: initial catalyst optimization studies. *Industrial & Engineering Chemistry Research*, 27(8), 1339-1344.
50. Hutchings, G. J., van der Riet, M., & Hunter, R. (1989). CO hydrogenation using cobalt/manganese oxide catalysts. Comments on the mechanism of carbon-carbon bond formation. *Journal of the Chemical Society, Faraday Transactions 1: Physical Chemistry in Condensed Phases*, 85(9), 2875-2890.
51. Liang, Q., Chen, K., Hou, W., & Yan, Q. (1998). CO hydrogenation over nanometer spinel-type Co/Mn complex oxides prepared by sol-gel method. *Applied Catalysis A: General*, 166(1), 191-199.
52. Jiang, M., Koizumi, N., Ozaki, T., & Yamada, M. (2001). Adsorption properties of cobalt and cobalt-manganese catalysts studied by in situ diffuse reflectance FTIR using CO and CO+ H₂ as probes. *Applied Catalysis A: General*, 209(1-2), 59-70.
53. Keyser, M. J., Everson, R. C., & Espinoza, R. L. (1998). Fischer-Tropsch studies with cobalt-manganese oxide catalysts: synthesis performance in a fixed bed reactor. *Applied Catalysis A: General*, 171(1), 99-107.
54. Keyser, M. J., Everson, R. C., & Espinoza, R. L. (2000). Fischer-Tropsch kinetic studies with cobalt-manganese oxide catalysts. *Industrial & Engineering Chemistry Research*, 39(1), 48-54.
55. Riedel, T., Claeys, M., Schulz, H., Schaub, G., Nam, S. S., Jun, K. W., ... & Lee, K. W. (1999). Comparative study of Fischer-Tropsch synthesis with H₂/CO and H₂/CO₂ syngas using Fe- and Co-based catalysts. *Applied Catalysis A: General*, 186(1-2), 201-213.
56. Das, D., Ravichandran, G., & Chakrabarty, D. K. (1997). Conversion of syngas to light olefins over silicalite-1 supported iron and cobalt catalysts: Effect of manganese addition. *Catalysis today*, 36(3), 285-293.
57. Das, D., Ravichandran, G., & Chakrabarty, D. K. (1995). Synthesis of light alkenes from syngas on silicalite-1 supported cobalt and cobalt-manganese catalysts. *Applied Catalysis A: General*, 131(2), 335-345.
58. Zhang, J. L., Ren, J., Chen, J. G., & Sun, Y. H. (2002). Effect of Manganese Promoter on the Performance of Co/Al₂O₃ Catalysts for Fischer Tropsch Synthesis. *Acta Physico-Chimica Sinica*, 18(03), 260-263.
59. Klabunde, K. J., & Imizu, Y. (1984). Bimetallic solvated metal atom dispersed catalysts. New materials with low-temperature catalytic properties. *Journal of the American Chemical Society*, 106(9), 2721-2722.

60. Voß, M., Borgmann, D., & Wedler, G. (2002). Characterization of alumina, silica, and titania supported cobalt catalysts. *Journal of Catalysis*, 212(1), 10-21.
61. Martínez, A., López, C., Márquez, F., & Díaz, I. (2003). Fischer–Tropsch synthesis of hydrocarbons over mesoporous Co/SBA-15 catalysts: the influence of metal loading, cobalt precursor, and promoters. *Journal of Catalysis*, 220(2), 486-499.
62. Dinse, A., Aigner, M., Ulbrich, M., Johnson, G. R., & Bell, A. T. (2012). Effects of Mn promotion on the activity and selectivity of Co/SiO₂ for Fischer–Tropsch Synthesis. *Journal of Catalysis*, 288, 104-114.
63. Morales, F., de Smit, E., de Groot, F. M., Visser, T., & Weckhuysen, B. M. (2007). Effects of manganese oxide promoter on the CO and H₂ adsorption properties of titania-supported cobalt Fischer–Tropsch catalysts. *Journal of Catalysis*, 246(1), 91-99.
64. Tan, B. J., Klabunde, K. J., & Sherwood, P. M. (1991). XPS studies of solvated metal atom dispersed (SMAD) catalysts. Evidence for layered cobalt-manganese particles on alumina and silica. *Journal of the American Chemical Society*, 113(3), 855-861.
65. Johnson, G. R., & Bell, A. T. (2016). Effects of Lewis acidity of metal oxide promoters on the activity and selectivity of Co-based Fischer–Tropsch synthesis catalysts. *Journal of Catalysis*, 338, 250-264.
66. Pedersen, E. Ø., Svenum, I. H., & Blekkan, E. A. (2018). Mn promoted Co catalysts for Fischer-Tropsch production of light olefins—an experimental and theoretical study. *Journal of Catalysis*, 361, 23-32.
67. Zhang, X., Su, H., Zhang, Y., & Gu, X. (2016). Effect of CeO₂ promotion on the catalytic performance of Co/ZrO₂ catalysts for Fischer–Tropsch synthesis. *Fuel*, 184, 162-168.
68. Liu, J. X., Su, H. Y., Sun, D. P., Zhang, B. Y., & Li, W. X. (2013). Crystallographic dependence of CO activation on cobalt catalysts: HCP versus FCC. *Journal of the American Chemical Society*, 135(44), 16284-16287.
69. Ojeda, M., Nabar, R., Nilekar, A. U., Ishikawa, A., Mavrikakis, M., & Iglesia, E. (2010). CO activation pathways and the mechanism of Fischer–Tropsch synthesis. *Journal of Catalysis*, 272(2), 287-297.
70. Gong, X. Q., Raval, R., & Hu, P. (2004). CO dissociation and O removal on Co (0 0 0 1): a density functional theory study. *Surface Science*, 562(1-3), 247-256.

71. Ma, X., Su, H. Y., Deng, H., & Li, W. X. (2011). Carbon monoxide adsorption and dissociation on Mn-decorated Rh (1 1 1) and Rh (5 5 3) surfaces: A first-principles study. *Catalysis Today*, 160(1), 228-233.
72. Gong, X. Q., Raval, R., & Hu, P. (2005). CH_x Hydrogenation on Co (0001): A density functional theory study. *The Journal of Chemical Physics*, 122(2), 024711.
73. Balakrishnan, N., Joseph, B., & Bhethanabotla, V. R. (2013). Effect of Pt and Ru promoters on deactivation of Co catalysts by C deposition during Fischer–Tropsch synthesis: a DFT study. *Applied Catalysis A: General*, 462, 107-115.
74. Balakrishnan, N., Joseph, B., & Bhethanabotla, V. R. (2012). Effect of platinum promoters on the removal of O from the surface of cobalt catalysts: A DFT study. *Surface Science*, 606(5-6), 634-643.
75. Yang, N., Yoo, J. S., Schumann, J., Bothra, P., Singh, J. A., Valle, E., ... & Bent, S. F. (2017). Rh-MnO Interface Sites Formed by Atomic Layer Deposition Promote Syngas Conversion to Higher Oxygenates. *ACS Catalysis*, 7(9), 5746-5757.
76. Enache, D. I., Roy-Auberger, M., & Revel, R. (2004). Differences in the characteristics and catalytic properties of cobalt-based Fischer–Tropsch catalysts supported on zirconia and alumina. *Applied Catalysis A: General*, 268(1-2), 51-60.
77. Liu, S., Li, Y. W., Wang, J., & Jiao, H. (2016). Mechanisms of H₂O and CO₂ formation from surface oxygen reduction on Co (0001). *The Journal of Physical Chemistry C*, 120(34), 19265-19270.
78. Luo, W., & Asthagiri, A. (2014). Density functional theory study of methanol steam reforming on Co (0001) and Co (111) surfaces. *The Journal of Physical Chemistry C*, 118(28), 15274-15285.
79. Papp, H. (1983). The chemisorption of carbon monoxide on a Co (0001) single crystal surface; studied by LEED, UPS, EELS, AES and work function measurements. *Surface Science*, 129(1), 205-218.
80. Gunasooriya, G. K. K., van Bavel, A. P., Kuipers, H. P., & Saeys, M. (2015). CO adsorption on cobalt: Prediction of stable surface phases. *Surface Science*, 642, L6-L10.
81. Kalhara Gunasooriya, G. K., & Saeys, M. (2018). CO Adsorption Site Preference on Platinum: Charge Is the Essence. *ACS Catalysis*, 8(5), 3770-3774.

82. Michaelides, A., Ranea, V. A., De Andres, P. L., & King, D. A. (2003). General model for water monomer adsorption on close-packed transition and noble metal surfaces. *Physical Review Letters*, *90*(21), 216102.
83. Teng, B. T., Wen, X. D., Fan, M., Wu, F. M., & Zhang, Y. (2014). Choosing a proper exchange–correlation functional for the computational catalysis on surface. *Physical Chemistry Chemical Physics*, *16*(34), 18563-18569.
84. Kizilkaya, A. C., Niemantsverdriet, J. W., & Weststrate, C. J. (2016). Oxygen adsorption and water formation on Co (0001). *The Journal of Physical Chemistry C*, *120*(9), 4833-4842.
85. Weststrate, C. J., Van Helden, P., & Niemantsverdriet, J. W. (2016). Reflections on the Fischer-Tropsch synthesis: Mechanistic issues from a surface science perspective. *Catalysis Today*, *275*, 100-110.

APPENDIX A

INPUT AND OUTPUT FILES

A.1 SAMPLE INPUT AND OUTPUT FILES

There are 4 main input files that are used to calculate with the help of VASP. These are INCAR, KPOINTS, POSCAR, POTCAR files.

INCAR file is prepared according to calculation types including, volume relaxation, clean surface optimization, adsorption energy, vibrational frequency, transition state, vibrational analysis for translational analysis. INCAR file includes smearing function, optimization algorithm, convergence criteria and other parameters.

```
SYSTEM = Co(111)
!ISTART = 0
!PREC = HIGH
!ISIF = 2
IBRION = 2 ; NFREE = 20;
NSW = 999
LREAL = AUTO
ISMEAR = 1 ; SIGMA = 0.2;
ENCUT = 600
!NBANDS = 320
EDIFFG = -0.01
IDIPOL = 3
LDIPOL = .TRUE.
ADDGRID = .TRUE.
MAGMOM = 20*3
IALGO = 48
ISPIN = 2
```

Figure A.1. A sample INCAR file

A sample INCAR file is shown in Figure A.1.

KPOINTS specify used kpoint number to the Brillouin zone in calculation. POSCAR file is formed unit cell vectors, lattice constant atom numbers, input coordinates for system.

A sample KPOINTS file is shown in Figure A.1.

```

K-Points
0
Monkhorst-Pack
5 5 1
0. 0. 0.

```

Figure A.2. A sample KPOINTS file

POSCAR file is the initial coordinates of structure geometry.

```

Co-fcc-111-22
1.0000000000000000
4.9725999832153320 0.0000000000000000 0.0000000000000000
-2.4863002425925131 4.3063977634163706 0.0000000000000000
-0.0000010106117090 -0.0000017504309440 23.1201000213622159
20 1 1
Selective dynamics
Direct
0.3333300237726533 0.1666700035846631 0.0000000000000000 F F F
0.8333299758261887 0.1666700035846631 0.0000000000000000 F F F
0.3333300236972434 0.6666700488532058 0.0000000000000000 F F F
0.8333299757507788 0.6666700488532058 0.0000000000000000 F F F
0.0000000000500719 0.0000000001001510 0.0878000049663470 F F F
0.5000000178942017 0.0000000001001510 0.0878000049663470 F F F
0.9999999940899897 0.4999999979110896 0.0878000049663470 F F F
0.4999999940899897 0.4999999979110896 0.0878000049663470 F F F
0.1666699924383153 0.3333300023368508 0.1756100127450253 F F F
0.6666699921687140 0.3333300023368508 0.1756100127450253 F F F
0.1666700501720513 0.8333300199234870 0.1756100127450253 F F F
0.6666700501720513 0.8333300199234870 0.1756100127450253 F F F
0.3338871512165821 0.1644172813714273 0.2648969008443437 T T T
0.8368966102708381 0.1631033692398024 0.2635532790700811 T T T
0.3354278799295475 0.6645721871326910 0.2612829317292162 T T T
0.8355826980638030 0.6661129215090591 0.2648969008443437 T T T
-0.0049175854723002 0.0049175860732346 0.3513812595710575 T T T
0.4843291013362726 -0.0138662140647484 0.3478905500569118 T T T
0.0138662123180069 0.5156709165545398 0.3478905500569118 T T T
0.4944898532286560 0.5055101388803617 0.3476053258022696 T T T
0.6706593054185418 0.3293406945714604 0.4260693647982158 T T T
0.6675531992802375 0.3324468007097650 0.4954039702824391 T T T

```

Figure A.3. A sample POSCAR file

POTCAR file consists pseudopotential type for calculation, atomic information such as ENMAX. POSCAR atomic order must be same with POTCAR atomic order. Individual atom's POTCAR files are merged and only one POTCAR is formed. A sample POTCAR file first lines are shown in Figure A.4.

```

PAW_PBE Co 02Aug2007
9.000000000000000
parameters from PSCTR are:
VRHFIN =Co: d8 s1
LEXCH  = PE
EATOM  = 813.3670 eV, 59.7808 Ry

TITEL  = PAW_PBE Co 02Aug2007
LULTRA = F use ultrasoft PP ?
IUNSCR = 1 unscreen: 0-lin 1-nonlin 2-no
RPACOR = 2.000 partial core radius
POMASS = 58.933; ZVAL = 9.000 mass and valenz
RCORE  = 2.300 outmost cutoff radius
RWIGS  = 2.460; RWIGS = 1.302 wigner-seitz radius (au A)
ENMAX  = 267.968; ENMIN = 200.976 eV
RCLOC  = 1.203 cutoff for local pot
LCOR   = T correct aug charges
LPAW   = T paw PP
EAUG   = 477.818
DEXC   = 0.000
RMAX   = 2.360 core radius for proj-oper
RAUG   = 1.300 factor for augmentation sphere
RDEP   = 2.393 radius for radial grids
RDEPT  = 1.864 core radius for aug-charge

```

Figure A.4. A sample “POTCAR” file (first lines)

```

Error from kinetic energy argument (eV)
NDATA = 100
STEP = 20.000 1.050
102. 100. 99.7 98.2 97.4 95.8 94.0 93.1
91.2 89.2 88.1 86.0 83.8 81.5 79.1 76.7
74.2 71.7 69.1 65.2 62.6 60.0 56.1 53.5
50.9 47.1 43.3 40.9 37.4 34.0 30.7 27.6
24.7 22.0 19.4 17.1 14.2 12.3 10.1 8.56
6.82 5.36 4.14 3.14 2.34 1.71 1.22 0.771
0.519 0.304 0.171 0.106 0.604E-01 0.389E-01 0.301E-01 0.289E-01
0.288E-01 0.276E-01 0.246E-01 0.202E-01 0.153E-01 0.108E-01 0.724E-02 0.459E-02
0.342E-02 0.290E-02 0.282E-02 0.279E-02 0.255E-02 0.215E-02 0.160E-02 0.110E-02
0.763E-03 0.598E-03 0.550E-03 0.545E-03 0.512E-03 0.431E-03 0.313E-03 0.224E-03
0.169E-03 0.153E-03 0.151E-03 0.138E-03 0.110E-03 0.790E-04 0.596E-04 0.535E-04
0.524E-04 0.468E-04 0.353E-04 0.262E-04 0.221E-04 0.216E-04 0.194E-04 0.148E-04
0.110E-04 0.101E-04 0.965E-05 0.795E-05
END of PSCTR-controll parameters
local part
81.2582175088937
0.47064101E+02 0.47061564E+02 0.47053981E+02 0.47041338E+02 0.47023629E+02

```

Figure A.5. A sample POTCAR files (last lines)

A sample POTCAR last lines are shown in Figure A.5.


```

 2 F= -.15128375E+03 E0= -.15127850E+03 d E =-.830339E-03 mag= 32.9171
trial-energy change: -0.000830 1.order -0.000134 -0.000260 -0.000007
step: 1.0017(harm= 1.0296) dis= 0.00084 next Energy= -151.283749 (dE=-0.830E-03)
bond charge predicted
      N      E              dE              d eps              ncg              rms              rms(c)
RMM:  1      -0.151283749482E+03      -0.84304E-06      -0.14868E-07      3403      0.877E-04      0.126E-03
RMM:  2      -0.151283752679E+03      -0.31971E-05      -0.20201E-07      3382      0.148E-03      0.217E-02
RMM:  3      -0.151283749508E+03      0.31706E-05      -0.18270E-07      3364      0.174E-03      0.181E-03
RMM:  4      -0.151283749521E+03      -0.12544E-07      -0.19826E-08      2831      0.563E-04
 3 F= -.15128375E+03 E0= -.15127850E+03 d E =-.830756E-03 mag= 32.9171
curvature: -0.06 expect dE=-0.318E-04 dE for cont linesearch -0.100E-07
trial: gam= 2.11523 g(F)= 0.558E-03 g(S)= 0.000E+00 ort = 0.677E-05 (trialstep = 0.149E+00)
search vector abs. value= 0.175E-02
bond charge predicted
      N      E              dE              d eps              ncg              rms              rms(c)
RMM:  1      -0.151283780717E+03      -0.31208E-04      -0.77461E-03      5780      0.192E-01      0.429E-02
RMM:  2      -0.151284035553E+03      -0.25484E-03      -0.25278E-04      5789      0.631E-02      0.213E-01
RMM:  3      -0.151283967761E+03      0.67792E-04      -0.68382E-05      5780      0.283E-02      0.150E-01
RMM:  4      -0.151283853923E+03      0.11384E-03      -0.32757E-05      5772      0.196E-02      0.931E-02
RMM:  5      -0.151283816106E+03      0.37817E-04      -0.14933E-05      5728      0.140E-02      0.440E-02
RMM:  6      -0.151283807374E+03      0.87311E-05      -0.51155E-06      5266      0.841E-03      0.130E-02
RMM:  7      -0.151283806261E+03      0.11135E-05      -0.80857E-07      3597      0.317E-03      0.103E-02
RMM:  8      -0.151283806761E+03      -0.50049E-06      -0.15534E-06      3684      0.477E-03
 4 F= -.15128381E+03 E0= -.15127862E+03 d E =-.572404E-04 mag= 32.9169
trial-energy change: -0.000057 1.order -0.000055 -0.000085 -0.000024
step: 0.2082(harm= 0.2082) dis= 0.00068 next Energy= -151.283809 (dE=-0.595E-04)
bond charge predicted

```

Figure A.7. A sample "slurm.out" file (first lines)

At the end of calculation, stopping code writes at the end of slurm.out file.

```

      N      E              dE              d eps              ncg              rms              rms(c)
RMM:  1      -0.151283915298E+03      0.17535E-05      -0.21725E-04      5777      0.322E-02      0.908E-03
RMM:  2      -0.151283936574E+03      -0.21276E-04      -0.95134E-06      5668      0.116E-02      0.609E-02
RMM:  3      -0.151283927714E+03      0.88600E-05      -0.40653E-06      4962      0.714E-03      0.350E-02
RMM:  4      -0.151283920279E+03      0.74356E-05      -0.12869E-06      3564      0.417E-03      0.126E-02
RMM:  5      -0.151283922179E+03      -0.19004E-05      -0.71173E-07      3477      0.336E-03      0.133E-02
RMM:  6      -0.151283922520E+03      -0.34075E-06      -0.34615E-07      3383      0.255E-03
 16 F= -.15128392E+03 E0= -.15127894E+03 d E =-.698160E-04 mag= 32.9141
curvature: -1.62 expect dE=-0.476E-04 dE for cont linesearch -0.130E-06
trial: gam= 0.33840 g(F)= 0.293E-04 g(S)= 0.000E+00 ort = 0.568E-05 (trialstep = 0.275E+00)
search vector abs. value= 0.793E-04
bond charge predicted
      N      E              dE              d eps              ncg              rms              rms(c)
RMM:  1      -0.151283930627E+03      -0.84482E-05      -0.10106E-03      5780      0.688E-02      0.151E-02
RMM:  2      -0.151283955678E+03      -0.25050E-04      -0.29194E-05      5750      0.200E-02      0.581E-02
RMM:  3      -0.151283958010E+03      -0.23325E-05      -0.82831E-06      5662      0.960E-03      0.548E-02
RMM:  4      -0.151283945579E+03      0.12431E-04      -0.41526E-06      4966      0.698E-03      0.376E-02
RMM:  5      -0.151283940494E+03      0.50845E-05      -0.18213E-06      3898      0.529E-03      0.120E-02
RMM:  6      -0.151283940124E+03      0.36976E-06      -0.34350E-07      3389      0.236E-03
 17 F= -.15128394E+03 E0= -.15127896E+03 d E =-.176045E-04 mag= 32.9139
trial-energy change: -0.000018 1.order -0.000006 -0.000009 -0.000004
step: 0.2881(harm= 0.4741) dis= 0.00003 next Energy= -151.283940 (dE=-0.177E-04)
reached required accuracy - stopping structural energy minimisation
writing wavefunctions

```

Figure A.8. A sample "slurm.out" (last lines)

```

POTCAR:   PAW_PBE Co 02Aug2007
VRHFIN =Co: d8 s1
LEXCH = PE
EATOM = 813.3670 eV, 59.7808 Ry

TITEL = PAW_PBE Co 02Aug2007
LULTRA = F use ultrasoft PP ?
IUNSCR = 1 unscreen: 0-lin 1-nonlin 2-no
RPACOR = 2.000 partial core radius
POMASS = 58.933; ZVAL = 9.000 mass and valenz
RCORE = 2.300 outmost cutoff radius
RWIGS = 2.460; RWIGS = 1.302 wigner-seitz radius (au A)
ENMAX = 267.968; ENMIN = 200.976 eV
RCLOC = 1.203 cutoff for local pot
LCOR = T correct aug charges
LPAW = T paw PP
EAUG = 477.818
DEXC = 0.000
RMAX = 2.360 core radius for proj-oper
RAUG = 1.300 factor for augmentation sphere
RDEP = 2.393 radius for radial grids
RDEPT = 1.864 core radius for aug-charge

Atomic configuration
9 entries
  n  l  j          E      occ.
  1  0  0.50    -7587.6674  2.0000
  2  0  0.50    -893.6084  2.0000
  2  1  1.50    -764.5805  6.0000

```

Figure A.9. A sample of "OUTCAR" (first lines)

reached required accuracy - stopping structural energy minimisation
writing wavefunctions

LOOP+: cpu time 52.94: real time 53.60
4ORBIT: cpu time 0.00: real time 0.00

total amount of memory used by VASP on root node 100446. kByte
=====

base : 30000. kBytes
nonlr-proj: 8326. kBytes
fftplans : 7884. kBytes
grid : 14569. kBytes
one-center: 684. kBytes
wavefun : 38983. kBytes

General timing and accounting informations for this job:
=====

Total CPU time used (sec): 1507.173
User time (sec): 1497.061
System time (sec): 10.111
Elapsed time (sec): 1510.381

Maximum memory used (kb): 273772.
Average memory used (kb): 0.

Minor page faults: 1129464
Major page faults: 0
Voluntary context switches: 4762

Figure A.10. A sample "OUTCAR" file (last lines)

